ECOLE POLYTECHNIQUE FEDERALE DE LAUSANNE
SCHOOL OF LIFE SCIENCES


Master's project in Bioengineering and Biotechnology

# Effects of Photodynamic Therapy in Combination with Anti-Angiogenic Drugs on the Chicken Chorioallantoic Membrane Model

Done by

**Andrea Weiss**

Under the direction of

Prof. Hubert van den Bergh

Co-director

Dr. Patrycja Nowak-Sliwinska

In the laboratory of The Medical Photonics Group
EPFL

External Expert Prof. Dr. Arjan W. Griffioen

Department of Medical Oncology

VU University Medical Center, Amsterdam, The Netherland

LAUSANNE, EPFL 2011

# Table of Contents

## Summary

Photodynamic therapy (PDT) is clinically-approved in the treatment of angiogenic disorders, particularly eye diseases such as age-related macular degeneration (AMD) and skin cancers, such as basal cell carcinoma. PDT causes vascular occlusion resulting in hypoxia and inflammation, which induces the activation of the hypoxia inducible factors and the release of vascular endothelial growth factor, amongst other pro-angiogenic factors. This leads to the activation angiogenic pathways and the biological response of revascularization of treated areas. Therefore, the use of PDT in combination with anti-angiogenic strategies could increase treatment efficiency for diseases such as AMD by extending the photodynamic angio-occlusive effects.

The aim of this research is to compare the effectiveness of Visudyne®-PDT in combination with one of two drugs targeting angiogenesis through different mechanisms: 1) direct targeting of VEGF, the clinically targeted pathway in AMD, by means of the antibody Avastin®, and 2) blocking the angiogenic signaling pathway with a receptor tyrosine kinase inhibitor, Sutent®. These compounds were tested on the chicken chorioallantoic membrane (CAM) with and without PDT. When drugs were topically applied during early stages of embryonic development to inhibit physiological angiogenesis, fifty percent inhibition ($ED_{50}$) is seen at 45 and 200 μM for Avastin® and Sutent®, respectively. To study the effects of drug inhibition on an induced angiogenic state, closure of small blood vessels is achieved through Visudyne®-PDT. Vascular regrowth following photodamage is significantly inhibited by both drugs, with an $ED_{50}$ of 7 and 17 μM for Avastin® and Sutent®, respectively. These results suggest the therapeutic potential of the tyrosine kinase inhibitor for application in combination with PDT strategies. The use of small molecule drugs could lead to more optimal application of anti-angiogenic compounds via droplets or slow-release drug delivery systems.

# Introduction

## Angiogenesis

Angiogenesis is defined as the formation of new blood vessels from pre-existing capillaries (1). This term was coined in 1935 in order to describe the formation of new blood vessels in placenta (2). The survival of all cells and tissues is dependent on angiogenesis, due to the transportation of gasses and nutrients in the blood through the vascular network. Angiogenesis is therefore incredibly important to many normal physiological processes such as normal tissue growth, embryonic development, wound healing and menstruation (1). In the same sense, the inability of the body to properly control angiogenesis can lead to many severe disease states. Inadequate angiogenesis can lead to ischemic tissues (tissues with restricted blood flow) and cardiac failure, while abnormally high levels of angiogenesis can result in pathological processes such as: cancer, age-related macular degeneration (AMD), cardiovascular diseases (atherosclerosis), chronic inflammation (rheumatoid arthritis, Crohn's disease), diabetes (diabetic retinopathy), psoriasis, endometriosis and adiposity (3; 4).

Blood vessels are lined by endothelial cells which are in direct contact with blood. Below the monolayer of endothelial cells, blood vessels are surrounded by pericytes (structural support cells), smooth muscle cells, fibroblasts, the basement membrane (BM) and the extracellular membrane (ECM) (1). Endothelial cells are metabolically active and selectively permeable to small solutes and peptides/proteins. They also play a key role in many regulatory processes in the body including: regulation of blood coagulation (5); directing cells of the immune system to specific sites in the body through the release of chemo-attractants, cytokines and chemokines (6); aiding in vascular remodeling and being directly involved in the angiogenic cascade (1).

The process of angiogenesis is characterized by the formation of new vessels from preexisting vessels, capillaries and postcapillary venules (7). Angiogenesis is initiated by the release of pro-angiogenic factors which activate signaling cascades. The increased release of pro-angiogenic factors is normally in response to the release of cytokines by cells in a hypoxic (low oxygen) or ischemic environment (1). The transition from quiescent or non-proliferative vasculature to angiogenic vasculature is marked by a change in the balance between pro- and anti-angiogenic factors.

Endothelial cell activity is always the first process to initiate angiogenesis in all situations. It is believed that vascular endothelial growth factor (VEGF) is the most important molecule involved

in the initiation of angiogenesis (1). This hypothesis is supported by the fact that the release of VEGF results in vasodilation through endothelial cell production of nitrous oxide, which increases endothelial cell permeability, a pre-requisite for endothelial cells to enter the angiogenic cascade (1; 8). Increased endothelial cell permeability allows plasma proteins to enter the tissue and form a fibrin-rich provisional network to support the growth of new blood vessels (9). VEGF's importance in initiating the angiogenic cascade is supported by the fact that its production is controlled by hypoxia inducible factors (HIF) and the fact that the VEGF receptor (VEGFR) is over expressed in hypoxic or ischemic conditions (10). Even though VEGF is arguably the most important factor involved in angiogenesis, evidence has shown that angiogenesis in not entirely VEGF dependent (11).

In the process of angiogenesis, activated endothelial cells migrate to the desired location of the body, degrading the BM of the parent venule in order to move towards an angiogenic stimulus. The endothelial cells elongate and align to create a solid sprout, while the lumen of the vessel is formed by a curvature in each endothelial cell (12). The endothelial cells continue to proliferate, increasing the length of the sprout, until finally two hollow sprouts will join at their tips to create a loop and allow blood to flow. Pericytes then line the base of the loop and new sprouts can grow from its apex (13).

The exact process of these last steps of angiogenesis is not entirely understood, but the process is believed to be guided by specialized cells at the front of the sprout called 'tip cells'. A study conducted by Gerhardt et al. on angiogenesis in the retina of mice found that retinal vessels grow in expanding circles (14). These sprouts were guided by specialized tip cells supported by highly proliferative stalk cells. This study revealed that the tip cells are highly polarized and uniquely responsive the VEGF-A isoform. Tip cells grow by extending along filopodia which follow astrocyte cell tracks. The filopodia can guide the tip cells by detecting VEGF-A gradients, which are created by astrocytes. The stalk cells are also specifically responsive to VEGF-A, but to its absolute concentration and not its gradient (14).

Adult vasculature is mainly quiescent with the exception of organs which undergo ongoing angiogenesis, such as the female reproductive organs, organs that undergo physiological growth, or injured tissues (15).

### Angiogenic factors

Physiologic angiogenesis is a very complicated process which involves many different pro- and anti-angiogenic stimuli including many growth factors and environmental factors. Vascular

endothelial growth factor (VEGF) is the most potent and best understood of these growth factors (1). It belongs to the VEGF-PDGF supergene family, which contains 5 isoforms based on alternative exon splicing (VEGF-A, VEGF-B, VEGF-C, VEGF-D and VEGF-E). Out of these factors, VEGF-A is the most potent growth factor and is frequently referred to as simply VEGF (16). VEGF is responsible for the regulation of angiogenesis through the following mechanisms: increasing micro-vascular permeability to plasma proteins (17); inducing endothelial cell division and migration (18; 19); promoting endothelial cell survival through interactions with ECM components, such as $\alpha_v\beta_3$ integrin, which prevents apoptosis (20) and reverses endothelial cell senescence (21; 22); promoting stromal degradation and possibly increasing the formation of extravascular fibrin substrate for endothelial and tumor cell growth (23; 24). VEGF is also believed to induce the expression of proteases and receptors involved in cellular invasion and tissue remodeling (25; 26). Loss of VEGF signaling can result in apoptosis of endothelial cells (15). This family of ligands interacts with three receptor tyrosine kinases: VEGFR-1/FLT-1, VEGFR-2/FLK-1/KDR and VEGFR-3/FLT-4; however its angiogenic effects are mainly due to binding with VEGFR-1 and -2 found predominantly on vascular endothelial cells (24; 27). VEGFRs, however, are not only expressed on the vascular endothelium, but also on monocytes, macrophages and some tumors cells (1). VEGF is mainly produced by angiogenic endothelial cells, but can also be produced in hypoxic tumor cells, macrophages and other immune cells (28). VEGF-A binds with greater affinity to VEGFR-1 than VEGFR-2, but it is believed that VEGFR-1 mainly acts as an intermediate receptor, controlling the availability of VEGF-A to VEGFR-2, which is mainly responsible for VEGF-related signaling (24; 29).

Other important pro-angiogenic factors include the basic fibroblast growth factor family, (bFGF also referred to as FGF2) and the platelet-derived growth factor (PDGF) (16). There are also many ECM components which can have effects on angiogenesis and endothelial cell morphology including: integrins, throbospondin, laminin and osteonectin. Integrin $\alpha_v\beta_3$ plays a particularly critical role in angiogenesis due to the fact that its inhibition results in endothelial cell apoptosis and the fact that it mediates cellular adhesion to many factors (30). In addition, it is minimally expressed in quiescent endothelial cells while being up-regulated in angiogenic endothelial cells (31).

In addition to the molecules and pathways mentioned above, there are also other cell types and environmental factor which can affect angiogenesis including: immune cells, periendothelial cells and environmental factors such as hypoxia (1). Hypoxic conditions are capable of inducing

angiogenesis through the activation of HIF, which in turn causes the release of VEGF and other pro-angiogenic factors (1).

The decision for a blood vessel to remain quiescent or become angiogenic is dependent on many different signals of varying importance, some of which are briefly discussed above. Interactions with these pathways can be achieved through many different mechanisms and can provide the ability to control angiogenesis for therapeutic purposes.

### Receptor tyrosine kinases

Many important angiogenic factors such as VEGFs, PDGF, FGFs, and epidermal growth factor (EGF) interact with endothelial cells through receptors which are transmembrane cell signaling proteins called receptor tyrosine kinases (RTKs) (32; 16). RTKs are responsible for transducing extracellular signals to the interior of cells and are involved in many different pathways in the body, including cell proliferation and migration (16). An overview of different pathways involved in angiogenesis which are activated by RTKs can be seen in Figure 1 (adapted from Gotink et al. (16)). The most common RTK involved in angiogenesis is the VEGFR (16).

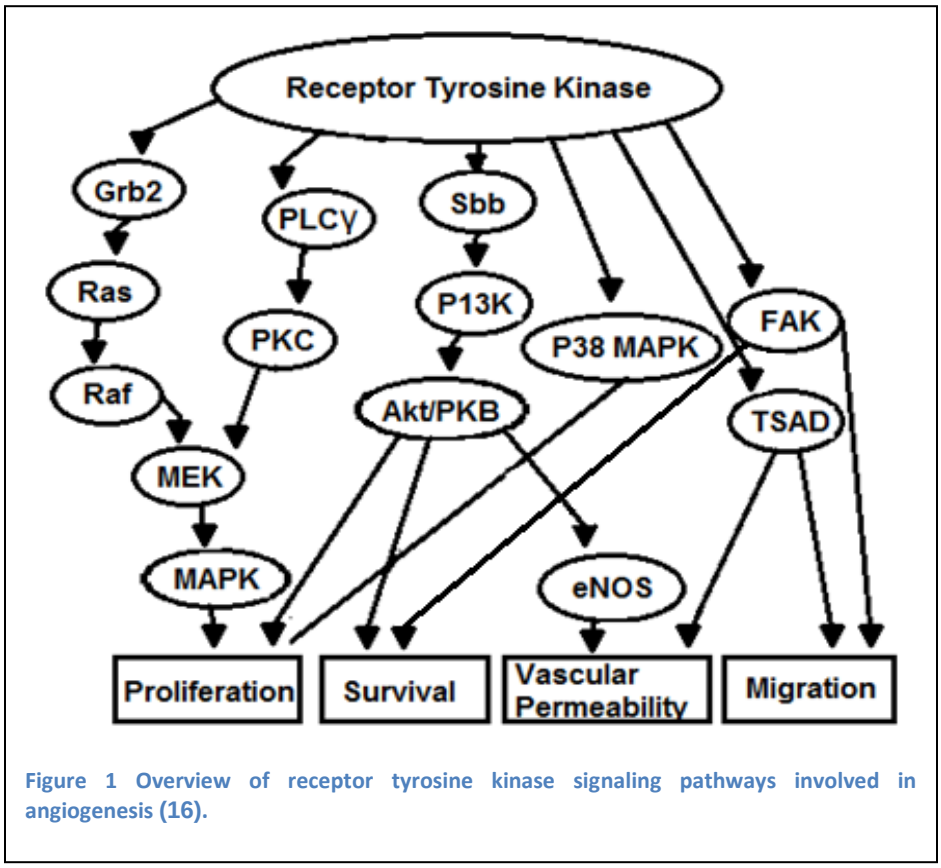


**Figure 1 Overview of receptor tyrosine kinase signaling pathways involved in angiogenesis (16).**

A typical RTK monomer is shown in Figure 2 (16). A monomer consists of an N-terminal extracellular ligand-binding domain, a transmembrane domain and a C-terminal intracellular domain with tyrosine kinase activity. The kinase domain has two lobes, with an ATP-binding cleft located between the N- and C-terminal lobes (16). An angiogenic factor can act as a ligand to a RTK by binding to its extracellular domain, inducing dimerization of the receptor and autophosphorylation of the kinase domain located on the interior of the cell (33). The RTK is then capable of transferring a phosphate group from a high-energy donor molecule, such as ATP, to a specific substrate (33). ATP normally binds to a kinase receptor by forming an H-bond from its adenine ring to the ATP-binding cleft of the kinase. The transfer of a phosphate group from the ATP molecule to the substrate results in the phosphorylation of the substrate, which induces a functional change (16). The substrate is then capable of transducing the signal through the activation of a specific signaling pathway. Simultaneous activation of many signaling pathways results in a biological response (34).

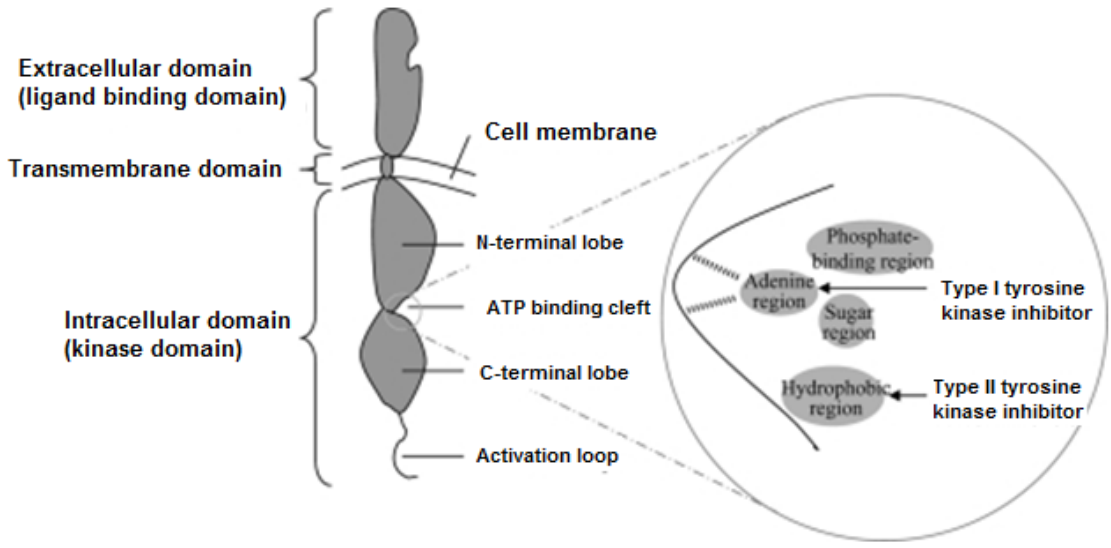


**Figure 2 The structure of a receptor tyrosine kinase, showing the ATP binding site which the receptor tyrosine kinase inhibitor competitively binds to (16).**

Due to their pivotal role in the activation of angiogenic signaling pathways, RTKs can be targeted as a means to control angiogenesis for therapeutic reasons. This can be achieved through the use of receptor tyrosine kinase inhibitors (RTKIs), which are small-molecules that

competitively interfere with the ATP binding site (shown in Figure 2) (16). There exist three categories of RTKIs. Type I kinase inhibitors, which include Sutent®, recognize the active conformation of the kinase and bind to the ATP-binding site by presenting one to three H-Bonds which mimic bonds normally formed by ATP. Due to the fact that the ATP binding site is mostly conserved in all RTKs, type I inhibitors always occupy the adenine region of ATP-binding site, and it is therefore hard to have a type I inhibitor which is highly selective (16). Type II kinase inhibitors recognize the inactive confirmation of the kinase and indirectly compete with ATP by occupying the hydrophobic pocket right next to ATP-binding site. Finally, type III kinase inhibitors, which are known as 'covalent' inhibitors, covalently bind to the cysteines at a specific site in the kinase, blocking the binding of ATP (16).

## Exudative age-related macular degeneration

### Overview

Age-related macular degeneration (AMD) is a retinal disease, which represents the leading cause of vision loss and legal blindness in the elderly populations of developed countries (35). AMD is characterized by abnormalities in four structure of the macular region: the photoreceptors, the retinal pigment epithelium (RPE), the Bruch's membrane and the choriocapillaries (36). An overview of these structures and their abnormalities in patients suffering from AMD is shown in Figure 3 (37). There are two variations of AMD: the atrophic form of AMD and the angiogenic or exudative form of AMD. Exudative AMD is the faster-progressing form of AMD, and is characterized by the growth of abnormally leaky blood vessels in the choroid layer of the eye, called choroidal neovessels (CNVs) (36). The choroid is a vascular layer located between the retina and sclera (38). In AMD, these CNVs cause the leakage of blood and fluids in the macular region of the eye responsible for the central field of vision, resulting in vision impairment (36). The exact cause of the growth of these CNVs is unknown, but is believed to be related to a lack of oxygen and other nutrients in the photoreceptors (39; 40). A typical example of the type of vision loss suffered by patients with AMD is shown in Figure 4 (41). The exudative form of AMD is the focus of this study and will be referred to as only AMD hereafter.

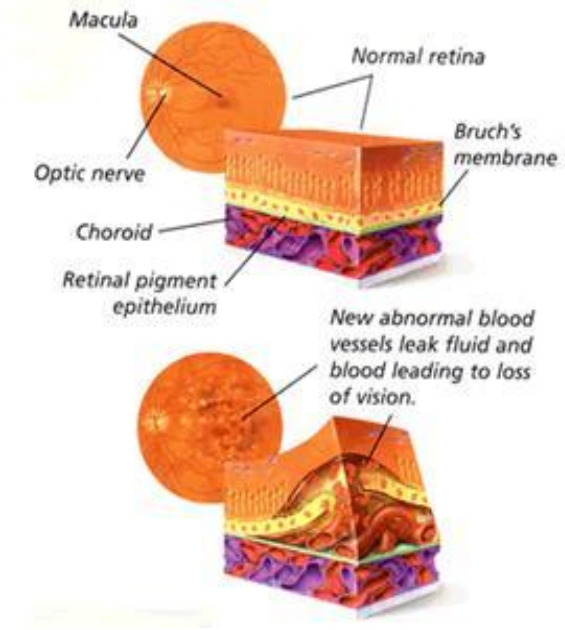


Figure 3 An overview of the structure in the eye affected by AMD. The top image shows a normal eye, while the bottom image shows the effects of AMD (37).

Figure 4 An example of vision loss as a result of AMD (41).

## Treatment options for AMD

Current forms of treatment for AMD, which can help to manage symptoms and slow disease progression, include: laser treatment (thermal laser photocoagulation and transpupillary thermotherapy) (42), PDT (43), and anti-angiogenic drug therapy (43). Laser treatment uses laser light in order to non-specifically photo-coagulate CNVs, sealing off leaky blood vessels. This form of treatment, however, results in many small retinal scars causing blinds spots in the patients' field of vision and, therefore, is no longer widely used (42). Both photodynamic and anti-VEGF therapies have been shown to be safe and effective treatments for AMD which specifically target abnormal blood vessels. The specific inhibition of diseased CNVs with PDT or anti-angiogenic drug therapy presents the advantage of resulting in minimal damage to retinal vessels, normal choriocapillaries, retinal pigment epithelium and nearby photoreceptors (43; 44). These therapies result in some degree of closure of malignant blood vessels, allowing normal choriocapillaries to regrow in their place resulting in improved visual acuity (45; 46).

Clinically-approved treatments for AMD include the use of Visudyne®-PDT and two anti-angiogenic drugs: Lucentis® (ranibizumab, Novartis) and Macugen® (pegaptanib sodium, EyeTech) (47; 48; 39). Both of these drugs target the pro-angiogenic growth factor VEGF to inhibit blood vessel growth (42). The anti-angiogenic drug Lucentis® is a humanized monoclonal antibody targeting VEGF, while Macugen® is an aptamer or pegylated modified RNA

oligonucleotide with a high affinity for VEGF (36). In addition to these drugs which have already been approved, there are additional anti-angiogenic drugs which are still under investigation, including: anecortave acetate (a steroid) (49); triamcinolone acetonide (50); squalamine lactate (a steroid compound) (51); Sirna-027 (a small interfering RNA) (52); VEGF-Trap (a decoy receptor) (53) and angiostatin, endostatin and PEDF (anti-angiogenic factor) (54; 36).

In the literature there are some studies examining the effect of small molecule-based RTKIs on eye disease. For example, the application of the RTKI CGP 41251 to CNVs growing in mice due to retinal damage caused by photocoagulation resulted in a dramatic decrease in the growth of CNVs in treated mice when compared to control mice, suggesting some support for the use of an orally bioavailable RTKI in the treatment of AMD (55).

The use of slow-release drug delivery systems has also been investigated for the treatment of vitreoretinal diseases, such as AMD (56). These devices can help to overcome some of the complications normally associated with drug delivery to the eyes. Complications include problems with delivery of systemically administered drugs to the retina, due to its unique situation of being separated from systemic circulation by the inner and outer blood retinal barriers (56). The application of drugs through eye drops is also not ideal, due to difficulties achieving therapeutically-relevant concentrations because of low absorption and washing away of drugs as a result of tear production (57). Due to these complications, most drugs must be administered directly into the eye through intravitreal injections. This, however, is also not without complications such as vitreous hemorrhage, endophthalmitis and retinal detachment (56). In addition, many low molecular weight drugs have short half-lives (as short as a few hours) in the vitreous cavity, requiring multiple drug applications in order to maintain therapeutic drug concentrations (58). All of these complications and limitations have resulted in a need for the development of slow-release drug delivery systems for the treatment of eye diseases such as AMD. Some of the devices which are under investigation and their potential for improving treatment of AMD are discussed in the paper by Yasukawa et al (56).

More recently, the use of implantable telescopes has also been approved for the treatment of AMD. These microscopes magnify images, thereby reducing the relative size of the blind spot in the center of the field of vision caused by the macular degeneration. This treatment, however, is only used in extreme cases for patients with severe vision loss, reaching the end stage of advanced macular degeneration (42).

### *Avastin® vs. Lucentis®*

Avastin®, one of the drugs under investigation in this study, is not clinically-approved for the treatment of AMD, but is frequently used 'off-label' for this indication. Avastin® is clinically-approved for the systemic treatment of certain forms of cancer such as colon cancer (59), and is currently under consideration for the treatment of AMD. Lucentis®, one of the anti-angiogenic drugs clinically-approved for the treatment of AMD mentioned above, is derived from the same anti-VEGF mouse monoclonal antibody as Avastin® (60). While Avastin® is comprised of the full length antibody; Lucentis® consists of only the antigen-binding fragment, making it a much smaller molecule (60). An overview of the modifications made to the antibody in order to generate these drugs can be seen in Figure 5 (61). Lucentis® was specifically developed and approved for the treatment of eye disease (60). Even though both molecules bind to VEGF at the same position, they vary in size, affinity, speed of clearance from the eye and cost (62). Both drugs are administered through intravitreal injection either on a monthly or an as-needed regiment. The widespread 'off-label' use of Avastin® for the treatment of AMD has developed as a result of the similarities between these drugs, the vast price difference between them (approximately $50 per dose of Avastin® compared to $2,000 per dose of Lucentis®), and an overall lack of evidence showing that Lucentis® is more effective than Avastin® (60).

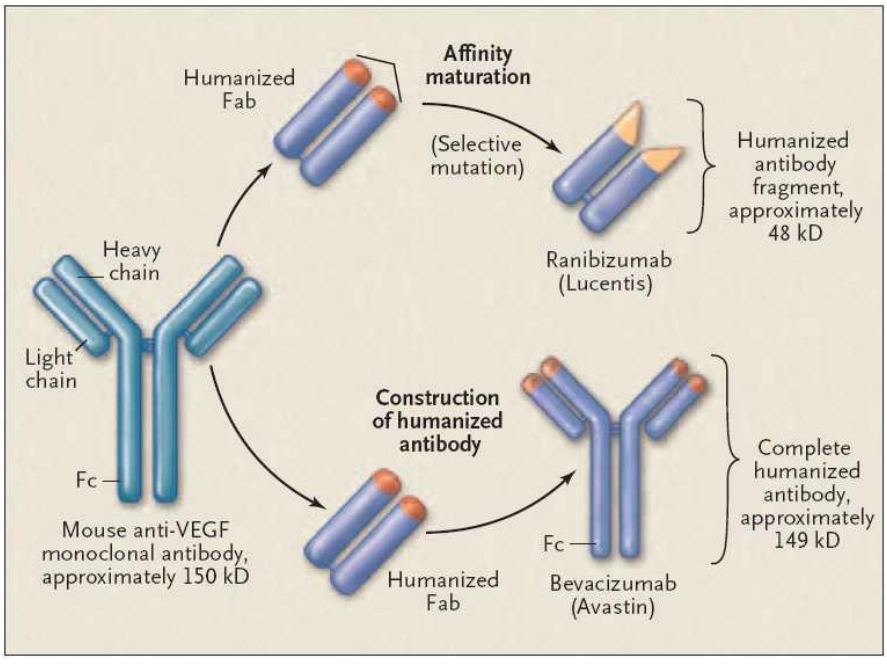


**Figure 5 An image of the mouse antibody which is used to generate Avastin® and Lucentis® and the modification made to the antibody to generate each of the drugs (61).**

In order to determine the efficacy of these two drugs, a large, prospective, multicenter randomized clinical trial was performed called the Comparison of AMD Treatment Trials (CATT) (63). In this study, optical coherence topographies (OCT) were used in order to monitor disease progression following treatment and identify fluid leakage from blood vessels. First-year results from this study showed that monthly use of Avastin® and Lucentis® resulted in the same visual acuity outcome. OCT results showed better retinal thickness measurements for Lucentis®-treated patients, which may be reflected in the visual acuity measurements for the second year check point, but were not evident at the end of the first year. This study also showed equivalent visual acuity outcomes for the monthly and as-needed treatment regime for Lucentis®. As-needed treatment for Avastin® and Lucentis® appeared similar, but the as-needed treatment regime for Avastin® was not as effective as the monthly regiment for either drug. This may be due to Avastin® therapy resulting in shorter treatment benefits for a subgroup of patients requiring more frequent drug administration (60; 63). Overall, these results are very positive for patients, as it supports the use of Avastin®, a much less expensive drug than Lucentis®, and suggests that monthly treatments may not always be necessary.

### *Visudyne®-PDT*

Visudyne®-PDT is commonly used for the treatment of AMD with relatively good results (36; 64). Studies have shown that Visudyne® preferentially accumulates in the neovasculature (including CNVs); however animal models have shown that some drug is also present in the retina (65). Visudyne®-PDT may, therefore, result in some damage to retinal pigmented epithelium and outer nuclear layers of the retina. Temporary occlusion of CNVs following Visudyne®-PDT in humans has been confirmed by fluorescein angiography (65).

Two double-masked, placebo-controlled, randomized studies on patients suffering from classic-containing subfoveal CNVs secondary to age-related macular degeneration were conducted in order to ascertain the effectiveness of Visudyne®-PDT (66; 65). A total of 609 patients (402 Visudyne® and 207 placebo) were involved in the two studies. Patients were treated and the vascular effects of the treatment were monitored using fluorescein angiograms. If blood vessel leakage was not entirely arrested or if a leakage returned, as detected by angiograms, retreatment was allowed every 3 months. The results of these studies showed that a statistically significant difference could be seen between patients treated with Visudyne®-PDT and control patients at both the 1 and 2 year check for visual acuity measurements. A subgroup of patients with classic CNV lesions (n=242, Visudyne®=159, placebo=83), defined as those where classic components comprised 50% or more of the whole lesion area, showed a difference of

approximately 28% between groups at 12 and 24 months for the primary efficacy endpoint (defined as the percentage of patients who lost <3 lines of visual acuity). In this subgroup, severe vision loss (≥6 lines of visual acuity from baseline) occurred in 12% of Visudyne®-treated patients compared to 36% of placebo-treated patients. Patients with predominantly classic CNV lesions without occult CNVs showed the greatest treatment benefit, with a 49% difference between treatment groups at the 1 year check point (assessed by <3 lines-lost definition). Older patients (≥75), patients with dark irises, occult lesions or less that 50% classic CNVs are less likely to benefit from PDT (66; 65).

These treatment modalities for AMD have been shown to be relatively effective; however, their beneficial results are only transient and no long term-cure is yet available. This is due to the fact that leaky blood vessels are only temporarily stabilized and the formation of new blood vessels which can become diseased in not prevented. In addition, PDT actually promotes the regrowth of new blood vessels by creating a hypoxic environment through vascular occlusion. Hypoxia results in the release of pro-angiogenic factors and initiation of angiogenic signaling pathways (43). This process accelerates the regrowth of malignant vasculature and therefore the recurrence of disease symptoms. The recurrence of vision loss necessitates re-treatment and is the major motivation for the adaptation of combination therapies, which could prevent or slow the regrowth of blood vessels following treatment.

## Cancer

Although exudative AMD is the primary focus of treatment for the research conducted in this study, many of the implications of these results can be carried over to cancer research. This is primarily due to the fact that like AMD, tumor growth is accompanied by abnormally angiogenic vasculature, and the fact that therapeutic benefit can be seen for cancer patient's treatment with anti-angiogenic drugs and PDT. In addition, the use of a combination of anti-angiogenic and photodynamic therapies present many potential benefits in the treatment of certain forms of cancer.

In 1971, Judah Folkman first proposed the theory that tumor growth is angiogenesis-dependent, and that targeting the neovascularization of tumors could provide a new form of cancer therapy (67). This theory was supported by a study performed in 1963, which showed that tumors implanted in isolated perfused organs failed to grow larger than a few millimeters, but when the same tumors were reimplanted into donor mice they grew rapidly killing the host (68). It was

believed that the perfused organ created an environment where neovascularization was inhibited, limiting the tumor's growth (13).

This was followed by a study in 1968, which showed that tumors could induce new capillary vessel growth even if they are separated from the vascular bed of the host by a Millipore filter (69). This lead to the hypothesis that tumors are capable of releasing a diffusible angiogenic factor or are capable of degrading an inhibitory factor, giving them the capability to initiating angiogenesis (13).

It is now widely accepted that tumors are angiogenesis-dependent and their ability to have sustained angiogenesis has been included as one of the hallmarks needed for the development and progression of cancer (70).

Cells initially lack the ability to induce angiogenesis, which limits their ability to grow. It is therefore believed that tumors must develop this ability, through what is referred to as an 'angiogenic switch', where the balance between angiogenesis inducers and inhibitors is switched to favor angiogenesis (70). The 'angiogenic switch' is believed to be the rate-limiting secondary step to developing multi-stage carcinoma (71).

The 'angiogenic switch' is normally accompanied by the increased expression of VEGFs and/or FGFs, or the down-regulated expression of angiogenesis inhibitors, such as thrombospondin-1 or β-interferon or both. Pro-angiogenic factors secreted by tumor cells stimulate proliferation and migration of endothelial cells, resulting in the outgrowth of new capillaries into the tumor (70). Each tumor type utilizes different molecular strategies to initiate the 'angiogenic switch' (70).

The theory that cancer is angiogenesis-dependent, and that the angiogenic phenotype is dependent on the expression of pro-angiogenic factors, is supported by the fact that serum concentrations of VEGF are 6.5 times higher in colon carcinoma patients when compared to healthy individuals, and that high serum levels of VEGF is strongly associated with reduced overall survival and disease-free survival (72; 73; 74).

The link between cancer and angiogenesis is further strengthened by evidence which shows that many cancer-related genetic changes thought to result from mutations in tumor suppressor genes and oncogenes also result in angiogenic endothelial cells. Many oncogenes, such as *c-myb*, *sis* and *src,* cause increased expression of molecules that induce angiogenesis. For example, the mutated *ras* gene strongly upregulates TGF- α, TGF-β, and VEGF, and can also indirectly affect angiogenesis through the production and activation of the BM and ECM-

degradation enzymes (1). Another example is the mutation of the VHL gene, which is normally involved in the degradation of HIF-1α. The mutated VHL gene is no longer capable of breaking down HIF-1α, which can result in upregulation of VEGF, EGFR, and PDGF, and the induction of angiogenesis (70; 75).

The 'angiogenic switch' is very dependent on the expression of VEGF, due to the fact that it is the most potent pro-angiogenic factor. The most common way to inhibit angiogenesis is, therefore, through drugs which target VEGF or its receptors (16).

### Tumor angiogenesis

The 'angiogenic switch' is viewed as a discrete phase of tumor growth, which can occur at any stage of tumor development depending on the tumor and its microenvironment (15). Tumor angiogenesis is thought to go through two distinct phases. The first stage is the avascular phase, characterized by a small, occult lesion with a diameter less than 1-2 mm; this type of lesion will stay dormant by reaching a steady state between proliferation and apoptosis (15). A small percentage of these tumors will leave the dormant stage to enter the second phase of tumor angiogenesis, considered the vascular phase, which is characterized by exponential growth (15).

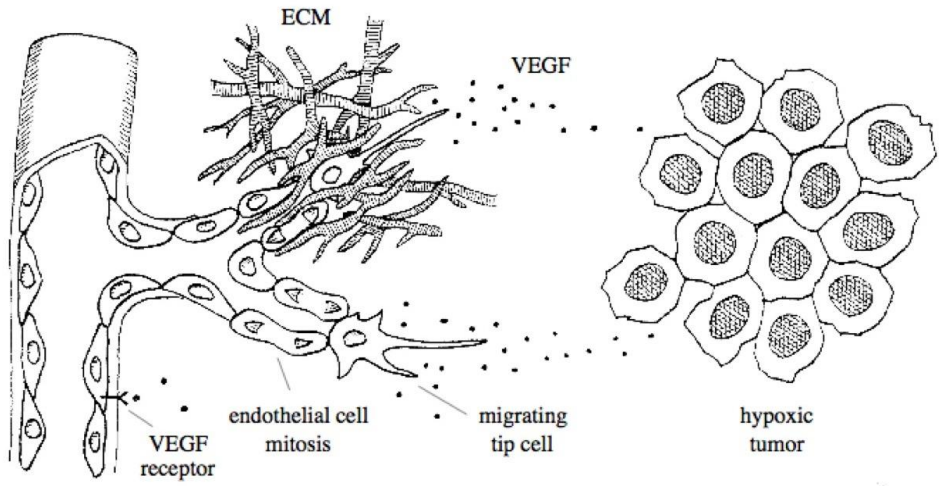


**Figure 6 Overview of the interaction between a blood vessel and tumor cells, which results in the growth of new blood vessels towards the tumor (76).**

There are many different pathways by which a tumor can induce angiogenesis, some of which are described below (13). Tumors can release their own angiogenic factors; each tumor type will release a combination of different factors in order to initiate angiogenesis. Macrophages can be attracted and activated to release angiogenic factors. Collagenases and heparanasese, which store angiogenic factors in the ECM, can be secreted and vascular permeability factors can be released, which cause leakage of fibrinogen from postcapillary venules to stimulate angiogenesis. An example of the type of interaction between tumor cells and nearby vasculature which can result in angiogenesis is shown in Figure 6 (76). This figure shows the tumor cells releasing pro-angiogenic factors (in this case VEGF) which activate nearby endothelial cells, resulting in angiogenesis toward the tumor.

Tumor vasculature is significantly different from normal vasculature due changes in the balance between pro- and anti-angiogenic factors (15). Some distinct characteristics of tumor vasculature include: aberrant vascular structures, i.e. vessels are irregularly shaped, dilated and tortuous, even having dead ends; altered endothelial-cell pericyte interactions characterized by loosely-associated pericytes and less dense pericyte coverage (77); abnormal blood flow which is slowed and sometimes oscillating, resulting in dysfunctional capillaries; increased vessel permeability causing leaky and hemorrhagic vessels due to over expression of VEGF and vessel characterized by delayed maturation (77; 15). These differences are due to the non-physiologic balance of pro- and anti-angiogenic factors and to the reduced association of pericytes with blood vessels. Reduced pericyte coverage allows for increased proliferation of endothelial cells resulting in vessels with abnormal structure, such as the increased thickness or tortuosity mentioned above, and results in vasculature which has increased sensitivity to the inhibition of VEGF signaling (15).

It has been hypothesized the unorganized nature of tumor vasculature may be due to misguiding of the filopodia which guide tip cells. One study showed that tumor vessels had misguided filopodia similar to those of transgenic mice overexpressing VEGF (14). Tumor hypoxia can also complicate the angiogenic activity of cancer cells and can result in tumor vasculature which is never quiescent and constantly growing. It should also be noted that research has shown that angiogenic activity does not necessarily correlate with the aggressiveness of a tumor (15).

## Anti-angiogenic drug therapy

### General information, advantages and disadvantages

Based on his theory regarding the dependence of tumor growth on angiogenesis, Judah Folkman proposed targeting the neovascularization of tumors as a new form of cancer therapy (67; 16). Now that cancer's dependence on angiogenesis has been widely accepted, targeting tumor angiogenesis has become a viable form of cancer therapy.

As previously described, angiogenesis is dependent on many pro- and anti- angiogenic signaling pathways. This study focuses on the use of two particular anti-angiogenic agents: the monoclonal antibody Avastin®, which directly target VEGF, and a RTKI, Sutent®, which inhibits VEGFR, thus preventing angiogenic signal transduction. An overview of many of the different pathways that can be targeted by anti-angiogenic drugs is shown in Figure 7 (78). The particular pathways of Sutent® and Avastin® are outlined in red and blue, respectively.

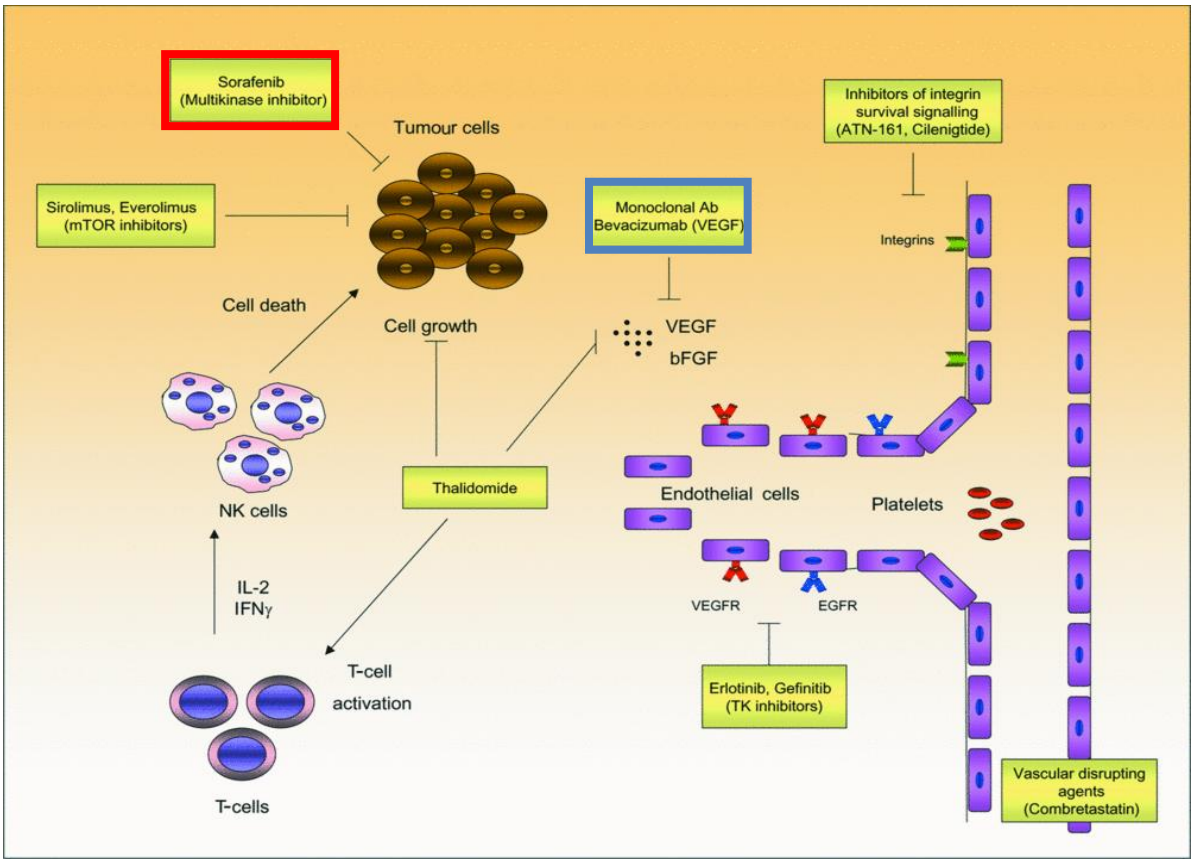


**Figure 7 Overview of potential targets of anti-angiogenic drugs in cancer treatment. Sutent® (sorafenib) (outlined in red in the figure) is shown targeting receptor tyrosine kinases in the tumors endothelium, while Avastin® (bevacizumab) (outlined in blue) is shown directly targeting VEGF molecules (78).**

Due to the fact that there are many angiogenic signaling pathways and many pro-angiogenic factors in the body, there exist many pathways by which angiogenesis can be targeted; but, there exist equally as many by which a tumor can evade this form of therapy, compensating for an inhibited factor through the increased expression of other factors (23). These mechanisms form the basis for one of the main complications associated with anti-angiogenic drug therapy: drug resistance. This also makes the combination of multiple anti-angiogenic drugs therapies an attractive therapeutic option, which could provide increased benefits (23). Even though the development of drug resistance has complicated the use of anti-angiogenic drug therapies in clinical applications, beneficial results are frequently seen with this form of therapy, as well as synergistic effects when they are used in combination with either chemo- or radiation therapy (23).

| Compound | Main targets | Preclinical models | Development status |
|---|---|---|---|
| Imatinib (Gleevec/ Glivec; Novartis) | BCR–ABL, KIT and PDGFR | FDC-P1 cells with KIT mutants cloned from patients with AML | • Approved for CML and GIST<br>• Pre-registration for ALL<br>• Phase II for solid tumours, sarcoma and melanoma |
| Nilotinib (Tasigna; Novartis) | BCR–ABL, KIT and PDGFR | Increased survival of mice injected with *Bcr–Abl*-transformed haematopoietic cell lines or primary marrow cells | • Approved for CML, including for patients who are resistant or intolerant to imatinib<br>• Phase III for melanoma and GIST |
| Sunitinib (Sutent; Pfizer) | FLT3, KIT, VEGFR and PDGFR | • MV4-11, RS4;11 and OC1-AML5 cells<br>• NOD–SCID mice | • Approved for RCC and GIST<br>• Pre-registration for pancreatic tumours<br>• Reached Phase III for breast, lung and prostate cancers and HCC, but development discontinued |
| Sorafenib (Nexavar; Bayer/Onyx) | KIT, Raf and VEGFR | • MDA-MB-231, NCI-H460, Colo-205, HT-29, DLD-1 and A549 cells<br>• NCr-nu/nu mice | • Approved for RCC and HCC<br>• Phase III for thyroid tumours and NSCLC<br>• Phase II for prostate cancer |
| Gefitinib (Iressa; AstraZeneca) | EGFR | HL-60, U-937 and Kasumi cells | • Approved for NSCLC<br>• Phase II for other tumour types |
| Semaxanib | FLT3, KIT, VEGFR and PDGFR | BaF3, MV4-11 and RS4;11 cells | Reached Phase III for colorectal cancer, but development discontinued |
| Midostaurin | FLT3, KIT, VEGFR and PDGFR | BaF3 cells with wild-type or mutant FLT3 | Phase III for AML |
| Lestaurtinib | FLT3 | BaF3 cells with wild-type or mutant FLT3 | Reached Phase II for AML and solid tumours, but development discontinued |
| Tandutinib | FLT3, KIT and PDGFR | BaF3, Molm-13, Molm-14, HL-60, AML-193, KG-1 and THP-1 cells | • Phase II for glioblastoma<br>• Discontinued for prostate cancer and AML |

**Figure 8 Table of selected anti-angiogenic receptor tyrosine kinase inhibitors, their target RTKs, clinical application and stage of development (79).**

The use of anti-angiogenic agents for the treatment of angiogenesis based disorders has shown a lot of therapeutic potential and is a field that is strongly researched. Many anti-angiogenic drugs are currently under development, involved in clinical trials or are being used in the treatment of angiogenesis disorders, particularly cancer. A table of selected RTKIs in different stages of development can be found in Figure 8 (79). Some of the general advantages and disadvantages of anti-angiogenic drug therapy will be discussed before each of the two drugs being specifically investigated in this study are described in more detail.

Anti-angiogenic drug therapy has been shown to be a relatively reliable and safe form of treatment for patients suffering from AMD and remains one of the best therapeutic options for this disease. More interestingly, however, is the use of anti-angiogenic drug therapy for the treatment of cancer, as it presents some unique advantages over other common forms of cancer drug therapy. Drug resistance is one of the major factors which contribute to the failure of certain types of cancer treatments, such as chemotherapy. It is believed to be caused by one of two mechanisms: through mutations in growth factor receptor signaling genes, or, as in the case of classic multi-drug resistance, the reduced energy-dependent uptake of anti-cancer drugs by drug efflux transporters due to the cloning of multidrug transporters such as P-glycoprotein (Pgp) (80; 81). It is believed that the development of drug resistance to anti-angiogenic drugs through these sorts of mutations may be avoidable as they target the tumor endothelium instead of the tumor cells themselves. Tumors must recruit these endothelial cells in order to create the vasculature they need to survive and grow. These endothelial cells are genetically more stable than the tumor cells, meaning that they are less susceptible to developing mutations that could lead to drug resistance (23). In addition, some RTKIs may be substrates and/or modulators of these multi-drug transporters, such as Pgp, and therefore may be able to bypass this mechanism of resistance (80; 81). This advantage, however, is considered controversial as much evidence has supported the ability of cancer to develop resistance to anti-angiogenic drugs, as well as results from clinical trials showing the development of drug resistance.

Although anti-angiogenic drug therapy is an effective form of treatment for AMD and some forms of cancer, it is still subject to limitations and has certain side effects and toxicities. Significant clinical toxicities to anti-angiogenic drug therapies have been observed and include: gastro-intestinal perforation, hypertension and reduced left ventricle ejection fraction (LVEF), thyroid disturbances and fatigue, kidney damage, sever bleeding, skin toxicities, and disturbed

wound healing (16; 82). An overview of anti-angiogenic drug therapy-related side effects and some of their underlying causes can be seen in Figure 9 (82).

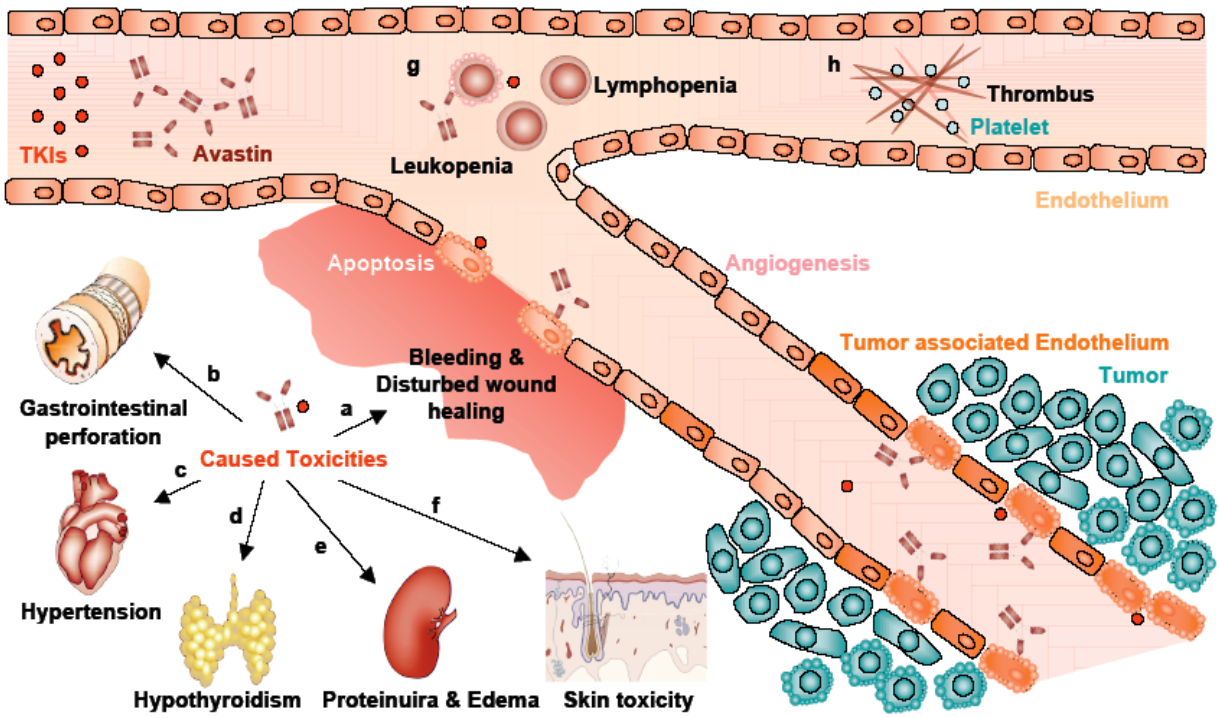


Figure 9 An overview of toxicities which can develop when using anti-angiogenic drug therapy including: bleeding and disturbed wound healing (a); gastrointestinal perforations due to disturbances to the intestinal villous capillaries (b); hypertension and reduced left ventricle ejection fraction (LVEF) (c); disturbances to thyroid gland homeostasis causing hypothyroidism and fatigue (d); kidney damage due to changes in osmotic pressure causing proteinuria and edema (e); skin toxicities due to changes in growth factor signaling cascades (f); leucopenia and lymphopenia (g) and thrombic events due to endothelial cell damage (h) (82).

Another possible drawback of anti-angiogenic drug therapy for cancer treatment is the suggestion by multiple sources that this form of therapy can result in “malignant progression of tumors to increased local invasion and distant metastasis” (83) or “accelerated metastasis” (84; 23). As with the development of resistance to this form of therapy, the relationship between anti-angiogenic drugs and metastasis is not well understood and is still a central point of debate.

Paez-Ribes et al. (83) reported that tumor-bearing RIP1-Tag2 mice with pancreatic neuroendocrine tumors (PNET) treated for 5 weeks with the anti-angiogenic drug Sutent® showed an increased in life span (median survival of an additional 7 weeks) and marked decrease in tumor burden (>75% compared to control). They also reported that smaller tumors treated with Sutent® began to develop an invasive phenotype with tumor cells which invaded

surrounding tissues. This, however, was accompanied by no significant increase in lymphatic metastasis but an increase in tumor micro-metastases in the liver of the Sutent® treated mice when compared to control mice (23; 83).

Another study by Ebos et al (84) reported that mice treated with short term Sutent® therapy (120 mg/kg/day) for 7 consecutive days, either directly before or after intravenous tumor implantation, showed accelerated tumor metastasis and reduced survival when compared to control mice who received a dose of Sutent® which was considered the minimum effective tumor-inhibiting dose (continuously administering 40-60 mg/kg/day), as determined by a previous preclinical study (85).

On the other hand, clinical data from more than 10,000 patients treated with anti-VEGF therapy reported that "it is unlikely that VEGF-targeted therapy accelerates metastasis" (23; 86). In addition, many sources have suggested that anti-angiogenic therapy may in fact help to prevent tumor metastasis, as it is believed that the process of metastasis is angiogenesis-dependent and may also be inhibited by anti-angiogenic drug therapy (87).

## Anti-angiogenic drugs

### *Avastin®*

Avastin® is a recombinant humanized monoclonal anti-body which specifically targets the VEGF-A isoform of vascular endothelial growth factor. It effective binds and neutralizes human VEGF, preventing it from binding with its target receptors, VEGFR-1 and 2. Avastin® is composed of a full length, 149 kDa, antibody derived from an anti-VEGF mouse monoclonal antibody. It is metabolized and eliminated by the reticuloendothelial system and has no active or inactive metabolites (88).

As previously discussed, Avastin® is not clinically-approved for the treatment of AMD, but is frequently used 'off-label' for this indication in a dose of 1.25 mg (89). Avastin® is the first clinically-approved angiogenesis inhibitor and was originally approved as a first-line treatment for patients with advanced, metastatic, colorectal cancer, preferably in combination with fluoropyrimidine-based chemotherapy (90). In 2008, it was also approved for the treatment of unresectable, advanced metastatic or recurrent non-squamous non-small cell lung cancer (NSCLC) in combination with paclitaxel/carboplatin, and has received conditional approval for the treatment of breast cancer and glioblastoma multiforme (88; 91; 71).

For cancer treatment, Avastin® is administered intravenously in a dose ranging from 1 to 10 mg/kg every two weeks. Avastin® is predominantly used in combination with chemotherapy, because it has been shown to increase the efficiency of treatment and improve progression free survival and response (90; 92; 93). It is hypothesized that by blocking VEGF signaling, Avastin® may help to transiently decrease blood vessel leakage in tumors, reducing VEGF-induced hemorrhaging and edema and the physiological effect of the tumor burden (71). This is believed to improve blood flow, increasing the bioavailability of chemotherapeutics in the tumor microenvironment, resulting in increased beneficial effects from chemotherapy treatment (71).

A phase II clinical trial performed by Yang et al. studied the effects of Avastin® therapy on 116 patients with treatment-refractory metastatic clear-cell renal cell carcinoma (RCC). Patients were either treated with a placebo, low-dose (3 mg/kg) or high-dose (10 mg/kg) Avastin® administered intravenously every 2 weeks (94). The high-dose treatment group showed significantly longer time to progression when compared to the placebo treatment group (4.8 vs. 2.5 months). No life-threatening toxicities or deaths were reported. The high-dose treatment group showed side effects including: hypertension of any grade (36%) and grade 3 hypertension (21%, not controlled by one standard medication) and asymptomatic proteinuria with no renal insufficiency (64%). All these side effects were reversible after treatment was stopped. Grade 1 and 2 haemoptysis was also seen in 2 patients in the Avastin® treatment group and in 2 patients in the placebo treatment group, no thromboembolic events were reported (94; 22).

### *Sutent®*

Sutent® is a broad spectrum, small-molecule RTKI which targets VEGFR (particularly VEGFR-2) and other RTKs including PDGF and c-kit receptors (22; 95). Being a broad spectrum or multiple target RTKI, Sutent® interacts with a variety of other RTKs having potential 'off-target' effects which may be at the origin of some of the side effects and toxicities associated with Sutent® therapy. It has been speculated that Sutent® may have an additional direct inhibitory effect on tumor cells by inhibiting one or more of their RTKs (96). Due to the fact that Sutent® primarily targets tumor vasculature, treatment may have additional effects on drug delivery to the tumor mass and result in sensitivity of specific vessels to the drug (96).

Sutent® can be administered orally, frequently in a salt form referred to as sunitinib malate, due to the fact that it is a small molecule (molecular weight of 532 Da) which is mostly hydrophobic. These characteristics make Sutent® capable of passing through cell membranes where it can directly interact with the intracellular domain of receptors and intracellular signaling molecules

(16). Sutent®'s bioavailability is not entirely understood, although it is known that its absorption occurs slowly and a steady-state concentration can only be achieved after 10-14 daily doses (97). Pharmacokinetic studies on animals have shown that at steady state, a minimum plasma concentration between 50 and 100 ng/ml of Sutent® and its primary metabolite (SU212662) are needed for pharmacological activity (98). The main route of elimination of Sutent® from the body is through fecal excretion (99; 16; 75).

Sutent® is an anti-angiogenic and anti-cancer drug, and, as such, is approved for the treatment of multiple forms of cancer. Sutent® was clinically approved for the treatment of RCC and imatinib-resistant gastrointestinal stromal tumor (GIST) in 2006 (100; 101). More recently, in 2010, the European Commission approved the use of Sutent® for the treatment of 'unresectable or metastatic, well-differentiated pancreatic neuroendocrine tumors with disease progression in adults' (102). A phase III clinical study on metastatic RCC showed that Sutent® monotherapy was a more effective treatment option than interferon alpha immune therapy, which is the first line of therapy for RCC which is chemotherapy resistant (103).Typical treatment regiments for cancer patients includes oral administration of Sutent® in 12.5, 25 or 50 mg daily doses, on a 6-week treatment cycle of 4-weeks on and 2-weeks off (100; 101). A study by Minkin et al. was aimed at developing a method to quantify the Sutent® plasma concentrations in patients treated with 25 mg/day on the 6-week cycle mentioned above. After 4 weeks of treatment, the steady state minimum concentration in these patients was reported to be 32 ng/ml (falling within the range predicted by the animal study discussed in the paragraph above) (104).

In clinical trials, many patients develop a resistance to Sutent® therapy and it has become evident that this may be a limitation of Sutent® therapy. Most patients experience at least transient benefits from treatment; however, a small percent experience no benefits. A study by McDermott et al. examining the effects of Sutent® therapy on 637 tumor cells lines showed that only two of the lines were highly sensitive to Sutent® at 1 μM due to activated PDGFRα signaling, indicating that the other lines had already developed a resistance to the drug (105).

Advanced in reversing drug resistance, however, are possible as the Researchers at the Van Andel Research Institute (VARI) studying the effects of Sutent® and its mechanism of action may have identified a way to reverse Sutent® resistance in clear cell RCC tumors. They found that these tumor cells are capable of developing Sutent® resistance through increased secretion of the protein interleukin-8 (IL-8), and that when Sutent® is administering in combination with IL-8 neutralizing antibodies, the tumors cells were resensitized to Sutent® therapy (106).

In addition to being approved for the treatment of RCC and GIST, Sutent® has also been investigated in Phase II clinical trials for the treatment of breast cancer, non-small cell lung cancer, and neuroendocrine tumors. A summary of selected Sutent® clinical trials adapted from a review published by Adams et al. can be seen in Figure 10 (75). These studies show the large therapeutic potential of an anti-angiogenic RTKI, such as Sutent®, in the treatment of a variety of different forms of cancer.

Enough evidence has supported the theory that anti-angiogenic drug therapy can provide a novel and effective form of therapy for cancer that it has become a standard form of therapy and is considered the fourth modality of cancer treatment after surgery, chemo- and radiation-therapy (23).

| First Author | Patients Treated | Sutent® Regiment | Patient Response |
|---|---|---|---|
| **Motzer et al. (95)** | Cytokine-resistant mRCC | 50 mg/d, 4 wk on, 2 wk off | PR, 40%; SD ≥ 3 mo, 27% |
| **Rini et al. (145)** | Bevacizumab-resistant mRCC | 50 mg/d, 4 wk on, 2 wk off | PR, 16%; SD, 61%; reduction in tumor size 56% |
| **George et al. (150)** | Imatinib-resistant GIST | 37.5 mg/d, continuous dosing | SD in 13/17 (2 unconfirmed PRs) at ≥ 12 wk |
| **Morgan et al. (148)** | Imatinib-resistant GIST (before approval) | 50 mg/d, 4 wk on, 2 wk off | CR, 0.7%; PR, 14%; SD, 63% |
| **Sociniski et al. (149)** | Second- or third-line treatment of NSCLC | 50 mg/d, 4 wk on, 2 wk off | Preliminary analysis: PR, 9.5%; SD at ≥ 8 wk, 42.9% |
| **Miller et al. (147)** | Metastatic breast cancer that has failed to respond to anthracycline and taxane | 50 mg/d, 4 wk on, 2 wk off | PR, 14%; SD at ≥ 6 mo, 2% |
| | | | |
| mRCC - metastatic renal cell carcinoma | | NSCLC - non-small cell lung cancer | |
| PR - partial response | SD - stable disease | CR - complete response | |

**Figure 10 Summary of clinical trials investigating the use of Sutent® in the treatment of various forms of cancer (75).**

## Photodynamic therapy

The concept of using light as a form of therapy has existed since antiquity. Many ancient civilizations such as the Egyptians, Indians and Greeks performed a type of photodynamic therapy using natural photosensitizers found in psolaren-containing plants and sunlight to treat skin disorders such as psoriasis and vitiligo (107).

Modern PDT utilizes a photosensitizing agent, most often a porphyrin-based compound, and light in the visual or near-infrared wavelengths. These photosensitizers (PSs) are activated when irradiated by light allowing them to react with oxygen in the environment creating highly reactive, short-lived singlet oxygen and reactive oxygen radicals, which causes local damage to the vascular endothelium and eventually results in vessel occlusion (65). Clinical applications, advantages and limitations of this therapy will be discussed before its mechanism of action and vascular effects are described in more depth.

### Clinical applications

In addition to being used in the treatment of AMD, PDT is frequently used in the treatment of early stage cancer with good results and is considered an efficacious, simple, minimally invasive, repeatable form of therapy (40). PDT is used in the treatment of head and neck tumors (108), breast cancer (109), brain tumors (110), gynecological tumors (111), non-small cell lung cancer (112), bladder carcinoma (113), esophageal and skin cancers (including basal cell carcinoma (BCC) (114) and Bowen's disease) (115; 116; 117). PDT is also extensively used in the treatment of dermatological disorders including, but not limited to: acne vulgaris, photo rejuvenation, psoriasis, cutaneous lymphoma, viral warts and scleroderma (116).

A multicenter study of a large number of patients with five-year follow up found that PDT treatment of patients suffering from BCC showed a success rate of approximately 95% in superficial BCC and 73-94% in nodular BCC (114). The recurrence rate of the superficial BCC was 22% (compared to 19% for other common forms of therapy) and 14% for nodular BCC (compared to 4% for other treatment forms which mainly include surgery) (114; 116)

### Advantages and limitations

PDT can provide therapeutic benefits for many forms of cancer, skin disorders and AMD. The use of PDT in the treatment of cancer is advantageous over other forms of therapy (surgery, chemotherapy or radiation-therapy) due to the fact that it is relatively non-invasive, results in selective tissue damage and can be used to treat more than one lesion at a time (116). PDT results in relatively limited damage to healthy tissue (due to both selective localization of the PS

and localized irradiation), uses non-ionizing radiation and allows for relatively rapid recovery (116). In addition, PDT can be used in combination with other therapies (such as anti-angiogenic drug therapies or chemotherapies) in hopes of achieving synergistic effects.

Although PDT is relatively non-invasive, it can still result in some side effects. These can include: burns, swelling, pain and scarring of nearby tissues; skin and eye sensitivity to light; stenosis, and perforation of hollow organs (115). In addition it has also been reported to result in DNA damage including strand breaks, alkali-labile sites, DNA degradation and DNA-protein cross links, and possibly causes chromosomal aberrations, such as sister chromatid exchanges and mutations (65). Other shortcomings of PDT include the limitation of treatment depth due to the penetration of light. Activation of PS is necessary in order to initiate the cytotoxic activity of PDT, which limits treatment to lesions which are mainly superficial and can be directly illuminated or are reachable by an endoscope for illumination, such as skin and hollow organ cancers. In general, the penetration depth in tissue of the visible or IR light used in PDT ranges from several mm to a 1 cm (116).

In addition to being limited by the penetration depth of light, PDT can also be limited by the revascularization of treated areas. PDT results in damage to the vascular endothelium, which causes increased vascular permeability as well as platelet aggregation, blood flow stasis, vasoconstriction and eventually vascular occlusion. This vascular damage induces inflammation and hypoxia, which in turn results in the activation of hypoxia inducible factors (HIF) and the expression of angiogenic and survival molecules, including VEGF (43). The activation of angiogenesis results in the revascularization of treated area, which is frequently accompanied by disease progression and the return of disease symptoms. A major limitation of PDT, therefore, is that its effects can be transient and re-treatment is frequently necessary.

### Mechanism of action

The mechanism of action of PDT is dependent on three requirements: the localization of the PS in the malignant tissue resulting is selective tissue damage; the activation of the PS by light, followed by a series of energy transfers leading to the creation of reactive singlet oxygen molecules, and vascular and cellular damage induced by the singlet oxygen molecules leading to endothelial cell damage, blood flow stasis, and vascular occlusion. Each of these elements will be discussed in more depth in the following sections.

### *PS selective uptake and retention*

The ‘selectivity’ of PDT depends on many factors including the drug, the drug carrier, the application of light, and the tissue properties (40). The first step to achieving selective tissue damage is to have selective PS uptake in the target tissue. In the case of AMD and cancer, increased permeability and leakiness of blood vessels can result in increased PS delivery. In addition, tumors may have increased expression of low density lipoprotein (LDL) and receptors such as albumin. This can increase delivery of hydrophobic PSs, which can be bound in a lipid core of lipoproteins, or hydrophilic PSs which can be transported by albumin. In addition, advanced cancers tend to have decreased lymphatic drainage and low pH environments, which can cause a decrease in the solubility of some porphyrins (40).

Following selective uptake of the PS, selective retention is needed in order to localize tissue damage. Selective retention can be achieved through properties which are specific to the diseased tissue or through chemical manipulations, such as a PS which is targeted to a certain receptor selectively expressed on tumor cells or tumor endothelium (40).

Due to its importance in regards to this research, the specific case of PDT treatment of the CNVs which develop in AMD will be addressed in more depth. A schematic of the macular region of the retina is shown in Figure 11 (40). The first layer of nerves below the macula consists of the photoreceptors, which are activated by light from above. Activated photoreceptors send a signal to the bipolar, horizontal, amacrine and ganglion cells for preprocessing before this signal is sent to the brain through to optic nerve. The retinal pigment epithelium (RPE) is a layer of ‘macro-phage-like’, highly pigmented cells, which are located below the photoreceptors. Blood flow in the eye is supplied by the following vascular networks (shown in Figure 11, from top to bottom) (40). The retina is supplied with blood from the retinal arteries and veins (labeled RV in the figure), which flows into the retinal capillary network (Ret Cap) around the macula (the macula itself has no vascular network because this would impair vision). The Bruch’s membrane is located below the RPE and receives its blood supply from the choroidal capillaries (Ch Cap) which are fed by the larger choroidal vessels (CV).

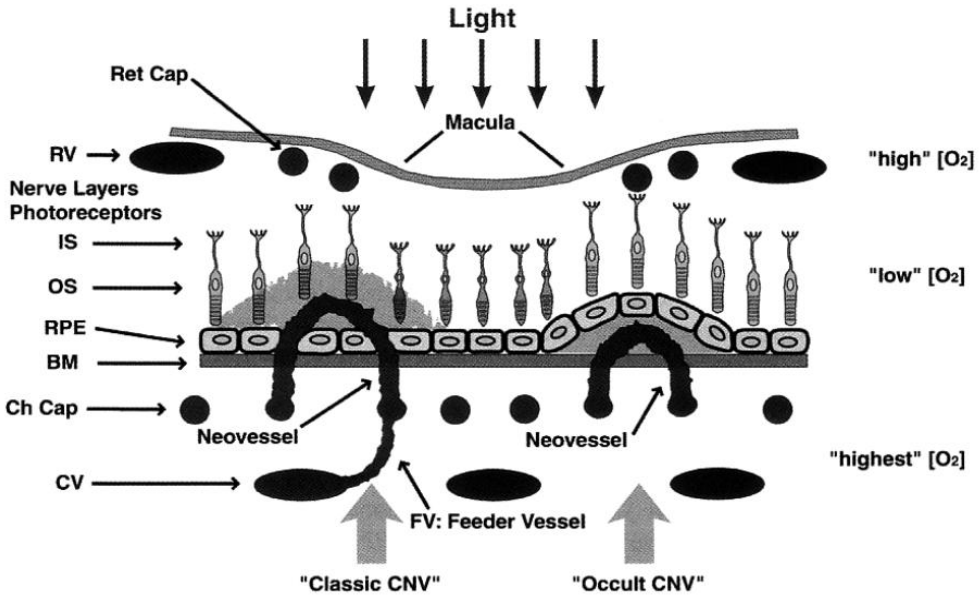


Figure 11 An overview of structure located in the macular region of the retina in eye (40).

Closure of blood vessels in the retina must be very selective, because closure of the wrong vessels could result in vision loss. In particular, closure of the retinal capillaries must be avoided (40). This can partially be avoided due to a lower partial pressure of oxygen in the retinal circulation compared to the choroidal circulation and oxygen gradients created by heterogeneous oxygen supply and consumption across the retina (40). Cellular damage is also mostly localized to the vasculature due to limited leakage of PSs into surrounding tissue when light is applied relatively quickly following PS injection. Limited PS leakage results in limited damage to photoreceptors and the RPE. Limiting damage to blood vessels, however, is not enough, because selective close of the malignant CNVs is desired without closure of the choriocapillaries or larger choroidal vessels (40). This is partially achieved due to the fact that the larger choroidal vessels have a significantly higher amount of collagen in the vessel walls, which may provide some degree of vascular protection (40). Additionally, the malignant vessels may have higher expression of LDL and albumin receptors, resulting in increased uptake of PSs. This selectivity, however, is not completely achieved as significant closure of choriocapillaries is seen even up to one week after PDT-treatment (as can be seen in the non-fluorescent part of the image shown in Figure 20) (40).

### *PS excitation and energy transfer*

Following the localization of the PS, it must be irradiated by the proper wavelength of light in order to be activated to its excited state (PS*). In order to become excited, the PSs must absorb

energy from light in the form of photons. An absorption spectrum describes the probability that light will be absorption as a function of wavelength for a given molecule or the probability that an incident photon will induce an energy level change (40). The absorption spectrum for Visudyne®, the PS used in these experiments and in the treatment of AMD, can be seen in Figure 17 (118).

Following excitation due to the absorption of a photon, the PS undergoes a series of energy transfers, which finally result in the production of a reactive singlet oxygen molecule. These energy transfers can be described using a Jablonski diagram, which shows the different energy levels of an electron and describes the possible transitions between them. A typical Jablonski diagram can be seen in Figure 12 (119). When a photon is absorbed by the PS, it becomes excited by making an energy transition from the ground singlet state ($S_0$) to a vibrationally excited level of the singlet excited state ($S_1$). The process of absorption is extremely fast, taking only $10^{-15}$ seconds. The excited PS (PS*) then undergoes internal conversion (IC) (taking ~$10^{-12}$ seconds), to the 'ground' $S_1$ state, from which a variety of different energy transfers can take place. In order for PDT to result in cellular damage, the PS* must then undergo intersystem crossing (ISC), a non-radiative change between electronic states with different multiplicity (e.g. a transition from $S_1$ to $T_1$, due to the higher energy of $S_1$, the transfer would be to the higher

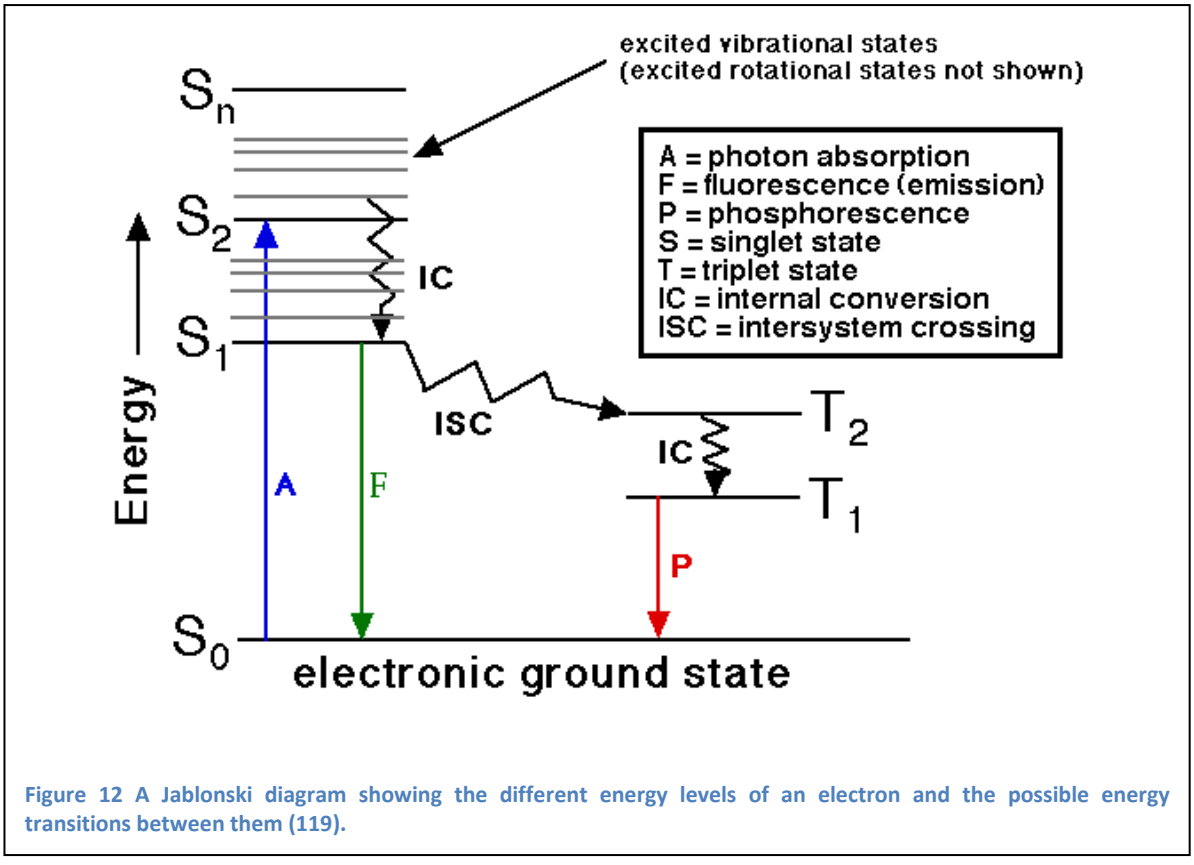


Figure 12 A Jablonski diagram showing the different energy levels of an electron and the possible energy transitions between them (119).

energy state of $T_1$ and would relax to ground state through IC). After undergoing ISC, the $T_1$ state PS can transfer its energy through a chemical reaction (e.g. $S_1$ chemical reaction by rearranging itself, connecting to another molecule or disassociating), exchange energy with a nearby molecule causing it to become excited to the singlet state, or it can relax through internal conversion to return to the $S_0$ state (40). In the situation of PDT, the triplet state PS will react chemically with molecules in the environment to generate reactive singlet oxygen.

There are three main pathways through which the triple PS can chemically react, as shown in Figure 13 (40). The first pathway (referred to as type II reactions) is an energy transfer to an oxygen molecule or to a substrate molecule. An energy transfer to ground state oxygen generates a singlet molecular oxygen, which can then react with the PS (bleaching it) or oxidize a nearby biomolecular target. The second pathway is a hydrogen atom exchange between the PS and a substrate molecule which can react with $O_2$, forming peroxide radicals as intermediary molecules in the process of oxidizing the substrate molecule. The final pathways is an electron transfer between the PS and a substrate molecule, generating radical ions which, in combination with $O_2$, can cause other oxidizing reactive intermediates, such as superoxide radical anion, $H_2O_2$, or hydroxyl radicals which are highly reactive. The second and third

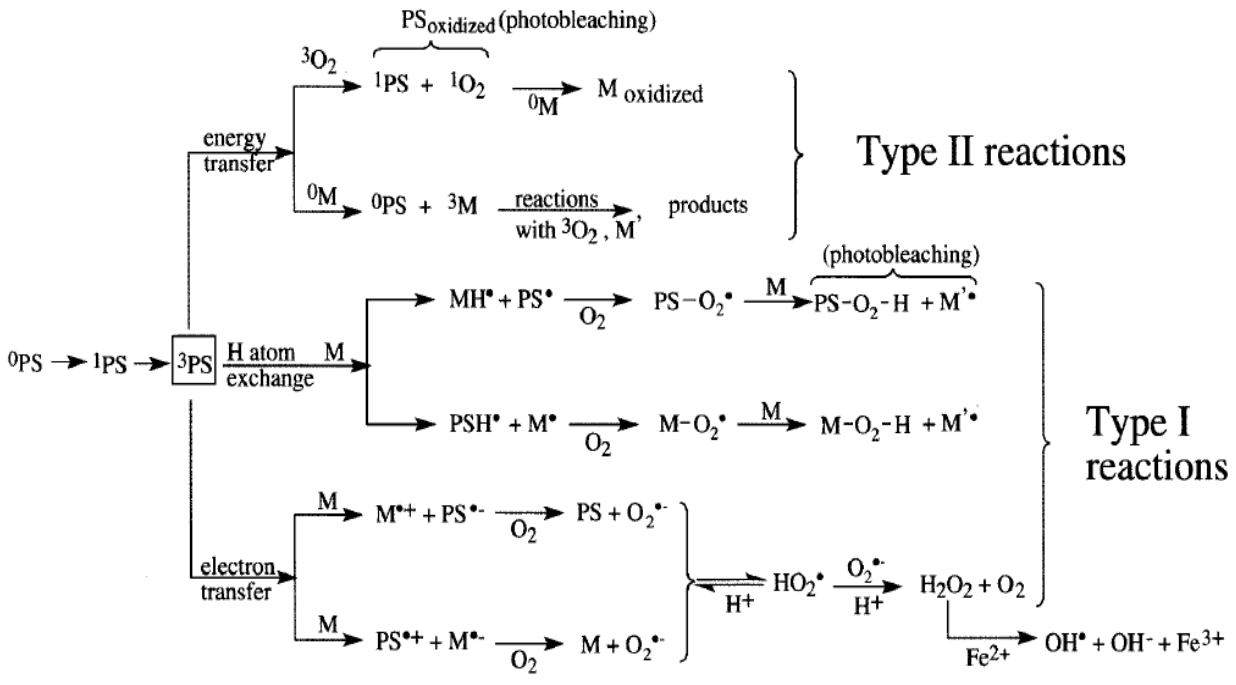


**Figure 13 Overview of the photo-oxidative reactions available to the triplet state photosensitizer ($^3$PS) which result in the generation of a sensitized biological substrate molecule (M) (40).**

pathways are known as type I reactions. Type II reactions require oxygen in the first step, while type I reaction require oxygen farther down in the chain of energy transfers. The photosensitizer Visudyne® primarily interacts through type two reaction. The singlet oxygen which is generated can react with proteins, lipids and nucleic acids to create free radicals leading to auto-oxidation and breakdown of these molecules (120). Vascular damage is highly localized due to the fact that singlet oxygen is highly reactive, and will either react very quickly or be quenched, so that distant reactions are only a fraction of nanometers away from the PS (40).

### *Cellular effects*

Following the activation of the PSs and the generation of reactive singlet oxygen molecules, these molecules can cause tissue damage through cellular, vascular and immunological effects (40). Tissue damage depends on the tissue, the sensitizer and the conditions of PDT applied (i.e. time between drug and light application, the drug delivery system which affects the localization of the PSs during therapy, and factors such as the quantity of drug or light applied).

PSs mainly target endothelial cells through either the mitochondria (for BPD-MA based PSs including Visudyne®) or through the lysosome and plasma membrane causing cell death through necrosis or apoptosis (40). Water soluble PSs, which localize in the lysosomes, normally cause cell death through necrosis and apoptosis due to the release of cathepsins and caspase 3. Mitochondrially-localized PS's, however, mainly cause cell death through apoptosis. It is generally more desirable to induce vascular damage through apoptosis than through necrosis, because it requires lower drug and light doses and may be easier to manipulate than necrotic cell death, allowing for more selective tissue damage (40).

PDT causes peroxidation in organelles where the PS has accumulated, which can result in organelle membrane disruption, changes in membrane potential or damage to membrane proteins (40). Cells partially damaged by PDT will activate rescue responses including the release of heat shock proteins, glucose-regulated proteins and heme oxygenase (40; 121). PDT can also affect cell surface receptors inducing the release of cytokines, which may have additional effects on the immune response (40).

Mitochondrially-localized PSs, such as the one used in the experiments for this study, Visudyne®, mainly cause cell death through apoptosis. An overview of the interactions which result in apoptosis can be seen in Figure 14 (40). Overall, it is believed that these PSs are capable of inducing the loss of mitochondrial membrane potential by opening a large conductance channel called the mitochondrial permeability transition pore complex (PTPC) (40).

This may result in the release of cytochrome-c into the cytosol, where it can react with apoptosis-activating factor-1 (APAF-1) and ATP to form a multi-protein complex called an apoptosome (122). This complex activates caspase 9, which activates caspase 3, which in turn activates caspase 6. Caspase 3 cleaves proteins involved in repairing damaged DNA (poly-ADP-ribose polymerase and DNA-PK) as well as activating a molecule (CAD) known to cause DNA damage. Caspase 6 cleaves the lamins of the cell's nucleus causing nuclear breakdown and interacts with other molecules know to be involved in apoptosis such as SHREBs, Gelsolin, caspase 7, caspase 9, MDM2, GAS2, Fodrin, FAK and more (40).

Another mechanism of apoptosis is through the activation of the cell surface "death receptors" such as TRAIL (TNF-related apoptosis-inducing ligand), FAS and TNFR1 (tumor necrosis factor receptor 1) (40). In this pathway, also shown in Figure 14, activation of these receptors will result in adopter proteins such as FADD (FAS associated death domain) to bind to other proteins in the cytosol. The complex they create induces the release of caspase 8, which causes the release of caspase 3, and cleaves Bid to create truncated Bid (t-Bid), which moves to the mitochondrial membrane to help release cytochrome-c. Cytochrome-c is also involved in apoptosis through indirect interactions with the caspases mentioned above (40; 122; 123; 124).

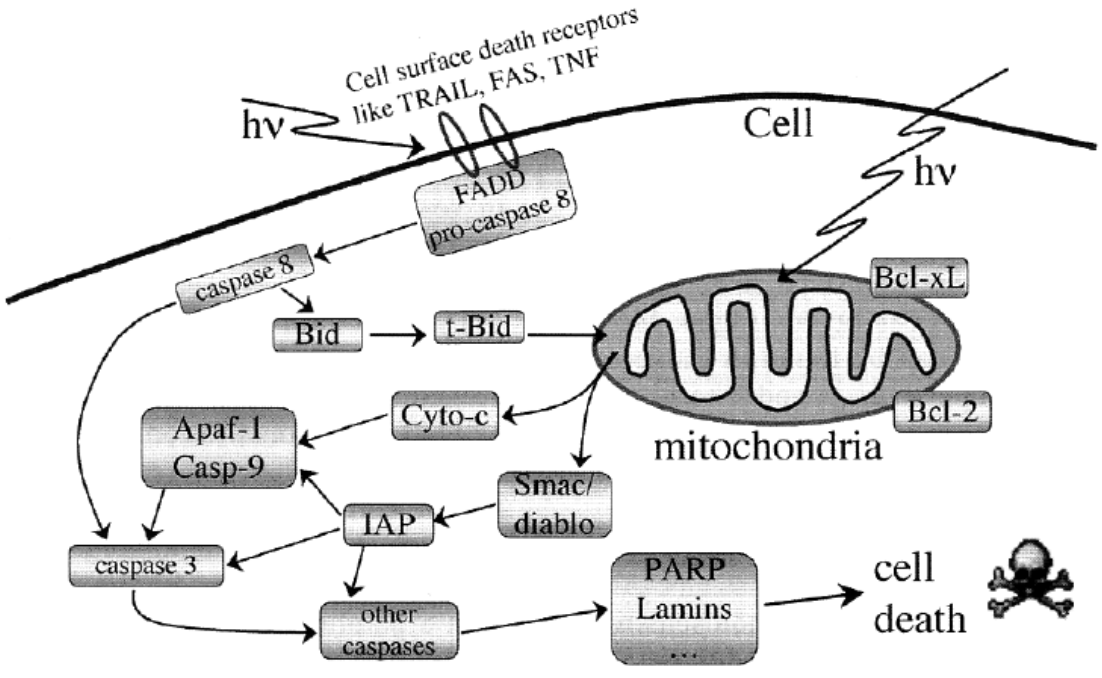


**Figure 14 An overview of the cellular pathways which result in cell death through apoptosis, the mechanism of cell death mainly achieved by mitochondrially-localized photosensitizers such as Visudyne® (40).**

### *PDT-induced vascular effects*

In certain indication, including the treatment of AMD, the main aim of PDT-treatment is to induce vascular damage. In the context of this study, it is therefore also important to examine the vascular effects of PDT. Predominantly vascular effects of PDT can be achieved by specifically selecting the conditions and PS used to perform PDT. The first visible vascular effect of PDT is vasoconstriction, which can be seen immediately following the application of light and up to several hours follow treatment (40). Early damage following PS injection and illumination has mostly been observed in the endothelial and sub-endothelial cells. Early changes to endothelial cells can be seen in the luminal surface, cytoplasmic microtubules, cytoskeletal proteins, and mitochondria. These changes cause the endothelial cells to retract, losing their tight junctions with neighbor cells and exposing the basement membrane. An overview of the vascular effects of PDT can be seen in Figure 15 (40). This figure shows the healthy vessel wall (a), the endothelial cells which have retracted following PDT damage (b), and the activation of platelets and polymorphonuclear leukocytes due to exposure of the basement membrane, which increase the release of eicosanoids, resulting in platelet aggregation on the basement membrane of the vessel (c) (40).

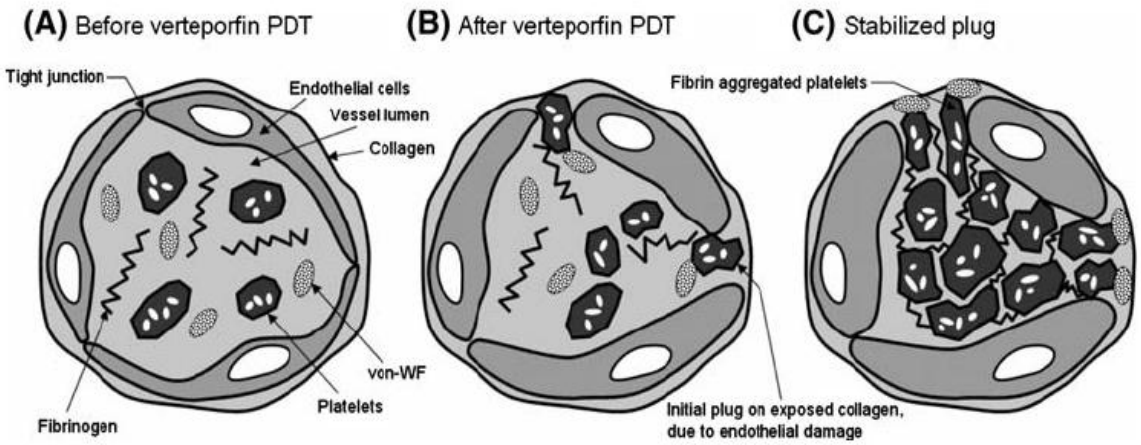


Figure 15 Overview of the mechanism by which PDT induces vascular damage resulting in blood flow stasis (40).

PDT causes polymorphonuclear leukocytes to attach to vessel walls, which results in a change in the release of biochemicals, such as eicosanoids thromboxane and leukotriene B4 and C4 (40). These factors disturb the balance between aggregation/disaggregation of platelets and vasodilation/vasoconstriction processes in blood vessels. These imbalances are counteracted

by increased smooth muscle activity resulting in vasoconstriction. Platelet aggregation, combined with vasoconstriction, results in the formation of a plug, which is then stabilized by fibrin (Figure 15C). The retraction of endothelial cells and biochemical changes initially causes an increase in vessel permeability and leakage, before finally leading to blood flow stasis and vascular occlusion (40).

Another mechanism leading to vascular occlusion is through PDT damage to membrane lipids. This causes the release of arachidonic acid, which initiates a biochemical cascade ending in the release of thromboxane, a vasoconstrictor. This, in addition to increased interstitial pressure due to increase vascular leakage, also contributes to blood flow stasis and vascular occlusion (40).

## Visudyne®

Visudyne® (Verteporfin for injection; Benzoporphyrin Derivative Monoacid Ring A (BPD-MA); Novartis AG), is the photosensitive molecule clinically used in the treatment of AMD and other eye disorders including pathological myopia, and presumed ocular histoplasmosis (69). Visudyne® is composed of a semisynthetic mixture of two porphyrin regioisomers shown in Figure 16 (120; 65).

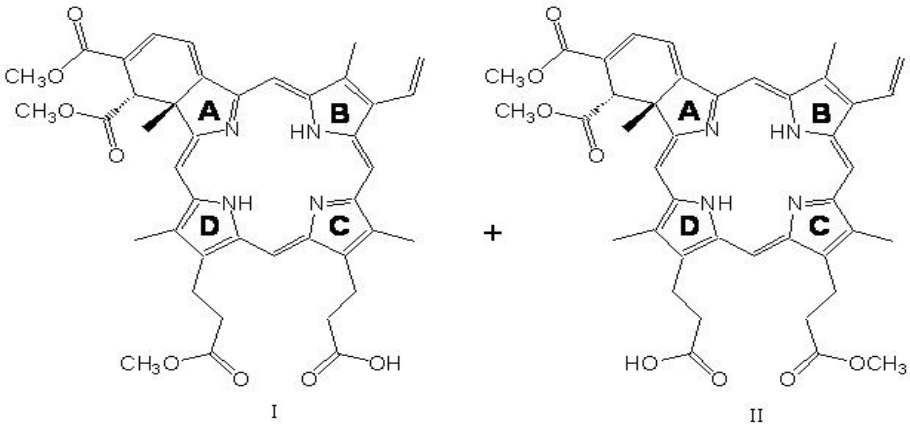


Figure 16 The chemical structure of the two isomers which make up Visudyne® (65).

The quantum yield for the production of singlet oxygen by Visudyne® is 0.76 in methanol (125) (meaning that approximately 8 out of 10 photons absorbed by Visudyne® result in the production of a singlet oxygen molecule). Approximated 500,000 singlet oxygen molecules can be produced by a Visudyne® molecule in one second (120). Desirable qualities for a PS include a

high quantum yield and a long-lived triplet state (40). The absorption spectrum of Visudyne® in ethanol and oxyhemoglobin in phosphate buffered saline is presented in Figure 17. Visudyne® has two absorption peaks, the Soret band at 420 nm and the Q-band at 689 nm. In clinical applications, the absorption peak at 689 nm is used to excite Visudyne® due to the increased penetration depth of red light and its decreased interaction with endogenous molecules. If the 420 nm absorption peak were used, oxyhemoglobin would have a strong interference with the excitation of Visudyne® as it has a large absorption peak at this wavelength (shown in Figure 17). In addition, the higher excitation peak is located in a range of wavelengths which have been shown to be safer for the retina (120). For the laboratory procedures in this study, however, the 420 nm absorption peak is used to excite Visudyne® molecules.

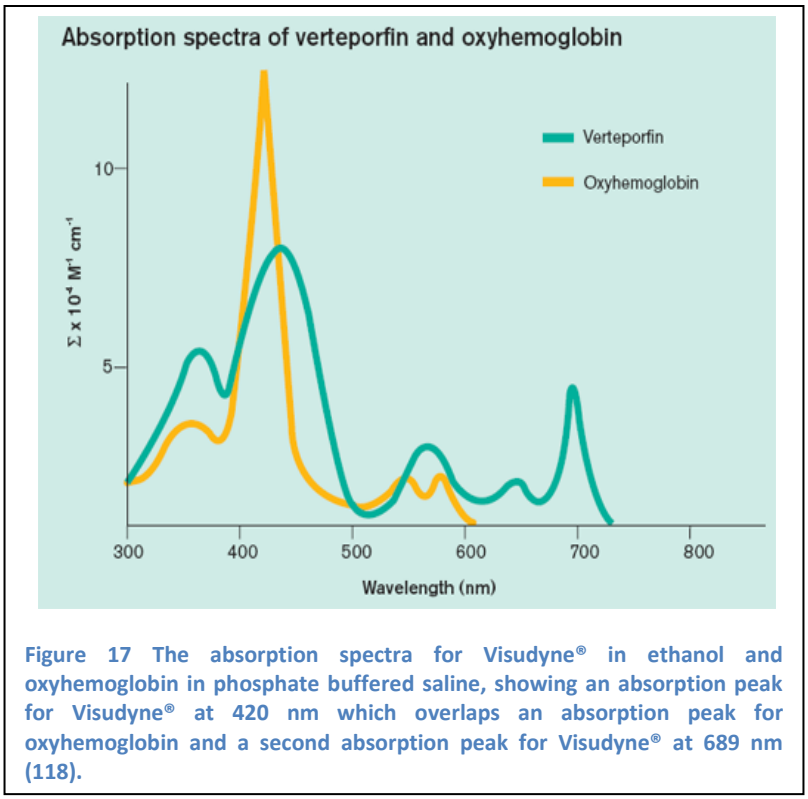


**Figure 17 The absorption spectra for Visudyne® in ethanol and oxyhemoglobin in phosphate buffered saline, showing an absorption peak for Visudyne® at 420 nm which overlaps an absorption peak for oxyhemoglobin and a second absorption peak for Visudyne® at 689 nm (118).**

After being intravenously administered, Visudyne® is primarily transported in the plasma by lipoproteins and exhibits a bi-exponential elimination, with a terminal elimination half-life of approximately 5-6 hours (65). Visudyne® is metabolized by human liver S9 and human liver microsomes into a 'diacid' metabolite (120). Exposure and maximal plasma concentration are proportional to the administered dose and range between 6 and 20 mg/m$^2$ (65). The primary route of Visudyne® excretion is through the bile and feces, due to its being a highly lipophilic molecule with a high molecular weight (120). The safety and efficacy of this drug has only been

demonstrated for a 2 year period following treatment. Common side effects and complications include: light sensitivity; severe decrease of vision (≥4 lines) within 1 week, and extravastion of Visudyne® at the injection site causing pain, inflammation, swelling and discoloration (65).

## Comparative study of PDT and anti-angiogenic treatment of AMD

A study was conducted by Brown et al. to compare the effects of treating AMD with PDT or anti-angiogenic drug monotherapies (126). Patients primarily suffered from classic, subfoveal CNVs and had not been previously treated with either form of therapy. Treatment was administered to three randomized groups receiving either: Visudyne®-PDT plus a fake intravitreal injection or non-active PDT plus monthly intravitreal injection of Lucentis® at a low- or high-dose (0.3 mg or 0.5 mg) (423 patients total, 143 PDT, 140 in each of the 2 Lucentis® groups). The need for repeat PDT treatment (real or non-active) was examined every 3 months using fluorescein angiography.

The effects of treatment were examined from months 12 through 24 in terms of the percentage of patients losing <15 letters from baseline visual acuity (12 month primary efficacy outcome measure), percentage gaining ≥15 letters from baseline, mean change over time in visual acuity scores and lesion characteristics monitored through fluorescein angiography.

The results at 12 and 24 months showed an increase in visual acuity for the Lucentis®-treated group which was statistically significant and clinically meaningful when compared to PDT-treated patients: approximately 90.0% of Lucentis®-treated patients had lost <15 letters from baseline compared to 65.7% of PDT-treated patients; 34% to 41.0% had gained ≥15 letters compared to 6.3% of PDT-treated patients; and, on average, visual acuity was improved from baseline by 8.1 to 10.7 letters compared to a mean decline of 9.8 letters in PDT-treated group) (126). In addition, the Lucentis®-treated group showed favorable changes in the anatomic characteristic of the lesion compared to the PDT-treated group. Overall, both treatment groups showed the same rate of serious ocular and nonocular adverse events (126).

## Clinical study on combination therapy for the treatment of AMD

Due to the fact that PDT is frequently accompanied by revascularization of the treated area resulting in limited treatment benefits, the use of anti-angiogenic drug therapy in combination with PDT has become a popular idea for improving the efficiency of therapy. One particular study examining the benefits of combination therapy is described below.

The study was conducted to assess the outcome of patients with AMD treated with combination Visudyne®-PDT and Avastin® anti-angiogenic drug therapy (127). The study included 1196 patients with CNVs due to AMD who received at least one combination treatment of 1.25 mg intravitreal Avastin® within 14 days of Visudyne®-PDT. After the initial combination treatment, patients received an average of 0.6 additional Visudyne®- PDT re-treatments and 2 Avastin® re-treatments over an average period of 15 months.

At the 12 month check point, 82% of patients (578/701) had stable or improved vision (loss of <3 lines or a gain in visual acuity), 36% (255/701) improved by ≥3 lines, and 17% (121/701) improved by ≥6 lines. By 12 months, patients gained an average of approximately 1.2 lines (6 letters) of visual acuity from their baseline. Patients who were treated for the first time gained significantly more visual acuity by month 12 (+8.4 letters) compared with those who had been previously treated (+2.4 letters; $P<0.01$). Most of the serious adverse events (26/30) were considered to be unrelated to any study treatment; however, there were 3 ocular events related to Avastin® alone and 1 ocular event was related to combination Avastin® and PDT treatment. Combination therapy with PDT and Avastin® led to vision benefit for most patients, particularly those who were being treated for the first time. It should also be noted that the need for retreatment was lower than reported for either monotherapy alone (127).

## Chicken Chorioallantoic Membrane (CAM) model

The chicken embryo chorioallantoic membrane (CAM) model is used in the experiments for this study in order to test anti-angiogenic agents alone and in combination with PDT. In recent years, the CAM model has become very popular and is now commonly used in the study of angiogenesis (29). This model provides a natural, *in vivo* environment of angiogenic blood vessels with all the complex host interactions on which angiogenic compounds can be tested (29). The main advantage of this model is its direct exposure to cells, tissues, biomaterial, drugs or other forms of therapy in order to determine their effects on angiogenesis (29).

The CAM is a membrane which forms around the embryo through the fusion of two of the four extraembryonic membranes, the chorion and the allantois, on embryo development day (EDD) 4 (29). It provides some basic physiological functions needed for the embryo to survive including: respiratory functions through the exchange of oxygen and carbon dioxide with the environment; absorbing calcium from the eggshell; providing a reservoir for waste products of the embryo (initially urea then mostly uric acid), and absorption of albumin by the allantois (29). In order to perform these functions, the CAM develops as a highly vascularized membrane in direct contact

with the eggshell. An image of a chicken egg and the CAM can be seen in Figure 18. In the following section, other common angiogenesis models will be discussed and the particular uses and advantages of the CAM model in the study of angiogenesis will be addressed.

**Figure 18 Image of a chicken egg showing the highly vascularized CAM above the embryo.**

## Angiogenesis models

There exist many alternative models, both *in vivo* and *in vitro*, which can be used to study angiogenesis. The process of angiogenesis involves disruption of basement membrane, cell migration, cell proliferation and tube formation, all of which can be examined individually *in vitro*. *In vitro* models can provide a lot of information, but they are limited in their ability to simulate more complicated pathways and interactions involved in biological processes, creating a need for *in vivo* models as well (29).

Some common *in vitro* angiogenesis models include: endothelial cell culture assays, endothelial cell proliferation assays (128), endothelial cell migration assays (chemokinesis and chemotaxis) (129), endothelial cell tube formation assays (130), endothelial apoptosis and viability assays (trypan blue) (131), angiogenesis factor-transfected endothelial cell lines and endothelial cell outgrowth or organ assays (aortic ring assay (132) and chick aortic arch assay (133)).

There also exist many alternative *in vivo a*ngiogenesis models including: transparent chamber models (rabbit ear chamber (134), hamster cheek pouch (135) and dorsal skin chamber (136)),

corneal micropocket assays (rabbit and rodent) (137), and various implants assays (subcutaneous injection using sodium alginate, subcutaneous disc implant made out of polyvinyl foam, matrigel plug (138) and sponge implants (139)).

Each of these models has unique advantages and disadvantages which make them desirable for use in different applications. The CAM model is particularly well suited to the research conducted for this study, because it is an inexpensive *in vivo* model which allows for relatively high throughput testing of multiple drugs at different concentrations. The CAM model combines the advantages of having an *in vivo* system without carrying the costs and regulatory issues normally associated with animal testing. In addition, due to the nature of the CAM model, test substances can be placed directly on the membrane and the effects of treatment can be directly visualized in real time.

### CAM as an angiogenesis model

There exist two variations of the CAM model: the *in ovo* and the *ex ovo* models. These studies were done using the *in ovo* model. In the *in ovo* model, the eggs is left to develop inside of the eggshell and the CAM is accessed by creating a hole in the eggshell, referred to as windowing, and allowing the membrane to drop and develop detached from the eggshell in a certain area (29). This method provides the advantage that it maintains a more physiological environment for the development of the membrane; however, it is limited due to the fact that only a small portion of the CAM is accessible, and there is an increased chance that the membrane may not drop properly, limiting access to the CAM at the time or in the manner desired (29).

The alternative CAM model is the *ex ovo* method where CAM is grow in a shell-less environment by transferring the contents of the eggs to an artificial eggshell container after 72 hours of incubation. This model allows for a greater area of the membrane to be viewed and experimented on, but provides a less physiologic environment for the development of vasculature (29). Embryos which develop in the shell-less environment normally develop to be smaller, when compared to *in ovo* embryos, and frequently die before coming to full term (29).

In addition to the *in ovo* and *ex ovo* models, there are many other variations in the methods used for experimenting on the CAM. These include variations in protocol (when and how long substances are applied and the vehicle used to administer the test substance). In literature, the application of drugs can range anywhere from EDD3 to 15 (29). The CAM vasculature grows rapidly until EDD9, so it is important to apply drugs before this time in order to examine the response of the rapidly-growing or angiogenic CAM. A previous study conducted in this

laboratory identified the ideal time for testing the effects of angiogenic agents on the naturally-developing CAM membrane to be between EDD7 and 9 (140).

Application vehicles used to administer test substances vary greatly and can include: methyl cellulose discs; Elvax™ polymer; matrigel; agarose gels (collagen gel inside parallel nylon meshes); gelatin sponges; filter discs (Millipore discs soaked in the solution); plastic cover slips (Thermanox cover slips onto which the stimulant has been dried); rings composed of silactic, Teflon or glass; flooding the CAM surface; direct inoculation into the cavity of the allantoic vesicle, or direct application of cells and tissues (29).

Common procedures include placing the test substance on the CAM during early development (EDD7 through 10) and examining the reaction after at least 2 days of incubation. Features which are commonly examined after treatment include vessel density, new vessel formation, vessel tortuosity, vessel disorganization, characteristics of vessel branching, and the size, area and number of avascular zones (29).

In addition, the CAM is also particularly well suited for studying the treatment of AMD, due to the fact that both the CAM and the retina are highly vascularized membranes. This can be seen by a study comparing leakage in the CNVs of the human eye to leakage in the small blood vessels of the CAM (40; 141). PS leakage is very important to treatment of AMD, because high levels of leakage can result in damage to areas of the retina which are not being targeted for treatment resulting in vision loss (40). This study showed strong localized leakage of fluorescein in the human eye over time, which is typical of aggressive ‘classical’ CNVs. Similar leakage was seen when the CAM was injected with a different water soluble dye. Images from these experiments can be seen in Figure 19 (40; 141), with images of dye leakage from the human eye shown of the left and the CAM shown on the right (time elapsed after injection increases from top to bottom images) (40; 141). These images show similar leakage properties in the human eye and in the CAM model, indicating similar pharmacokinetics.

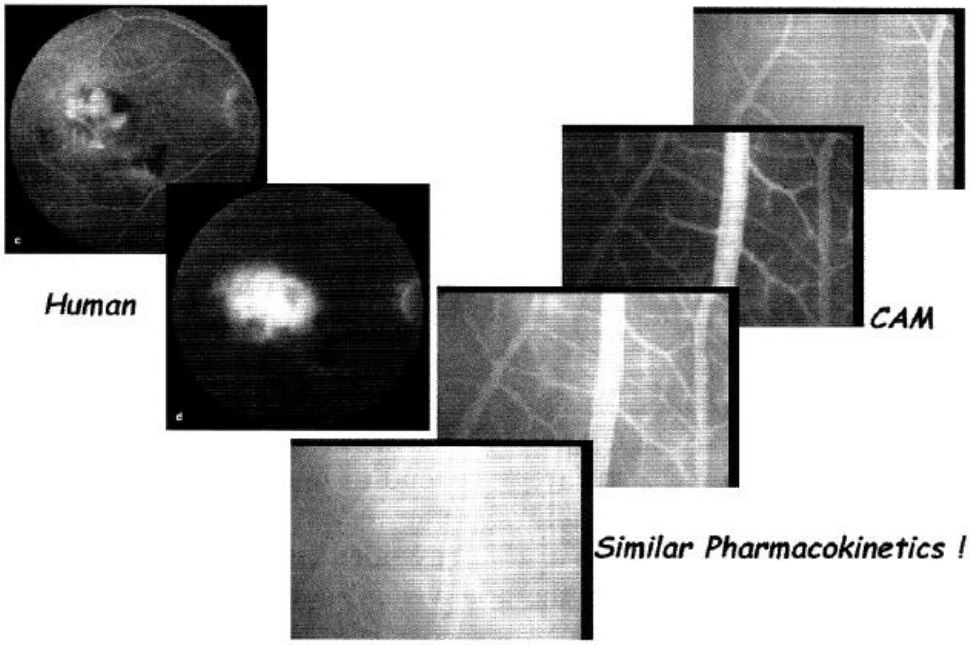


**Figure 19 Leakage of a fluorescent dye from the human eye (on the left) and the CAM vasculature (on the right) used to simulate photosensitizer leakage. Images progress with time from top to bottom, showing similar leakage of dye from the vasculature over time for the two models (40).**

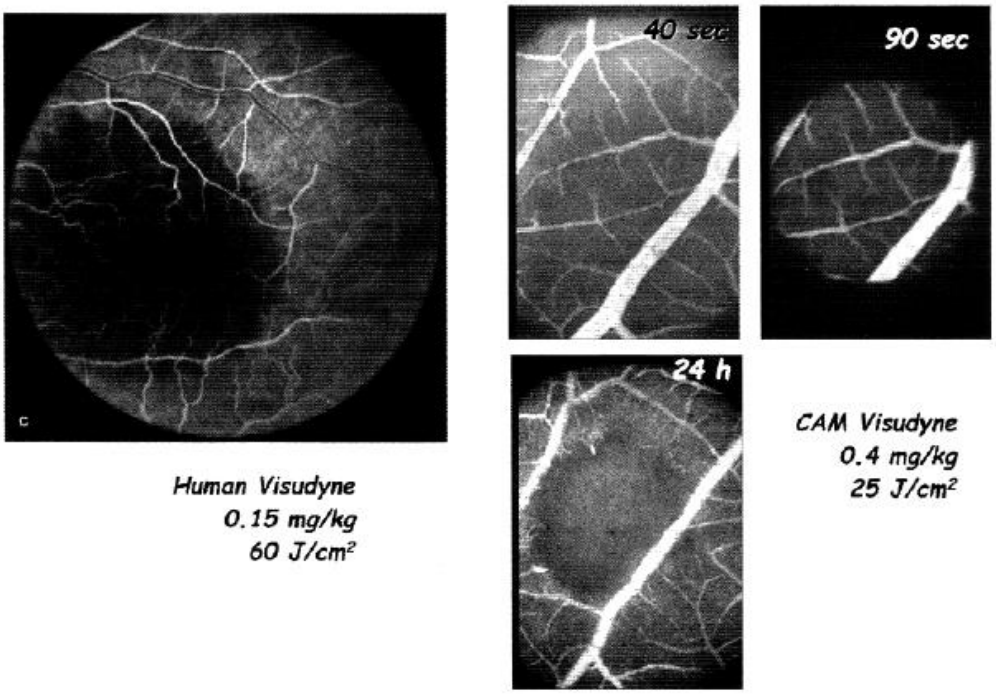


**Figure 20 Efficiency of blood flow stasis and vessel closure in the human eye following PDT (shown on the left) and in the CAM membrane (shown on the right, 40 seconds before PDT, a minute and a half into PDT and 24 hours following PDT) (40).**

Similarly, blood flow stasis efficacy was also compared between the human eye and the CAM one week following Visudyne®-PDT (40; 141). Figure 20 on the left shows images of the human eye one week following Visudyne®-PDT (40). The dark spot in this image shows the macular region where the leakage of the CNVs has been stopped and leakage of the partially closed choriocapillaries has been decreased due to treatment. The images on the right of Figure 20 show the CAM before, during and 24 hours following Visudyne®-PDT (40). These images show a dark spot on the CAM which is similar to the one seen following the clinical treatment of the human eye, indicating similar blood flow stasis in irradiated areas.

## Image-processing quantification programs

Images of the CAM's vascular morphology following therapy are obtained through fluorescent angiography. These images are processed using two different macros written in ImageJ (with the help of existing plug-ins). One of the programs analyzes the inhibition of the naturally-developing CAM due to anti-angiogenic drug therapy and the other quantifies vascular regrowth following PDT. Both programs were developed in this laboratory (The Medical Photonics Group, EPFL) specifically for this type of application. For more information on these programs the following two papers can be referenced (140; 142). Both of these programs will be briefly described in the following sections.

### Quantification of inhibition of the naturally-developing CAM

To study the effects of anti-angiogenic compounds on the developing CAM, drugs are topically applied in a polyethylene ring on EDD7 and 8. On EDD9, the results of treatment are visualized through fluorescence angiogram.

A flowchart giving an overview of the first image-processing program is shown in Figure 21 (140). Figure 21A shows the original 16-bit image of the CAM vasculature, which is obtained from the fluorescence angiogram. The image is first put through an "a posteriori" shading correction filter, which corrects for inhomogeneities in the fluorescence excitation intensity (Figure 21C). This is followed by the removal of noise by a Fast Fourier Transform (FFT) band-pass filter, which removes isolated single pixels and large "island-like" structures consisting of more than 90 pixels. From this point, the program runs two phases of analysis in parallel and superimposes the results onto each other to create the final skeletonized image of the vasculature. The first phase of processing extracts the main vessels through a threshold filter. The noise of this image is removed through a despeckle process, which removes individual

pixels, and a FFT band-pass filter removing islands of connected pixels less than 40 pixels in size. The result of this 'first phase of processing can be seen in Figure 21B.

In the second phase of processing, small vessels and capillaries are extracted from the image shown in Figure 21C using a rolling ball background filter. This is followed by a Laplacian filter (the result of which is shown in Figure 21D) and a Guassian filter. Part of the results from the Laplacian filter (-SD/2 to +SD/2) are used to generate an 8-bit image with a threshold put between 0 and 100. "Islands" of pixels less than 200 pixels are removed to produce the final image from the second phase of processing which can be seen in Figure 21E. The final skeletonization of the vasculature is generated by superimposing the images from the two phases of processing, and can be seen in Figure 21F. The final image shows all connections

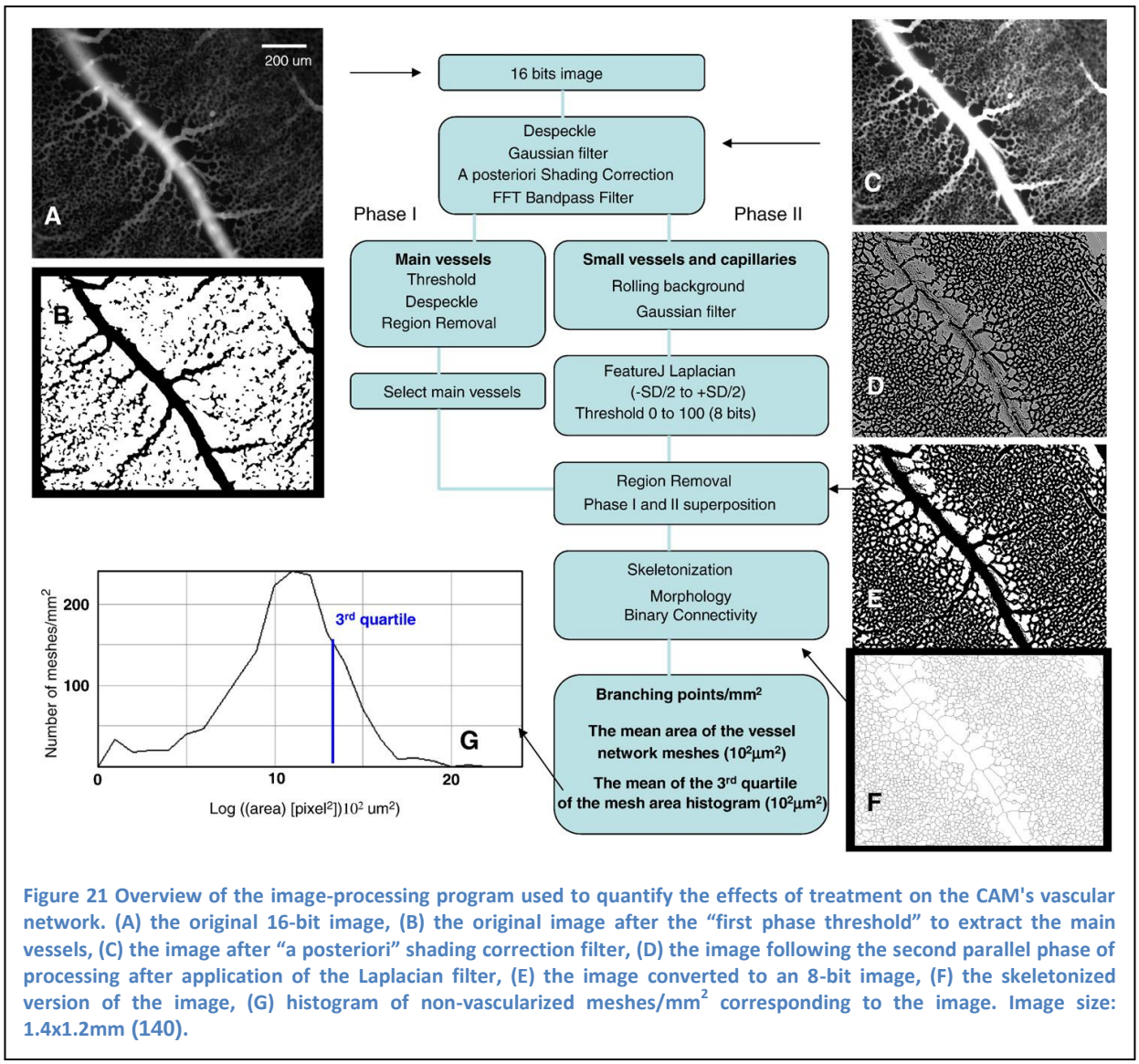


**Figure 21 Overview of the image-processing program used to quantify the effects of treatment on the CAM's vascular network. (A) the original 16-bit image, (B) the original image after the "first phase threshold" to extract the main vessels, (C) the image after "a posteriori" shading correction filter, (D) the image following the second parallel phase of processing after application of the Laplacian filter, (E) the image converted to an 8-bit image, (F) the skeletonized version of the image, (G) histogram of non-vascularized meshes/mm$^2$ corresponding to the image. Image size: 1.4x1.2mm (140).**

between vessels and capillaries, and capillaries and capillaries in the form of single pixel connecting lines. A morphology binary connectivity plug-in can be applied to determine the number of connected skeleton pixels.

Before quantification, the angiogram is divided into 9 equal areas to be processed individually so that unfocused parts of the image can be removed. The program returns a skeletonized version of the vasculature, a 'potential hypoxia map' and parameters describing the degree of vascular inhibition.

### Quantification of vascular regrowth following vaso-occlusive PDT

To study the effects of vascular regrowth on PDT-induced angiogenesis, Visudyne®-PDT is performed on the CAM on EDD11. Combination therapy is performed by topically applying the desired drug directly following PDT and again 24 hours following PDT, while control (or PDT only) experiments are followed by the application of physiological water. The effects of these treatments are then visualized on EDD13 using a fluorescence angiograms. The ImageJ macro can be used to quantify the vascular regrowth, vessel density and architecture (142).

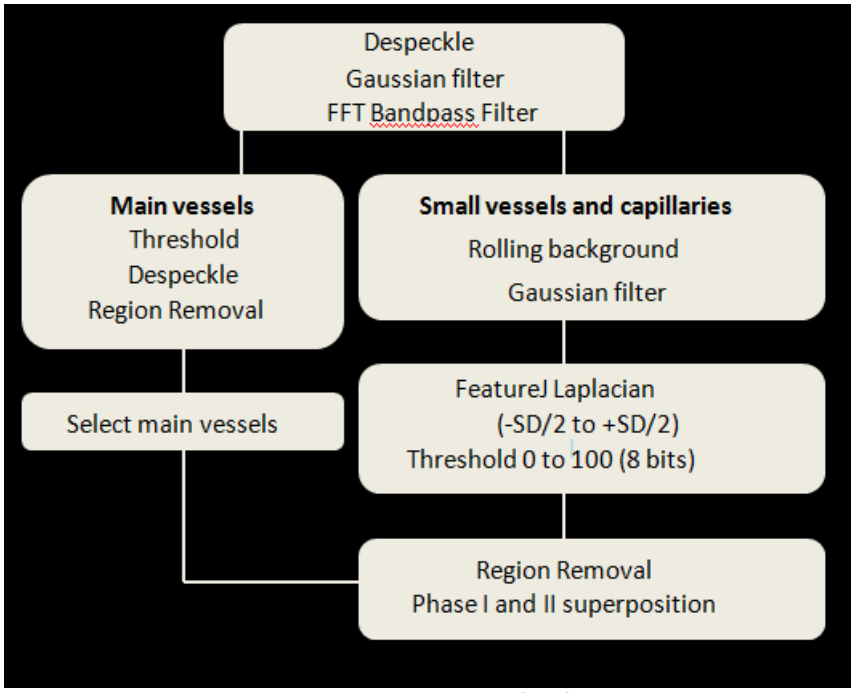


Figure 22 Overview of image quantification process (143).

A flowchart of the image-processing program described below can be seen in Figure 22 (143). The program also begins with the 16-bit image obtained from fluorescence angiograms. Three

points, manually inputted by the user, are used to determine the boarder of the treated area marking a circular region of interest. The macro then automatically generates 3 concentric circles, with identical widths, inside the original circle. The outermost circle is referred to as area 4 and is the first zone to be revascularized, while the innermost circles is referred to as area 1 and is the last to be revascularized.

Once the program has marked the different areas of regrowth, noise is removed from the image using a despeckle process followed by a Gaussian filter. This is followed by a FFT band-pass filter, which removes all single pixels and large “island-like” structures more than 90 pixels in size. From this point two parallel phases of processing are run in parallel, the results of which are superimposed on each other to generate the final skeletonized image of the vasculature.

The first phase of processing is used to isolate the main blood vessels. This is achieved through the application of a grey threshold value, which is empirically set at the mean grey value of the histogram + ½ SD. Isolated pixels are then removed using a despeckle process followed by the removal of small “islands of connected pixels” containing less than 40 pixels per “island”.

The second phase of processing is used to isolate small vessels and capillaries. This is achieved by the application of a rolling ball background filer, followed by a Laplacian filer. A part of the results from the Laplacian (-SD/2 to +SD/2) are removed and transformed into an 8-bit image with a threshold set between 0 and 100. “Islands” less than 300 pixels are then removed.

The skeletonization of the vasculature is then created by superimposing the results of these two phases of processing. The skeletonization shows all connections between vessel and capillaries, and capillaries and capillaries as single pixel connecting lines. The morphology binary connectivity plug-in can be used to determine the number of connected skeleton pixels.

The program returns a skeletonized version of the vasculature, a ‘potential hypoxia map’, and parameters describing the degree of vascular regrowth.

## Materials and Methods

The research conducted for this study utilizes two different experimental platforms involving the chicken embryo CAM model. The first experimental platform is the investigation of the effects of anti-angiogenic drugs on the physiologic angiogenic state of the developing CAM (EDD7-9). The second platform investigates the effects of anti-angiogenic drugs on the angiogenic state induced through vascular damage due to PDT on the mature CAM vasculature (EDD11-13). The materials and methods provided here are based on the material and methods published in previous articles from The Medical Photonics Group (140; 142).

### Materials and chemicals

This study is based on the investigation of two anti-angiogenic drugs, Avastin® and Sutent®. Avastin® (bevacizumab) is purchased from Genetech (San Fancisco, USA) and Sutent® (sunitinib) is purchased from Pfizer Inc. (New York, USA). Visualization of blood vessels is achieved through fluorescent angiography using fluorescein isothiocyanate dextran (FITC-Dextran, 20 kDA, 25 mg/ml), which is purchased from Sigma-Alrich (Buchs, Switzerland). India ink purchased from Pelikan (Witzikon \Switzerland) is injected into the extra-embryonic cavity to increase contrast during fluorescent angiography by blocking additional fluorescence from the embryo. A 0.9% NaCl solution, which is purchased from Bichsel AG (Interlaken, Switzerland), is used as a solvent to create dilutions for both drugs or alone as a control. Chicken embryos are purchased from AnimalcoAG (Staufen Switzerland). In order to perform PDT, the photosensitizer Visudyne® is acquired from Novartis Pharma, Inc. (Hettlingen Switzerland, the liposomal formulation of verteporfin (144)) and filtered through a sterile cellulose acetate membrane (0.8 μm pores, Renner GmbH, Darmstadt, Germany). Laboratory wrapping film used to cover the eggs protecting them from dehydration and possible contamination is purchased from Parafilm® (Pechiney, Menasha, USA). Injections into the CAM's vasculature are achieved using a Microliter™ syringes equipped with 33-guage metal HUB (N) needles from Hamilton (Reno, USA). Injection of india ink under the CAM is achieved using a sterile 5 mL Luer purchased from Codan Medical Aps and sterile 23-guage neolus needle purchased from Terumo® (Leuven, Belgium).

### The *in ovo* CAM model

Fertilized chicken eggs are received from Animalco AG (Staufen, Switzerland), labeled and placed into a hatching incubator with a relative humidity of 65% and a temperature of 37$^{o}$ C. Incubators are equipped with an automatic rotator (Savimat, Chauffry, France). Eggs are

automatically rotated by the incubator until EDD3, when a hole of approximately 3mm in diameter is opened in the narrow apex of the shell using sterilized tweezers. The hole is then covered using Scotch® Magic™ transparent adhesive tape to prevent dehydration or contamination. When topically applying compounds to the CAM, a polyethylene ring (diameter 5 mm, wall thickness 0.5 mm, height 1 mm) is placed on the surface and the drug is deposited inside the ring. These rings are cut from Pasteur pipettes purchased from Copan (Brescia, Italy) in sterile conditions. In order to visualize the CAM vasculature or perform PDT, the egg is placed under an epi-fluorescence microscope and the protocol described below is followed. When the egg is finished undergoing treatment, it is covered with Parafilm® and returned to the incubator in a static position until a new treatment protocol is needed.

## Microscope and image acquisition

Visualization of the CAM's vasculature and light irradiation during PDT are achieved with an epi-fluorescence Eclipse 600 FN microscope with Nikon objectives (Plan Apo 4x/0.2, working distance: 20mm or Plan Fluor 10x/0.3, working distance: 16 mm). A 100 W high pressure Hg-arc lamp (Osram, GmbH, Ausburg, Germany) is used to illuminate specimens. Light doses applied during PDT are measured using a calibrated Filed-Master GS power meter (Coherent, Santa Clara USA) and can be adjusted using neutral density filters. While performing PDT, a BV-2A filter set ($\lambda_{ex}$ = 420 ± 20 nm, $\lambda_{em}$ > 470 nm, Nikon, Japan) is used in order to select for the appropriate excitation and detection wavelengths of Visudyne®. In order to visualize vasculature by fluorescent angiography, excitation light is passed through a band-pass excitation filtered (470 ± 20 nm) and emission light is passed through a long-pass emission filter (λ > 520 nm). Fluorescence images are taken using an F-view II 12-bit monochrome Peltier-cooled digital CCD camera being run by 'analySIS DOCU' software from Soft Imaging System GmbH (Munster, Germany).

## Inhibition of developmental angiogenesis in the CAM

For experiments examining the response of the developmental CAM to topical application of drugs, the hole in the eggshell is increased to a diameter of approximately 3 cm on EDD7 providing access to a portion of the CAM. Twenty micoliters of the appropriate drug is then topically applied in the polyethylene ring on EDD7 and EDD8. Fluorescence angiograms are taken approximately 48 hours following the first drug application in order to visualize the response of the CAM to the test compound. Fluorescence angiographies are performed through i.v. injection of 20 µl of FITC-dextran (20 kDa, 25 mg/ml) into one of the main blood vessels of the CAM (diameter of ~200µm) and injection of a known light absorber, India ink, into the extra-

embryonic cavity directly below the topically treated area of the CAM. Light from an Hg-arc lamp filtered for excitation wavelength of 470 ± 20 nm and with a long-pass emission filter (λ > 520 nm) is used for illumination during the florescence angiography. Images are stored in a 16-bit TIF file and are later analyzed using the image-processing software previously described. Data points in the graphs provided in the results section represent the average of measurements from at least five embryos, with four different areas of 1.4 x 1.12 $mm^2$ (taken with the x10 objective) being analyzed per embryo.

## Visudyne®-photodynamic therapy

For experiments where PDT is performed, the hole in the eggshell is increased to a diameter of approximately 3 cm on EDD11. Twenty µl of Visudyne is intravenously administered and given one minute to evenly distribute in the circulating blood. The CAM is then irradiated with a light dose of 20 $J/cm^2$ ($\lambda_{ex}$ = 420 ±20 nm). The irradiation area is limited to 0.02 $cm^2$ using an optical diaphragm and a polyethylene ring used for topical drug application is placed around the irradiated area. Twenty micoliters of physiological water is topically applied within the polyethylene ring immediately following PDT and 24 hours following PDT. The conditions described above result in similar angio-occlusion efficiency as observed clinically after Visudyne®-PDT in human eye vessels of approximately the same diameter as the choroidal neovessels (approximated ≤ 70 µm) (142). Optimal PDT-induced vascular closure is defined as the closing of vessel of 70 µm or smaller in diameter, while larger vessels are left open (142). Fluorescent angiograms are taken of the treated area before, directly following and 48 hours following PDT treatment. Angiograms taken 48 hours following PDT are processed using the image-processing software previously described.

## Combination Visudyne®-PDT and anti-angiogenic drug therapy

Visudyne®-PDT is performed as described above and combined with topical or intravenous application of Avastin® or Sutent® at different concentrations. The appropriate drug is administered immediately following PDT and 24 hours following PDT in a quantity of 20 µl. Angiographies are then taken 48 hours following the original treatment in order to visualize the effects of therapy.

## Image-processing quantification method

Image-processing quantification is performed on images obtain from the florescence angiographies using a macro written for ImageJ (version 1.40 a; National Institute of Health;

Bethesda; USA) and existing plug-ins. The image-processing programs are described in more detail in the section of the introduction entitled: image-processing quantification programs.

In order to perform image quantification, the image must fulfill the following criteria: a resolution recorded at 1280 x 1024, dynamic range of 12 bits and 4095 grey levels, magnification with x10 (for quantification of vascular inhibition) or x4 (for quantification of vascular regrowth following PDT) objectives, and high contrast obtained by i.v. injection of a fluorescent contrast agent (FITC-dextran) and 20 µl of India ink as previously described.

The macro returns values for parameters to indicate vascular inhibition. The parameters reported for in this study were selected based on their ability to best describe the phenomena seen in the fluorescence angiograms. The outputs of this image-processing macro include a skeletonized version of the vascular network, a 'potential oxygenation map' and parameters describing the degree of angiogenesis inhibition. A typical example of these outputs can be seen in Figure 23. Figure 23A shows the original fluorescence angiogram of the CAM vasculature. Figure 23B shows the skeletonization network produced by the ImageJ macro and Figure 23C shows the 'potential hypoxia map' where black areas represent potential hypoxic areas.

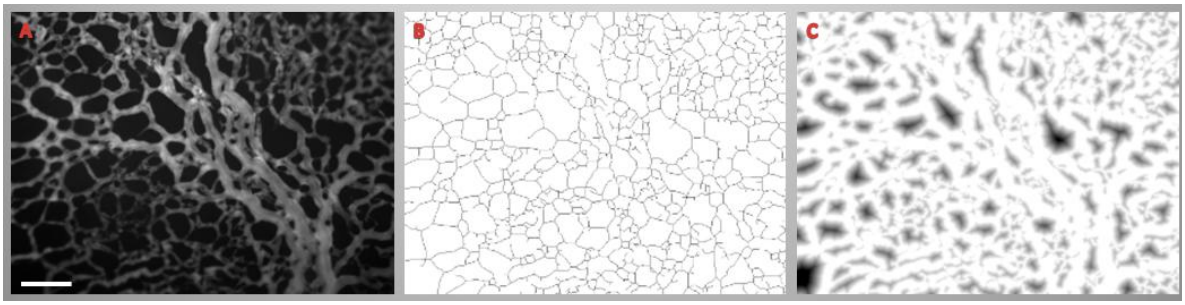


**Figure 23 An overview of the results from the image-processing program quantifying the degree of inhibition to the developmental CAM. A. The original fluorescent angiogram. B. The skeletonized version of the vasculature showing the connection between all vessels and capillaries, and capillaries and capillaries as single pixel connecting lines. C. The "potential oxygenation map" where possible hypoxic areas are shown in black.**

The parameters reported to describe the degree of inhibition of the naturally developing CAM include: the number of branching points per $mm^2$, defined as all equivalent and non-equivalent bifurcations (i.e. ≥ 3 neighbors), and the mean mesh size (or mean avascular zone) per $10^2$ $\mu m^2$.

The image-processing program which analyzes vascular regrowth following PDT is slightly different than the one analyzing inhibition of angiogenesis, but again produces the outputs of a skeletonized version of the vasculature, a 'potential oxygenation map' and parameters describing the vascular density and degree of regrowth. In analyzing the regrowth of vessels into the PDT treated area of the CAM, four concentric circles are placed on the treated area, the outer most circle marking the entire treated area or the region of interest (this circle is drawn based on user input). The four concentric circles create four zones of revascularization, each of which is analyzed separately by the software. The outer most region, area 4, is the first region to be revascularized while the inner most region, area 1, is the last to be revascularized. A typical example of these outputs can be seen in Figure 24, with the original image shown in Figure 24A, the skeletonized version of the image shown in Figure 24B and the 'potential hypoxia map' shown in Figure 24C.

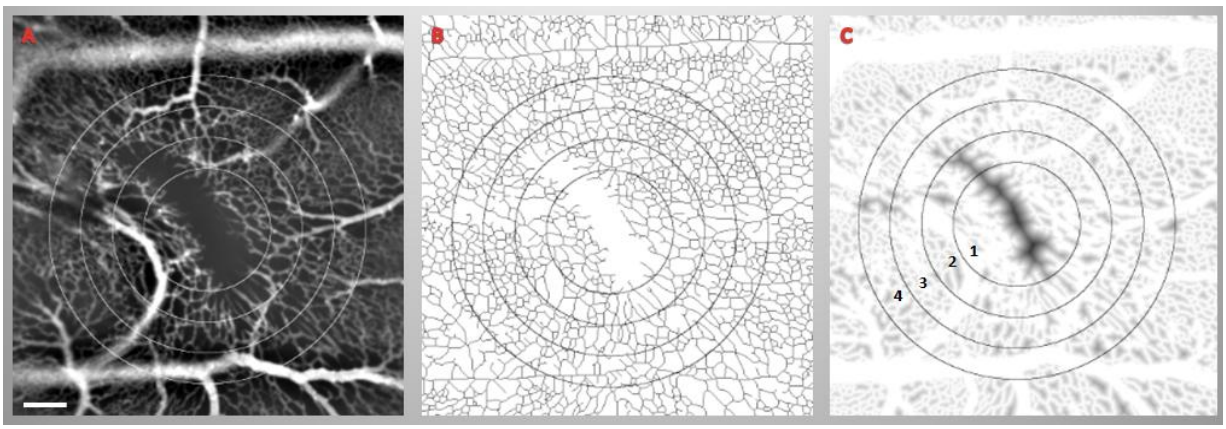


**Figure 24 An overview of the results of the image-processing program analyzing vascular regrowth following PDT, with rings marking the areas of regrowth following PDT and the outermost rings marking the entire treated area. A. The original fluorescent angiogram. B. The skeletonized version of the vasculature showing the connection between all vessels and capillaries and capillaries and capillaries as single pixel connecting lines. C. The "potential oxygenation map" where possible hypoxic areas are shown in black. The white bar in the lower left corner represents 200 µm and is valid for all images.**

The descriptors provided in this report to indicate vascular regrowth following PDT include: the branching points (per $mm^2$); a relative measure of mean mesh size as represented by the mean distance between vessels in µm; and the vessel density measured as the percentage of black pixels in the skeletonized image scaled to the surface area analyzed. All of the graphs provided in the results section indicate the average value of these parameters in area 1 (the inner most

region) of vascular regrowth for low and high concentrations of each drugs. Data from the inner most region was selected, because this region showed the most significant difference between conditions due to the fact that it is the last region to be revascularized. Graphs also indicate if results are statistically significant in regards to the control condition based on the results of a student t-test. Graphs are labeled as follows: data sets with a p-value > 0.1 have no indication; data sets with a p-value between 0.05 and 0.1 are marked by one asterisks above the bar (‘*’), and data sets with a p-value < 0.05 are marked by two asterisks above the bar (‘**’).

# Results

## Inhibition of developmental angiogenesis in the CAM

In the first experimental model, the inhibition of the physiologically-developing CAM membrane is investigated with the two anti-angiogenic agents: Avastin® and Sutent®. These drugs are topically applied to the immature membrane (embryo development days (EDD) 7 and 8) in concentrations ranging from 0.2 to 80 µM for Avastin® (corresponding to 0.06 to 238 µg/embryo/day) and 2 to 1000 µM for Sutent® (corresponding to 0.02 to 10.6 µg/embryo/day). Physiological water (0.9% NaCl) is used as a control condition.

Treatment of the CAM with anti-angiogenic compounds during the phase of development characterized by exponential vascular growth inhibits the natural development of capillaries and vessels and indicates the anti-angiogenic properties of the agents applied. The effects of these drugs are visualized by means of the fluorescence angiograms, which can be seen in Figure 25. Application of low drug concentrations (up to 10 and 100 µM for Avastin® and Sutent®, respectively) results in small avascular zones and inhibition of capillary development. The size of avascular zones increases with drug concentration, until capillary beds are completely inhibited, being replaced by networks of small blood vessels (as can be seen in the vascular treated with 40 µM Avastin®). Finally, at high concentrations (for 80 µM Avastin® and 700 to 1000 µM Sutent®), nearly all capillaries and blood vessels are inhibited, leaving only large blood vessels. In these images, it can also be seen that both drugs act similarly at low to medium concentration, but that at higher concentrations, Avastin® reaches a saturation point where increasing drug concentration does not result in increased vascular inhibition. Sutent®, on the

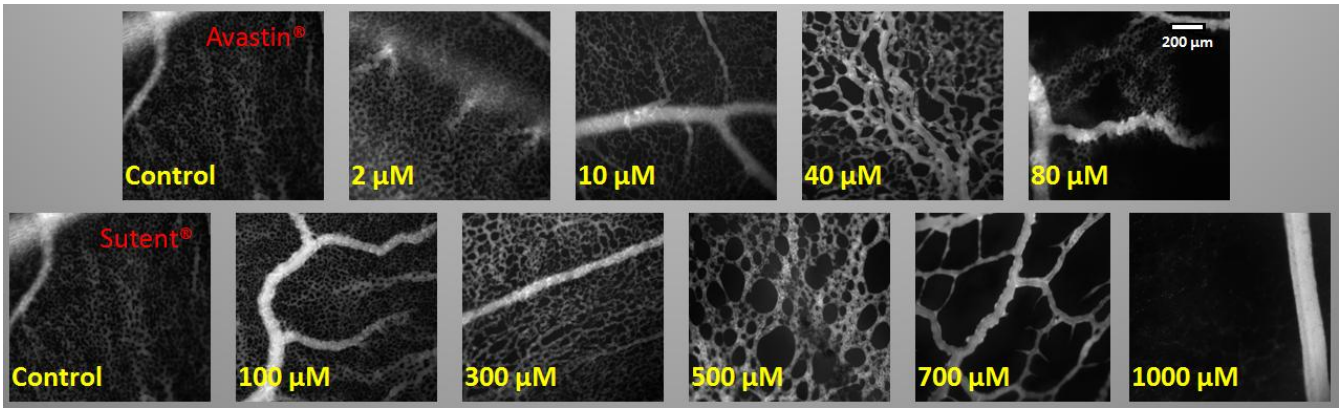


**Figure 25 Fluorescent angiogram images of the developmental CAM treated with Avastin® (top row) and Sutent® (bottom row) at the concentrations indicated. These images are obtain on EDD9, following two days of topical drug application. Fluorescent angiograms are obtained using FITC-dextran (25 mg/kg, 20kDa, $\lambda_{ex}$= 470 nm). The white bar in the upper right corner represents 200 µm and is valid for all images.**

other hand, does not saturate in this manner for the molarities tested and the concentration can be increased until almost all blood vessels growth is inhibited (occurring at approximately 1000μM). It should be noted that the images shown here are selected based on providing the most representative examples of the phenomena observed; however, results did vary between eggs and even within the treated area of the same egg.

In order to obtain a more quantitative analysis of angiogenesis inhibition, images obtained from angiograms are processed using the image-processing program previously described (140). The graph of branching points as a function of drug concentration, presented in Figure 26, shows Sutent® and Avastin® in red. This graph shows a dose-dependent decrease in the number of branching points (per $mm^2$) for both drugs. Similar to what can be seen in the morphological images shown above, a decreasing number of branching points indicates an increasing level of inhibition as the vascular network becomes less complex and the number of capillaries is decreased. At the lowest concentration of Avastin® (0.2 μM) a small degree of stimulation can be seen, as the number of branching points slightly increases. Following this increase, the number of branching points decreases to a greater degree than the number of branching points for Sutent® at similar concentrations. Therefore, it appears that Avastin® is a more effective inhibitor of angiogenesis at low concentrations. Overall, however, the trends of inhibition for both drugs at low concentrations appear to be relatively similar. At high

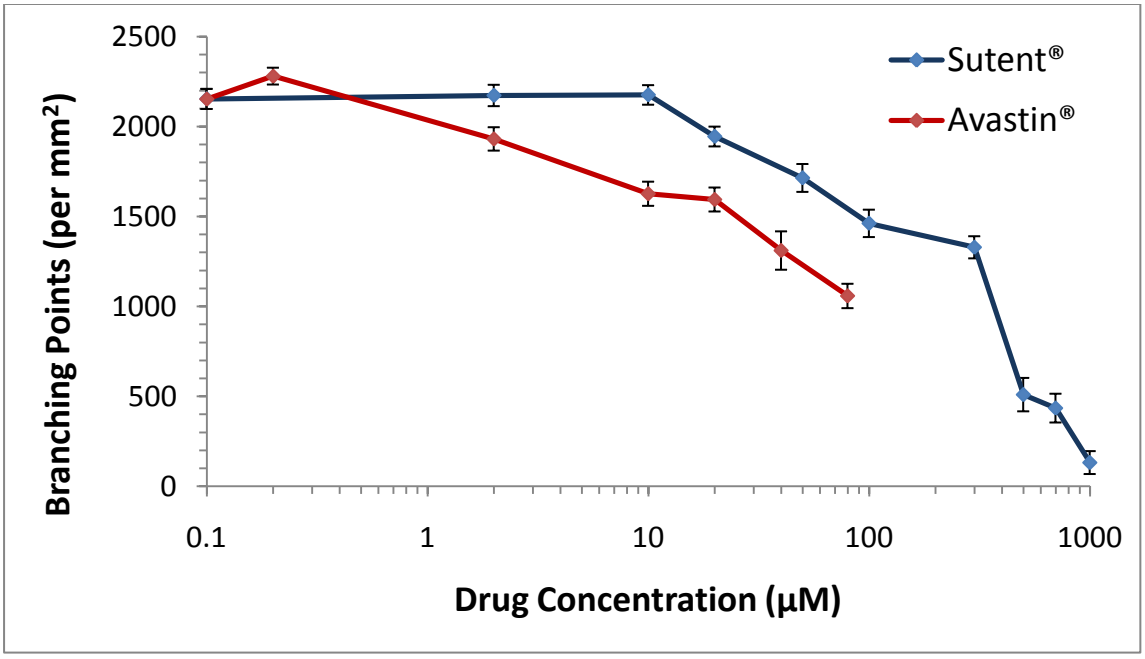


Figure 26 Number of branching points (per $mm^2$) as a function of drug concentration. Error bars represent the Standard Error of the Mean (SEM) of measurements.

concentrations, Sutent® continues to inhibit angiogenesis until nearly all vasculature is destroyed. The efficiency of Sutent® at high concentrations is much greater (approximately two times higher) than Avastin® at its most effective concentration.

The graph of mean mesh size as a function of drug concentration is presented in Figure 27. This graph again shows a dose-dependent increase in the mean mesh size as drug concentration is increased. A log scale was selected for both axes in order to better show the effects of each drug at low concentrations. Increased inhibition is reflected by an increase in the mean mesh size, as the inhibition of blood vessel and capillaries growth results in an increase in the area of avascular zones. In addition, the trends of the mean mesh size and the number of branching points are similar, as these parameters are fundamentally related to each other. These results again show a small amount of stimulation of angiogenesis for Avastin® at very low concentrations. This is followed by a mean mesh size which increases as drug concentration is increased. Based on this parameter, Avastin® is still seen to be a more effective inhibitor of angiogenesis than Sutent® at low concentrations, while greater Sutent® efficiency is seen at higher concentrations. In addition, the mean mesh parameter better shows the saturation of Avastin® seen in the fluorescence angiograms between the concentrations 40 and 80 μM. Between these concentrations, the mean mesh size of the vascular treated actually slightly decreases, within the margin of error, showing no significant increase in the ability of the drug to

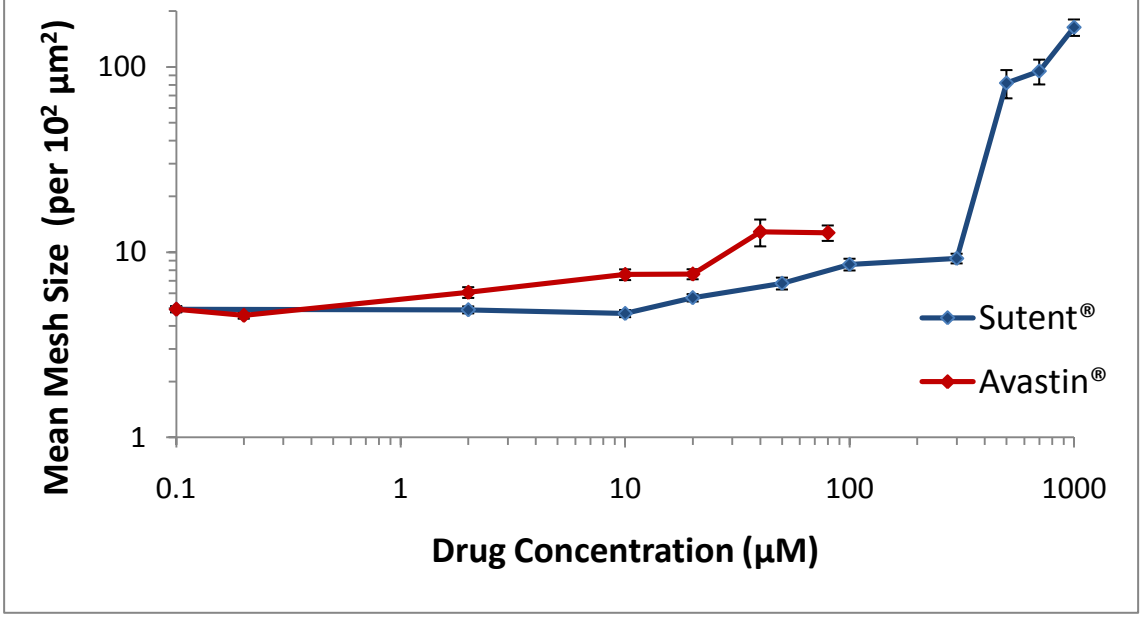


Figure 27 Mean mesh size (per $10^2$ $\mu m^2$) as a function of drug concentration. Error bars represent the SEM.

inhibit angiogenesis with increased concentration. Sutent®, on the other hand, shows no saturation as the mean mesh size continues to increase with drug concentration.

Both drugs showed effective inhibition of angiogenesis in the physiologically-developing CAM. The effective dose to achieve 50% inhibition ($ED_{50}$) for each drug was determined based on the percent of inhibition in comparison to the control condition averaged for the two parameters provided above. $ED_{50}$ was seen at 45 and 200 µM for Avastin® and Sutent®, respectively, corresponding to doses of 134 and 2.1 µg/embryo/day.

## Inhibition of PDT-induced angiogenesis in the CAM

In the second experimental model, the effects of anti-angiogenic drugs on the regrowth of blood vessels following photodynamic damage to the CAM vasculature are examined. Visudyne®-PDT applied to the mature CAM on EDD11 results in the effective closure of small blood vessels (diameter of 100 µm or less) followed by the induction of angiogenesis. Regrowth of vasculature can be seen following PDT and complete revascularization is seen for control conditions (PDT with physiological water) 48 hours following PDT (143). Figure 28 shows a typical example of vascular regrowth in control conditions following PDT: the CAM vasculature before PDT treatment (Figure 28A), the same area of the CAM directly following PDT (B), the start of vascular regrowth at 24 hours following PDT (C) and complete revascularization at 48 hours following PDT (D). This figure not only serves to show the complete revascularization of the treated area 48 hours following treatment, but also shows the changed morphology of new vasculature compared to untreated vasculature (which can be seen outside of the treated area).

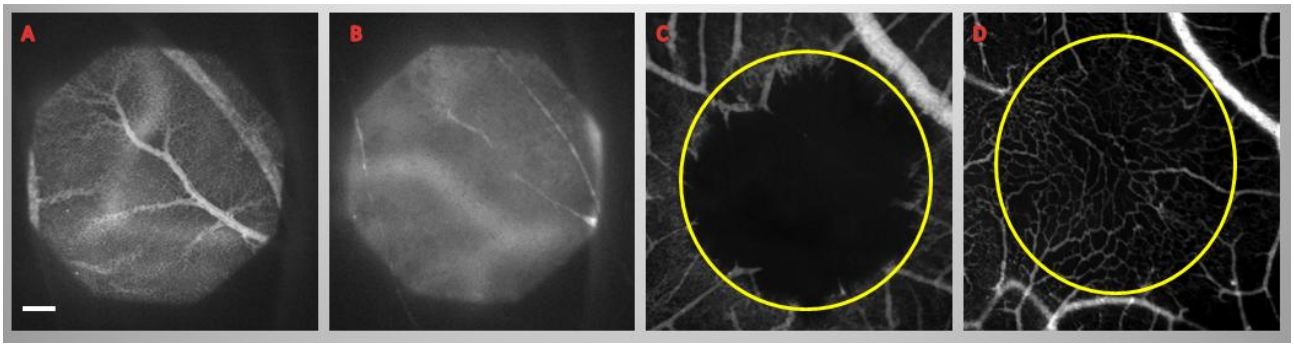


**Figure 28 The CAM vasculature before PDT (A), directly following PDT (B), 24 hours following PDT (C) and 48 hours following PDT (D). Under control conditions (shown here) vascular regrowth is complete 48 hours after treatment. Visualization of vasculature is achieved through fluorescence angiograms using FITC-dextran (25 mg/kg, 20kDa, $\lambda_{ex}$= 470 nm). The white bar in the lower left corner represents 200 µm and is valid for all images.**

The morphological difference between new vessels and untreated vessels can be seen in the increased tortuosity or unorganized, chaotic nature of the regrown vessels. An image showing vascular abnormalities can be found in Figure 29. In addition to showing increased tortuosity, this vasculature is characterized by increased mesh size (larger avascular zones) and occasionally increased thickness of regrown blood vessels (indicated by the arrows). These changes in vasculature most likely reflect the induction of angiogenesis in the treated area due to vascular damage from PDT through the activation of different pathways than those normally activated in the physiological development of the CAM.

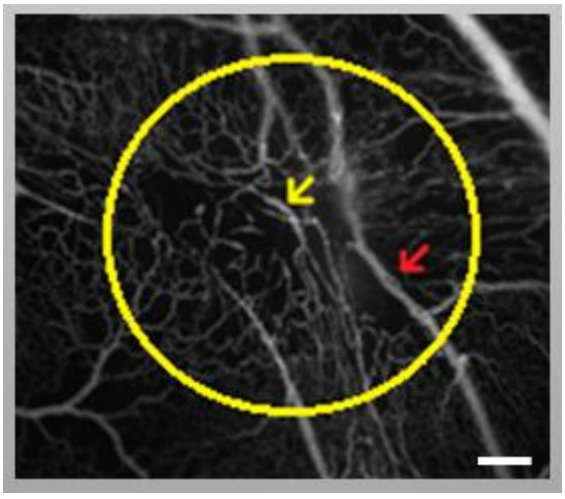

**Figure 29 Image showing abnormalities in the revascularized PDT treated area. The treated area is indicated by the yellow circle. Regrown blood vessels appear tortuous with abnormally large avascular zones and increased vessel diameters (indicated by the arrows). The white bar in the lower right corner represents 200 µm.**

### Topically administrated angiogenesis-inhibitors

In order to test the effects of anti-angiogenic drugs on PDT-induced angiogenesis, Visudyne®-PDT is performed on the mature CAM vasculature on EDD11 and drugs are topically applied directly following and 24 hours following therapy. Vascular regrowth is then visualized 48 hours following the original therapy using fluorescence angiograms. For each drug, concentrations of 2 or 20 µM are tested, corresponding to 6 or 60 µg/embryo/day for Avastin® and 0.02 or 0.2 µg/embryo/day for Sutent®. The morphological effects of these drugs on vascular regrowth 48 hours following vascular occlusion due to PDT can be seen in Figure 30. These images show

the varying abilities of these anti-angiogenic agents to prevent vascular regrowth. It can be seen that even low drug concentrations (much lower than concentrations needed to inhibit physiological angiogenesis) are capable of inhibiting the angiogenic state induced by photodynamic vascular damage when compared to the control condition. There appears to be dose-dependent inhibition for both drugs, as the percent of the treated area to be revascularized appears to decrease with increasing concentration. It can be seen that Avastin® appears to results in stronger inhibition of angiogenesis than Sutent® at low and high concentration. The different effects of each drug on angiogenesis, however, are more pronounced at 20 µM than at 2 µM. In Figure 30, it can be seen that using Sutent® as an anti-angiogenic agent results in less inhibition, as well as more organized and physiologically normal appearing regrown blood vessels. On the other hand, when Avastin® is applied at 20 µM, it results in the growth of blood vessels which are much more chaotic and are characterized by much larger avascular zones, as can be seen in Figure 30.

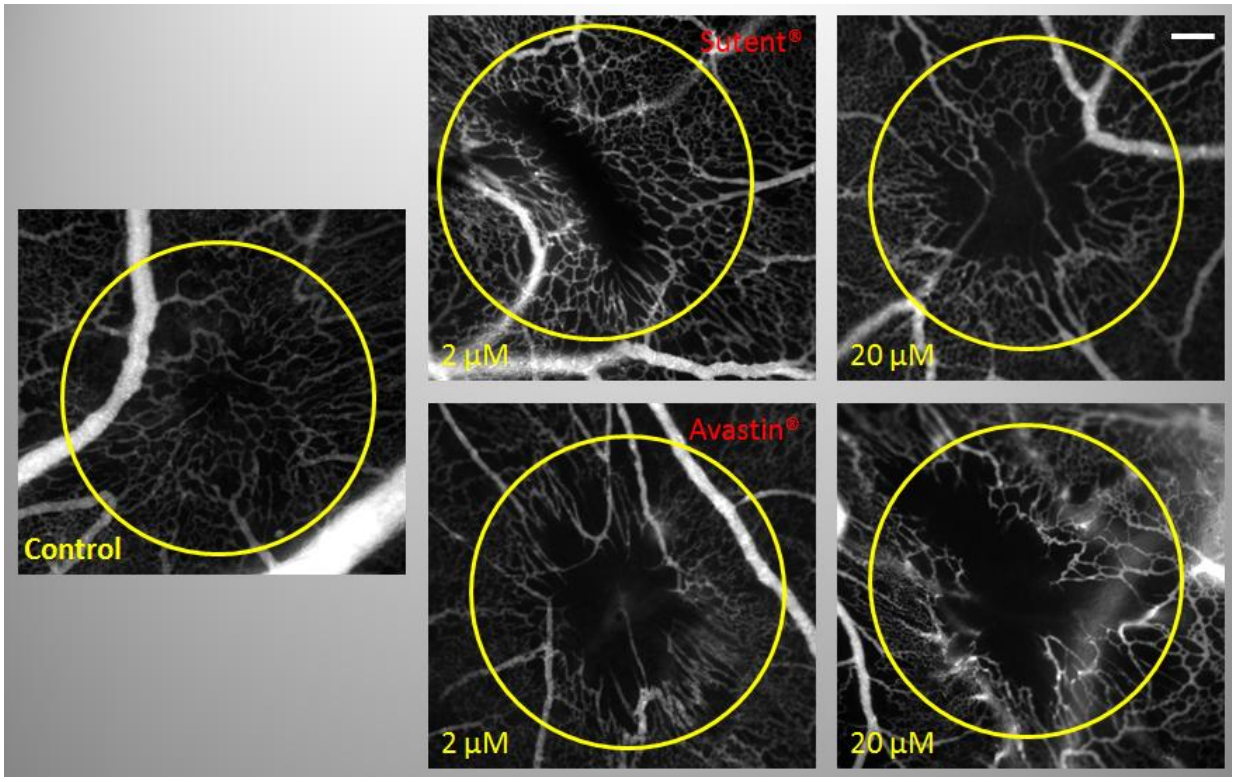


**Figure 30 Examples of fluorescence angiograms obtain 48 hours follow Visudyne®-PDT (0.2 mg/kg embryo weight, $\lambda_{ex}$ = 420 nm, $\lambda_{em}$ > 470 nm; light dose of 20 J/cm$^2$, irradiance 50 mW/cm$^2$, drug-light interval 1 minute). The control condition is shown on the left, Sutent® low and high concentrations are shown on the top row and Avastin® low and high concentrations are shown on the bottom row. The original treatment area is outlined by the yellow circles. The vasculature is visualized using FITC-dextran fluorescence angiography (25 mg/kg, 20 kDa, $\lambda_{ex}$ = 470 nm, $\lambda_{em}$ > 520 nm). The white bar in the upper right corner represents 200 µm and is valid for all images.**

Again, more quantitative information can be obtained through image-processing of fluorescence angiogram obtained on EDD13, 48 hours following PDT treatment.

The graph of branching points in region 1 of vascular regrowth, presented in Figure 31, shows the control condition of PDT monotherapy in the first column (red), PDT in combination with low drug concentration, 2 µM, in the second set of columns, with Avastin® in blue and Sutent® in yellow, and PDT in combination with high drug concentration, 20 µM, Avastin® and Sutent® in the third set of columns. This graph shows that both drugs are capable of inhibiting vascular regrowth following PDT when compared to the control condition. In addition, both drugs show similar inhibition at low concentrations, while Avastin® appears slightly more effective at high concentrations (but not significantly, p-value 0.23). Based on this parameter, Avastin® shows dose-dependent inhibition as the difference between low and high concentration is significant given a confidence interval of 10% (p-value of 0.085). Sutent®, on the other hand, does not show dose-dependent inhibition as the difference between low and high concentration is not significant (p-value 0.5).

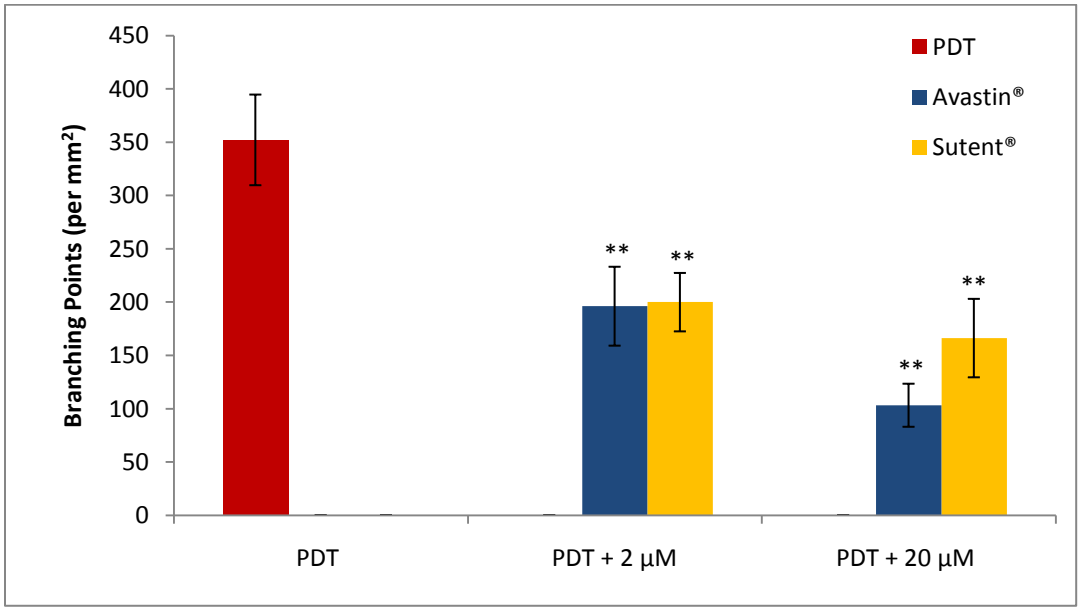


**Figure 31 Graph of branching points per mm² in region 1 of vascular regrowth following PDT. Control, low and high concentrations are shown for both Avastin® and Sutent®. Error bars show SEM. Data sets marked by '**' have a p-value < 0.05.**

The graph of relative mean mesh size in region 1 of vascular regrowth is presented in Figure 32. As the parameter for the mean distance to the next vessel increases, the area of the mean

mesh size also increases, indicating a greater degree of inhibition. Based on this parameter, both drugs show the ability to inhibit vascular regrowth in the central region of the PDT-treated area in comparison to the control condition. Both drugs appear to show dose dependent inhibition, as inhibition increases between low and high concentration, however neither difference is statistically significant (p-value 0.23 and 0.37 for Avastin® and Sutent®, respectively). In addition, Avastin® again appears to be a better inhibitor of vascular regrowth than Sutent®; however, at both high and low concentrations, the difference between the performances of the two drugs is not statistically significant (p-value 0.55 and 0.23 for high and low concentration, respectively).

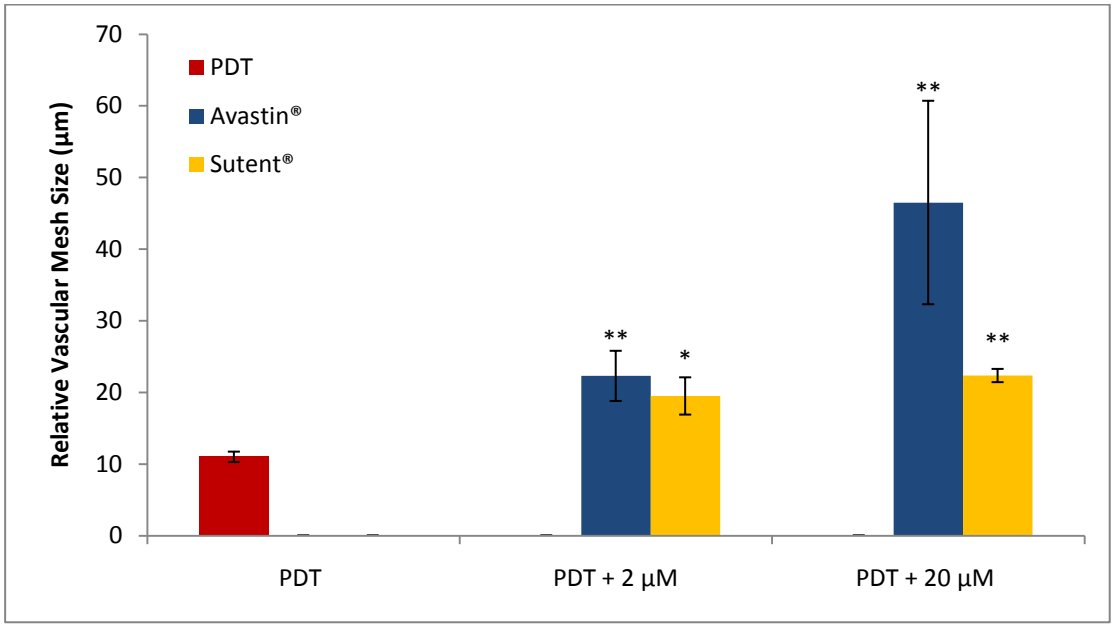


**Figure 32 Graph of the relative vascular mesh size in region 1 of vascular regrowth following PDT. Control, low and high concentrations are shown for both Avastin® and Sutent®. Error bars show SEM. Data sets marked by '*' have a p-value between 0.05 and 0.1, and data sets marked by '**' have a p-value < 0.05.**

The graph of percent vessel density in region 1 of the PDT-treated area is shown in Figure 33. The vessel density represent the percentage of the region being analyzed covered in regrown blood vessels. Smaller vessel density values indicate a greater degree of inhibition of angiogenesis, as it indicates that a smaller percentage of the treated area has been revascularized. Based on the parameter of percent vessel density, both drugs show the ability to inhibit angiogenesis in comparison to the control condition. Again this parameter shows Avastin® to be a slightly more effective inhibitor of angiogenesis at both concentrations, but again neither of these differences are statistically significant (p-value 0.64 and 0.23 for low and

high concentration, respectively). Inhibition also appears to be dose dependent for both drugs, but the differences between low and high concentration for each drug are also not significant.

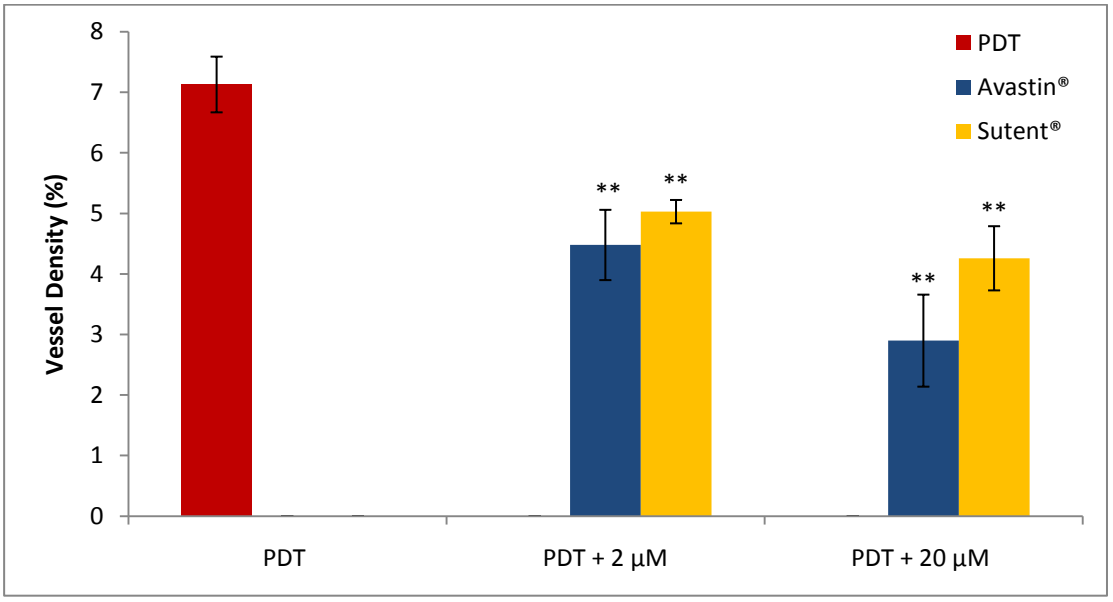


**Figure 33 Graph of percent vessel density in region 1 of vascular regrowth following PDT. Control, low and high concentrations are shown for both Avastin® and Sutent®. Error bars show SEM. Data sets marked by '**' have a p-value < 0.05.**

Both drugs showed effective inhibition of the angiogenic state induced by photodynamic damage in comparison to the control. The differences between Avastin® and Sutent® at high or low concentrations are not statistically significant based on any of the parameters analyzed. In addition, the difference between Sutent® low and high concentration is not statistically significant, while the difference for Avastin® between low and high concentration is statistically significant given a 10% confidence interval, but only for the branching points parameter (p-value of 0.085).

The estimated effective doses of 50% inhibition ($ED_{50}$) for each drug is determined based on the percent of inhibition in comparison to the control condition averages for the parameters presented above. The estimated $ED_{50}$ for inhibition of the PDT-induced angiogenic state was seen at 7 and 17 µM for Avastin® and Sutent®, respectively, corresponding to a treatment dose of 20.9 and 0.18 µg/embryo/day. These concentrations had to be estimated due to the fact that 50% inhibition was not attained for the parameter of vessel density for Sutent® and had to be calculated assuming a linear trend.

### Intravenously administrated angiogenesis-inhibitors

Subsequently, the effects of intravenously applied Sutent® following PDT were investigated in order to determine the relationship between intravenous and topical drug uptake and delivery. These experiments were performed for both drugs; however, due to time limitations, only adequate results were obtained for Sutent®. Images depicting the morphological effects of Sutent® therapy are provided in Figure 34. In this figure, the effects of topical drug application can be seen in images in the top row (low and high concentration) and effects of intravenous drug application can be seen in images on the bottom row (low and high concentration). These images show more effective inhibition of PDT-induced angiogenesis by Sutent® when it is topically administered compared to when it is intravenously administration. Intravenously administered Sutent® at low concentration appears to have little to no effect on angiogenesis, as the treated area is completely revascularized 48 hours after treatment. At high concentration, intravenously administered Sutent® does appear to inhibit revascularization of the treated area, but not very strongly as the area is partially regrown and looks very similar to the 2 µM topical

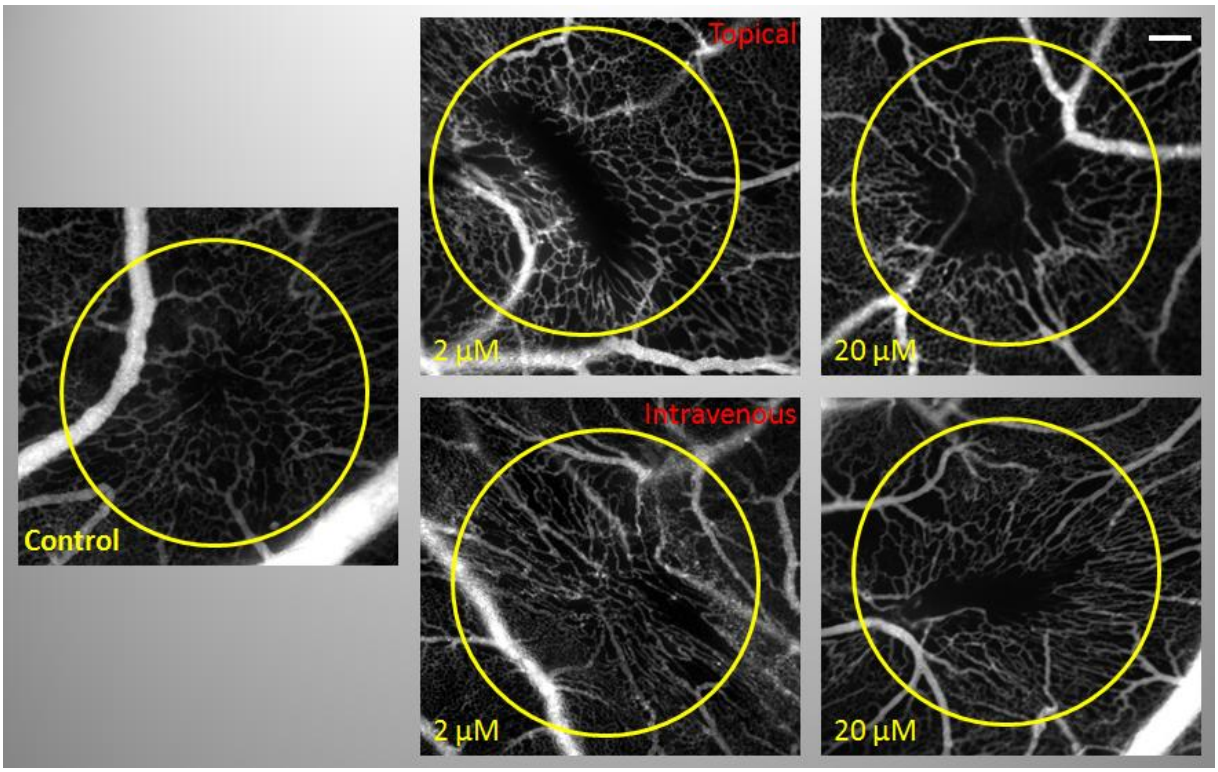


**Figure 34 Examples of fluorescence angiograms obtain 48 hours follow Visudyne®-PDT (0.2 mg/kg embryo weight, $\lambda_{ex}$ = 420 nm, $\lambda_{em}$ > 470 nm; light dose of 20 J/cm$^2$, irradiance 50 mW/cm$^2$, drug-light interval 1 minute). The control condition is shown on the left, Sutent® low and high concentration topically applied are shown in the top row, and Sutent® low and high concentration are shown in the bottom row. The original treatment area is outlined by the yellow circles. The vasculature is visualized using FITC-dextran fluorescence angiography (25 mg/kg, 20 kDa, $\lambda_{ex}$ = 470 nm, $\lambda_{em}$ > 520 nm). The white bar in the upper right corner represents 200 µm and is valid for all images.**

Sutent® treatment condition shown in the top row. In addition, these images show that the morphology of regrown blood vessels in the presence of topical and intravenously administered Sutent® are relatively similar, both being less tortuous and disorganized when compared to blood vessel that regrow in the presence of Avastin®.

Data obtained from image-processing allowed for the generation of the graph of the percent vessel density provided in Figure 35. This graph presents the percent vessel density, in region 1 of vascular regrowth, for the control PDT condition (first column, red), 2 µM, low concentration of Sutent® (the second set of columns, topical in yellow and intravenous in blue), and 20 µM, high concentration of Sutent® (the third set of columns, topical in yellow and intravenous in blue). Based on this graph, topically applied Sutent® is significantly more effective at inhibiting vascular regrowth following PDT than intravenously applied Sutent® given a confidence interval of 10% (p-value of approximately 0.09 for low and high concentration). In addition, neither of the intravenous conditions showed significant inhibition in comparison to the control. Based on the parameter of vessel density, the estimated $ED_{30}$ for topically and intravenously applied Sutent® was seen at 2 and 38 µM, corresponding to 0.02 and 0.4 µg/embryo/day, respectively. The $ED_{30}$ was calculated for this parameter, because a level of inhibition in comparison to the control high enough to calculate the $ED_{50}$ was not achieved for intravenously administered Sutent®.

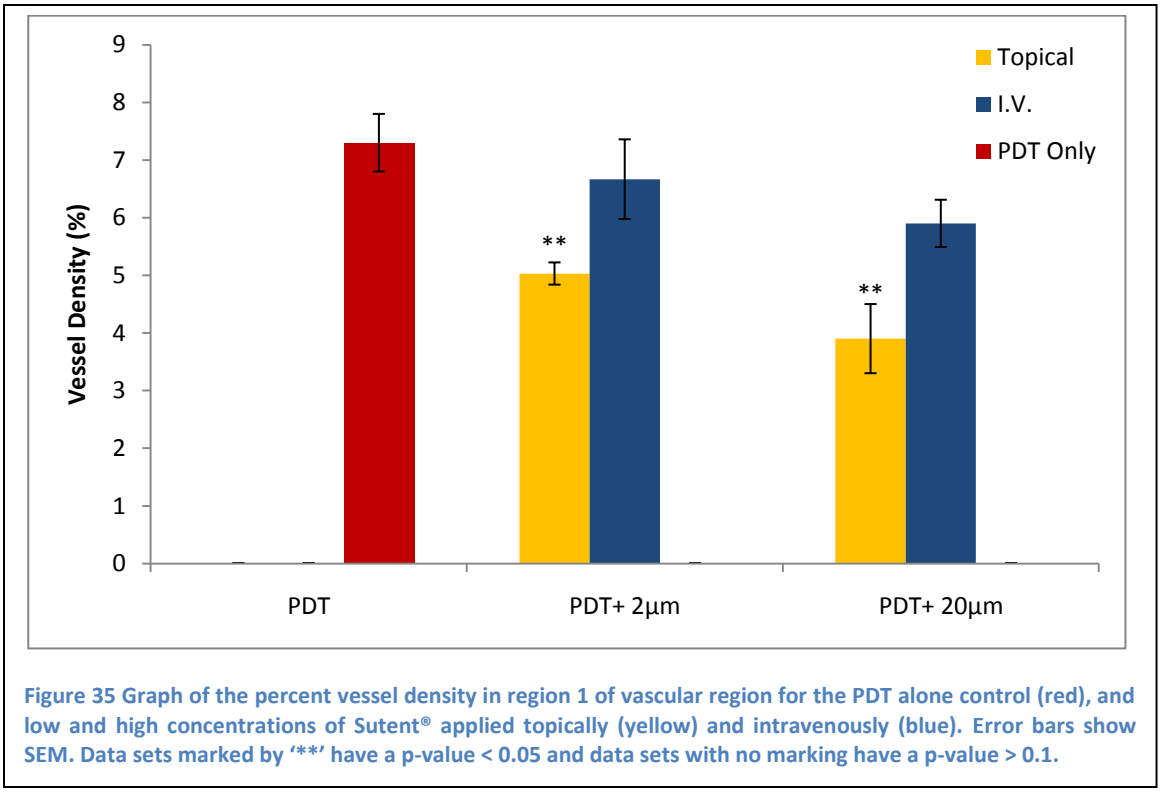


**Figure 35 Graph of the percent vessel density in region 1 of vascular region for the PDT alone control (red), and low and high concentrations of Sutent® applied topically (yellow) and intravenously (blue). Error bars show SEM. Data sets marked by '**' have a p-value < 0.05 and data sets with no marking have a p-value > 0.1.**

## Discussion and Conclusions

The CAM model is extensively used in angiogenic research and is particularly well suited for the study of diseases characterized by proliferative retinal vasculature, such as age-related macular degeneration (29).

In the present work, this model was used in order to study the effects of vascular regrowth following photodynamic occlusion of vessels in the presence of anti-angiogenic drugs targeting two different mechanisms: direct inhibition of vascular endothelial growth factor (VEGF) through a monoclonal antibody, such as Avastin®, or inhibition of VEGF and other pro-angiogenic signaling through the receptor tyrosine kinase inhibitor (RTKI) Sutent®.

The aim of showing the efficiency of a RTKI in preventing angiogenesis and vascular regrowth following photodynamic vascular occlusion is to open up the possibility for a new therapeutic modality, which would present unique advantages over current therapeutic options. The advantage of using a small molecule-based drug, such as Sutent®, in the treatment of AMD in the place of a large molecule, such as Avastin®, is based on the bioavailibity of the drug. Being a small molecule which is mostly hydrophobic, Sutent® can pass through cell membranes to interact with the intracellular domains of receptor tyrosine kinases involved in the angiogenic signaling cascade. This properties of Sutent® may well make it possible for drug application to be achieved both locally and topically through either slow release drug delivery systems or eye drops (56). This presents a potential advantage over Avastin®, which is currently administered through intravitreal injection. Multiple treatments of anti-angiogenic drugs are required and, as one can imagine, the advantages of a less invasive mode of drug administration would be great. In addition to this practical advantage, a locally-administered RTKI drug would likely bypass many of the common complications associated with anti-angiogenic drug therapy. First of all, local drug administration will probably decrease the development of systemic side effects and hopefully result in only the desired therapeutic effects of the drug. More importantly, drug resistance is less likely to develop when using a RTKI for the treatment of AMD, as the believed mechanisms by which resistance can develop are based on the abilities of cancerous cells to mutate and circumvent some of the pathways inhibited by the anti-angiogenic drug therapy. It is believed that because the vasculature being treated here is genetically stable, these mechanisms of resistance will not be available, and drug resistance will not develop.

It is also possible that by targeting a new pathway additional benefits or increased efficiencies may be seen which was not predicted. Targeting RTKIs opens up the possibility for new

combination therapies which have not previously been available. The use of multiple RTKIs or the combination of a RTKI with a VEGF-targeting molecule could provide additional benefits and synergistic effects not foreseen. In addition to additional therapeutic benefits from combination therapies, however, there is also the risk that combining anti-angiogenic drugs could result in unforeseen side effects and complications. Local administration of anti-angiogenic drugs can also improve the effectiveness of PDT, as drug application prior to PDT results in vascular normalization, increasing the availability of both PSs and oxygen in the blood vessels during treatment, improving the efficiency of PDT (142).

The results of this research showed that both of the drugs tested were able to inhibit physiologic and PDT-induced angiogenesis. In both situations, Avastin® appeared to be a slightly more effective inhibitor of angiogenesis than Sutent®, but statistical analysis of the data revealed that these differences were not significant. In the physiological angiogenic state, Avastin® appeared to reach a saturation point which was not seen for Sutent®. This saturation was most likely due to the fact that Avastin® is a large molecule which has a limited ability to penetrate blood vessels to bind and neutralize VEGF, while Sutent® concentration can be increased until it completely floods cells blocking nearly all of its target RTK pathways. The therapeutic relevance of this result, however, is not very significant due to the fact that concentrations higher than this saturation point (or concentrations of Sutent® needed to completely inhibit blood vessel growth) are much greater than any concentration which would be used in a clinical setting.

It should be noted that it is difficult to make direct comparisons between the two drugs being examined in this study. This is due to the fact that the drugs have drastically different molecular weights (Avastin® is three orders of magnitude larger than Sutent®), have different properties and bioavailabilities, and the fact that they target different. In this study, the drug molarity is predominantly used to indicate doses applied the CAM; however this can be misleading as a relatively high molarity of Sutent® still represents a relatively small dose in terms of µg of drug administered embryo when compared to the dose given in µg of even very low molarities of Avastin®. For this reason, all effective doses are provided in molarity and in terms of µg per embryo.

The $ED_{50}$ for Avastin® and Sutent® to inhibit the developmental angiogenic CAM was seen when 20 µl of 45 or 200 µM drug were applied to the CAM topically each day for two days, respectively, which corresponds to 134 and 2.1 µg/embryo/day. In clinical treatment of cancer, Avastin® is applied in an intravenous dose of 1 to 10 mg/kg which corresponds to 20 µl of 3.4 to

33.6 μM applied to the CAM. Sutent® is administered orally in a dose of 12.5, 25 or 50 mg per day. Taking the middle dose (25mg) and assuming an average mass of 70 kg for a person, this dose corresponds to 0.357 mg/kg which corresponds to 20 μl of 335 μM Sutent® applied to the CAM. Therefore, the $ED_{50}$ of Avastin® needed to inhibit the naturally-developing CAM vasculature is slightly higher than what is clinically used (45 instead of 33.6 μM) and the Sutent® needed is lower than the clinical doses (200 instead of 335 μM).

The estimated $ED_{50}$ for Avastin® and Sutent® to inhibit the PDT-induced angiogenic state on the CAM was seen when 20 μl of 7 or 17 μM drug were applied to the CAM topically each day for two days, respectively, corresponding to 20.9 and 0.18 μg/embryo/day. The effective dose of Avastin® fell within the clinically-used range of doses while the effective dose of Sutent® was approximately 20 times lower than the clinically-used dose for cancer therapy.

In addition to determining the effective concentration of each drug to inhibit the physiologic and PDT-induced angiogenic states, this research allows for a fundamental comparison of these two angiogenic states to be made. A notable result is the fact that inhibition of the PDT-induced angiogenic state was achieved at a much lower concentrations than inhibition of the physiologically angiogenic CAM. Inhibition of the PDT-induced angiogenic state occurred at a concentration approximately 2-3 fold lower than the developmental CAM for Avastin® and 4-fold for Sutent®. This result could reflect fundamental differences between the angiogenic states and the pathways they activate in order to achieve their desired biological responses. It may be the case that PDT-induced angiogenesis only activates specific pathways associated with the vascular damage done by PDT. For example, PDT induces hypoxia through vascular occlusion, resulting in the activation of HIF and the release of VEGF. One could speculate that while physiologic angiogenesis is a result of the activation of many closely regulated angiogenic pathways (such as VEGF, angiopoietins, EGF, PDGF or PIGF (143)), PDT-induced angiogenesis may be mainly a result of one or a few pathways activated due to hypoxia, inflammation and cell damage (143). Morphological characteristics of the vasculature which regrows after PDT damage also appear to support the hypothesis that this form of angiogenesis may be mainly VEGF-driven. This vasculature is abnormally tortuous and disorganized, having characteristics similar to tumor vasculature, which is known to be mainly VEGF-driven (142).

The estimated $ED_{30}$ for topically and intravenous applied Sutent® was seen when 20 μl of 2 and 38 μM drug were applied each day for two days, respectively, corresponding to 0.02 and 0.4 μg/embryo/day, respectively. Again doses are much lower than what is clinically used for cancer

treatment and would remain lower even if it were possible to calculate the $ED_{50}$ for this parameter.

The method of direct topical drug application was selected because it most closely reflects topical drug application via droplet to the eye, or application through a slow release drug delivery system, which are the primary models being investigated by this research. Intravenous drug application, however, was also performed for low and high concentrations of Sutent® in order to obtain more information about the activity of the drug and determine the relationship between these modes of drug administration. The results of these experiments showed that topical Sutent® application results in stronger inhibitions than intravenous application. This result can be explained by the fact that Sutent® is a small molecule drug, which when applied locally and topically has no problems entering cells to have its desired effect. By administering Sutent® systemically through intravenous injection, the drug concentration is effectively diluted by the volume of blood in the system and the concentration of drug reaching the desired area is reduced. This characteristic of Sutent® may also explain why effective angiogenesis-inhibiting doses could be achieved at lower concentrations than those used in the clinical treatment of cancer, which is also achieved through systemic administration. This result strongly supports the hypothesis that local application of Sutent® in the form of eye drops or slow-release drug delivery systems could provide an effective form of treatment for the choroidal neovessels which develop in age-related macular degeneration.

The preliminary results obtained with Avastin® show stronger inhibition of angiogenesis when this drug is administered intravenously as compared to topical application (data unshown). This result could be explained by the fact that Avastin® is a large molecule, which can enter in direct contact with VEGF when injected into the blood, allowing it to have a stronger effect than when it must pass into blood vessels due to being topically applied.

In addition, a recent study conducted in this laboratory (The Medical Photonics Group) was done to compare the effects of three different RTKIs, including Sutent®, with Avastin® in inhibiting developmental angiogenesis and vascular regrowth following PDT-induced vascular occlusion. This study showed Sutent® to have similar effectiveness as one of the RTKIs (erlotinib) and to be less effective than the other RTKI (sorafenib). In addition, morphological characteristics of regrown vasculature varied not only between Avastin® and the RTKIs, but between the different RTKIs as well. This indicates that different pathways are being inhibited by the different RTKIs, and that inhibition of different pathways results in angiogenesis achieved

through different mechanisms which is reflected in the structure and morphology of regrown vessels (143). These results further support the potential of using RTKIs in the treatment of angiogenic disorders.

Finally, it should be noted that it is complicated to translate the concentrations or doses applied to the CAM into doses administered in clinical applications. This is due to the following difficulties. The method of drug administration in clinical applications varies with the methods used in the research protocol (oral administration for Sutent® and intravenous administration for Avastin®), which results in different absorption and bioavailability of the drugs. There is effectively an overall lack of information concerning serum and blood concentrations of drugs, and there are important difficulties in translating results between a chicken and human. The two drugs examined are targeted to human VEGF and human RTKs. It can be seen that these drugs have an affinity for the chicken counterpart of their target molecule (by the fact that they have anti-angiogenic effects), but it is impossible to determine how a decrease in affinity can change the effectiveness of these drugs. This model and this research, therefore, are not being used to determine exact effective concentrations or to make a direct translation to clinical application, but instead serve to determine general trends and interactions of molecules and drugs in order to determine if these therapies are viable treatment options which should be investigated in more depth.

Experiments testing the effectiveness of the inhibition of physiologic and PDT-induced angiogenic states on the CAM showed that both the drugs tested were capable of inhibiting angiogenesis in comparison to the control condition and, more importantly, that there was no statistically significant difference between the activity of the two drugs. The results of this research support the theory that a small-molecule receptor tyrosine kinase inhibitor, such as Sutent®, is capable of inhibiting PDT-induced angiogenesis and that molecules such as this one could provide effective anti-angiogenic properties in the treatment of angiogenic disorders such as age-related macular degeneration and cancer. In addition, topically applied Sutent® was seen to be a more effective inhibitor of the PDT-induced angiogenesis than intravenously administered Sutent®, supporting the theory that a locally-applied receptor tyrosine kinase inhibitor could be used in the treatment of age-related macular degeneration.

## Abbreviations

| | |
|---|---|
| **AMD** | Age-related macular degeneration |
| **Ang** | Angiopoietin |
| **BCC** | Basal cell carcinoma |
| **BM** | Basement membrane |
| **BPD-MA** | Benzoporphyrin derivative monoacid |
| **CAM** | Chorioallantoic membrane |
| **CATT** | Comparison of AMD treatment trials |
| **CNV** | Choroidal neovessel |
| **Da** | Daltons |
| **ECM** | Extracellular matrix |
| **$ED_{50}$** | Effective dose of 50% |
| **EDD** | Embryo development day |
| **EGF** | Epidermal growth factor |
| **FFT** | Fast Fourier transform |
| **FGF** | Fibroblast growth factor |
| **FGFR** | Fibroblast growth factor receptor |
| **GIST** | Gastrointestinal stromal tumor |
| **HIF** | Hypoxia inducible factor |
| **IC** | Internal conversion |
| **ISC** | Intersystem crossing |
| **LDL** | Low density lipoprotein |
| **OCT** | Optical coherence topographies |
| **PDGF** | Platelet-derived growth factor |
| **PDGFR** | Platelet-derived growth factor receptor |
| **PDT** | Photodynamic therapy |
| **Pgp** | P-glycoprotein |
| **PNET** | Pancreatic neuroendocrine tumor |
| **PS** | Photosensitizer |
| **PS*** | Excited state |
| **PTPC** | Permeability transition pore complex |
| **RCC** | Renal cell carcinoma |
| **RPE** | Retinal pigment epithelium |
| **RTK** | Receptor tyrosine kinase |
| **RTKI** | Receptor tyrosine kinase inhibitor |
| **$S_0$** | Ground state |
| **$S_1$** | Singlet state |
| **SD** | Standard deviation |
| **SEM** | Standard error of mean |
| **$T_1$** | Triplet state |

| | |
|---|---|
| **TGF** | Tumor growth factor |
| **VEGF** | Vascular endothelial growth factor |
| **VEGFR** | Vascular endothelial growth factor receptor |

## Works Cited


1. *Angiogenesis: Potential for pharmacologic intervention in the treatment of cancer, cardiovascular diseases and chonic inflammation.* **Griffioen, A. W. and Molema, G.** 2000, Pharmacological Reviews, Vol. 52, pp. 237-68.

2. *Angiogenesis in the early human chorion and in primary placenta of the macaque monkey.* **Hertig, A. T.** 1935, Contributions to Embryology, Vol. 25, pp. 37-81.

3. *Angiogenesis in cancer, vascular, rheumatoid and other disease.* **Folkman, Judah.** 1995, Nature Medicine, pp. 27-30.

4. *Patterrns and emerging mechanisms of the angiogenic switch during tumorogenesis.* **Hanahan, D. and Folkman, J.** 1996, Cell, Vol. 86, pp. 353-64.

5. *Endothelial cell-mediated coagulation, anti-coagulation and fibrinolysis.* **Verstraete, M.** Stuttgert, New York : Schattauer, 1995, The Endothelial Cell in Health and Disease.

6. *Leukocyte-endothelial adhesion molecules.* **Carlos, T. M. and Harlan, J. M.** 1994, Blood, Vol. 84, pp. 2068-2101.

7. *Mechanisms of angiogenesis.* **Risaue, W.** 1997, Nature, Vol. 386, pp. 671-74.

8. *Nitric oxide synthase lies downstream from vascular endothelial grwoth factor-induced but not basic fibroblast growth factor-induced angiognesis.* **Ziche, M., et al.** 1997, Journal of Clinical Investigation, Vol. 99, pp. 2625-2634.

9. *Tumors: Wounds that do not heal. Similarities between tumor stroma generation and would healing.* **Dvorak, H. F.** 1986, New England Journal of Medicine, Vol. 315, pp. 1650-1659.

10. *Activation of vascular endothlial growth factor gene trascription by hypoxia-inducible factor 1.* **Forsythe, J. A., et al.** 1996, Molecular Cell Biology, Vol. 16, pp. 4604-4613.

11. *Second wave of angiogenesis during KDR/Flk-1 antibody therapy (Abstract).* **Hansen-Algenstaedt, N., et al.** 199, Proceedings of the American Association for Cancer Research, Vol. 40, p. 620.

12. *Migration and proliferation of endothelial cells in preformed and newly formed blood vessels during tumor angiogenesis.* **Ausprunk, D. H. and Folkman, J.** 1977, Microvascular Research, Vol. 14, pp. 53-65.

13. *Angiogenic Factors.* **Folkman, Judah and Klagsbrun, M.** 1987, Science, Vol. 235, pp. 442-447.

14. *VEGF guides angiogenic sprouting utilizing endothelial tip cell filopodia.* **Gerhardt, Holger, et al.** 2003, Journal of Cell Biology, Vol. 161, pp. 1163-1177.

15. *Tumorogenesis and the angiogenic switch.* **Bergers, Gabriele and Benjamin, Laura E.** 2003, Nature Reviews, pp. 401-410.

16. *Anti-angiogenic tyrosine kinase inhibitors: what is their mechanism of action.* **Gotink, K. J. and Verheul, H. M.** 2010, Angiogensis, pp. 1-14.

17. *Induction of a fibrin-gel investment: an early event in line 10 hepatocarcinoma growth mediated by tumor-secreted products.* **Dvorak, H. F., et al.** 1979, Journal of Immunology, Vol. 122, pp. 166-74.

18. *Vascular permeability factor/ vascular endothelial growth factor, microvascular hyperpermeability, and angiogenesis.* **Dvorak, H. F., et al.** 1995, American Journal of Pathology, Vol. 146, pp. 1029-39.

19. *The biology of vascular endothlial growth factor.* **Ferrara, N. and Davis-Smyth, T.** 1997, Endocrine Review, Vol. 18, pp. 4-25.

20. *Selective ablation of immature blood vessels in established human tumors follows vascular endothelial growth factor withdrawal.* **Benjamin, L. E., et al.** 1999, Journal of Clinical Investivation, Vol. 103, pp. 159-65.

21. *Vascular permeability factor/vascular endothelial growth factor (VPF/VEGF) delays and induces escape from senescence in human dermal microvascular endothelial cells.* **Watanabe, Y., et al.** 1997, Oncology, Vol. 14, pp. 2025-32.

22. *Therapy targeted at vascular endothelial growth factor in metastatic renal cell carcinoma: biology, clinical results and future developments.* **Rini, B. I., et al.** 2005, British Journal of Urology International, Vol. 96, pp. 286-90.

23. *Evading tumor evasion: Current concepts and perspectives of anti-angiogenic cancer therapy.* **Abdollahi, Amir and Folkman, Judah.** 2010, Drug Resistance Updates, pp. 16-28.

24. *Role of vascular endothelial growth factor in the regulation of angiogenesis.* **Ferrara, N.** 2001, American Journal of Cell Physiology, Vol. 280, pp. C1358-C1366.

25. *Vascular endothelial growth factor: Basic biology and clinical implications.* **Ferrara, N. and Keyt, B.** 1997, EXS, Vol. 79, pp. 209-232.

26. *VEGF prevents apoptosis of human microvascular endothelial cells via opposing effects on MAPK/ERK and SAPK/JNK signaling.* **Gupta, K., et al.** 1999, Experimental Cell Research, Vol. 247, pp. 495-504.

27. *Targeting VEGF ligands and receptors in cancer.* **Malik, A. K. and Gerberu, H. P.** 2003, Targets, Vol. 2, pp. 48-57.

28. *Vascular permeability factor/vascular endothlial growth factor: A multi-functional angiogenic cytokine.* **Brown, L. F., et al.** 1997, EXS, Vol. 79, pp. 233-269.

29. *The chick embryo chorioallantoic membrane as a model system for the study of tumor angiogenesis, invasion and development of anti-angiogenic agents.* **Tufan, A. C. and Satiroglu-Tufan, N. L.** 2005, Current Cancer Drug Targets, Vol. 5, pp. 249-266.

30. *Integrins: Structure, function and biological properties.* **Cheresh, D. A.** 1993, Advanced Molecular Cell Biology, Vol. 6, pp. 225-252.

31. *Requirements of vascular integrin αvβ3 for angiogenesis.* **Brooks, P. C. et al.** 1994, Science, Vol. 264, pp. 569-571.

32. *Hallmarks of cancer: the next generation.* **Hanahan, D. and Weinberg, R. A.** 2011, Cell, Vol. 144, pp. 646-74.

33. *Cell signaling by receptor tyrosine kinases.* **Schlessinger, J.** 2000, Cell, Vol. 103, pp. 211-225.

34. *Specificity in signal transduction: from phosphotyrosine-SH2 domain interactions to complex cellular systems.* **Pawson, T.** 2004, Cell, Vol. 116, pp. 191-203.

35. *Age-related macular degeneration.* **Fine, S. L., et al.** 2000, New England Journal of Medicine, Vol. 342, pp. 483-492.

36. *Age-related macular degeneration (AMD): patholgenesis and therapy.* **Nowak, J. Z.** 2006, Pharmacological Reports, Vol. 58, pp. 353-363.

37. *Disease.* DeCleene Optometry inc. Eyecare for Life*(TM).* [Online] 2009. [Cited: 06 2011, 03.] http://www.decleeneoptometry.com/pages/diseases.htm.

38. *Anatomy.* St. Luke's Cataract and Laser Institute. [Online] 2010. [Cited: 06 08, 2011.] http://www.stlukeseye.com/anatomy/choroid.html.

39. *Combination therapy using verteporfin and ranibizumab; optimizing the timing in the CAM model.* **Debefve, E., et al.** 2009, Photochemistry and Photobiology.

40. *Photodynamic therapy: basic principles and mechanisms.* **Van den Bergh, Hubert and Ballini, Jean-Pierre.** 2003, Lasers in Ophthalmology - Basic, Diagnostic, and Surgical Aspects, pp. 183-195.

41. Fish oil can halt Age-Related Macular Degeneration, a prominent eye disease for the elderly. *Fish Oil Blog.* [Online] 2011. [Cited: 06 2011, 03.] http://www.fishoilblog.com/fish-oil-treatment-age-related-macular-degeneration-blindness.php.

42. *Macular degeneration treatment*. **Haddrill, Marilyn.** All About Vision. [Online] July 2010. [Cited: April 11, 2011.] http://www.allaboutvision.com/conditions/amd-treatments.htm.

43. *Synergies of VEGF inhibition and photodynamic therapy in the treatment of age-related macular degeneration.* **Zuluaga, M-F., et al.** 2007, Investigative Opthalmology and Visual Science, Vol. 48, pp. 1767-1772.

44. *Wet age-related macular degeneration.* **Kulkarni, A. D. and Kuppermann, B. D.** 2005, Advanced Drug Delivery Review, Vol. 57, pp. 1994-2009.

45. *Managment of neovascular age-related macular degeneration.* **Schmidt-Erfurth, U. M. and Pruente, C.** 2007, Progess in Retinal and Eye Research, Vol. 26, pp. 437-451.

46. *Guidance for the treatment of neovascular age-related macular degeneration.* **Schmidt-Erfurth, U. M., et al.** 2007, Acta Opthalmol. Scand., Vol. 85, pp. 486-94.

47. *FDA News Release: FDA approves new biologic treatment for wet age-related macular degeneration*. **FDA, U. S. Food and Drug Administration.** [Online] 06 30, 2006. [Cited: 06 14, 2011.] http://www.fda.gov/NewsEvents/Newsroom/PressAnnouncements/2006/ucm108685.htm.

48. *FDA News Release: FDA approves new drug treatment for age-related macular degeneration*. **FDA, U. S. Food and Drug Administration.** [Online] 12 20, 2004. [Cited: 06 14, 2011.] http://www.fda.gov/NewsEvents/Newsroom/PressAnnouncements/2004/ucm108385.htm.

49. *Anecortave acetate for the treatment of subfoveal choroidal neovascularization secondary to age-realted macular degeneration.* **Schmidt-Erfurth, U., et al.** 2005, European Journal of Ophthalmology, Vol. 15, pp. 482-485.

50. *Intravitreal triamcinolone acetonide for treatment of intraocular proliferative, exudative and neovascular diseases.* **Jonas, J. B., et al.** 2005, Progress in Retinal and Eye Research, Vol. 24, pp. 587-611.

51. *Antiangiogenic steroids in human cancer therapy.* **Petras, R. J. and Weinberg, O. K.** 2005, Evidence Based Complementary and Alternative Medicine, Vol. 2, pp. 49-57.

52. *Supression of ocular neovascularization with siRNA targeting VEGF Receptor1.* **Shen, J., et al.** 2006, Gene Therapy, Vol. 13, pp. 225-234.

53. *VEGF-TRAP (R1R2) suppresses choroidal neovascularization and VEGF-induced breakdown of the blood retinal barrier.* **Saishin, Y., et al.** 2003, Journal of Cell Physiology, Vol. 195, pp. 241-248.

54. *Adenoviral vector-delivered pigment epithelium-derived factor for neo-vascular age-related macular degeneration: results of phase I clinical tiral.* **Campochiaro, P. A., et al.** 2006, Human Gene Therapy, Vol. 17, pp. 167-176.

55. *Dramatic inhibition of retinal and choroidal neovascularization by oral administration of a kinase inhibitor.* **Seo, M. S., et al.** 1999, American Journal of Pathology, Vol. 154, pp. 1743-1753.

56. *Intraocular sustained drug delivery using implantable polymeric devices.* **Yasukawa, T., et al.** 2005, Advanced Drug Delivery Reviews, Vol. 57, pp. 2034-2046.

57. *Ocular drug delivery: conventional ocular formulations.* **Lang, L. C.** 1995, Advanced drug delivery review, Vol. 16, pp. 39-43.

58. *Intravitreal administration of antisense oligonucleotides: potential of liposomal delivery.* **Bochot, A., et al.** 2000, Pregressive Retinal Eye Research, Vol. 19, pp. 131-147.

59. *FDA drug approval summary: bevacizumab plus FOLFOX4 as second-line treatment of colorectal cancer.* **Cohen, M. H., et al.** 2007, The Oncologist, Vol. 12, pp. 356-361.

60. *Bevacizumab versus ranibizumab - the verdict.* **Rosenfeld, Philip J.** Massachusetts Medical Society. s.l. : New England Journal of Medicine, 2011.

61. *Quand est-il du Lucentis* (ranibizumab)? **Lambert, Vincent.** Experimental Ophthalmology Laboratory of Liege, University of Liège. [Online] March 2009. [Cited: 05 06, 2011.] http://www.ophtalmo.ulg.ac.be/lucentis.html.

62. *Predicted biological activity of intravitreal bevacizumab.* **Stewart, M. W.** 2007, Retina, Vol. 27, pp. 1196-200.

63. *Ranibizumab and bevacizumab for neovascular age-related macular degeneration.* **CATT Research Group, The.** 2011, New England Journal of Medicine, p. DOI:10.1056/NEJMoa1102673.

64. *New treatments in age-related macular degeneration.* **Hooper, C. Y. and Guymer, R. H.** 2003, Clinical Experimental Opthalmology, Vol. 31, pp. 376-391.

65. *Visudyne (verteporfin for injection), Rx only, Perscribing Information.* **Novartis.** East Hanover, New Jersey : Novartis Pharmaceuticals Corporation, 2007.

66. *Photodynamic therapy of subfoveal choroidal neovascularization in age-related macular degeneration with verteporfin: two-year results of 2 randomized clinical trials-tap report 2.* **Bressler, N. M. and TAP, Treatment of Age Related Macular Degeneration with Photodynamic Therapy Study Group.** 2001, Archives of Opthalmalogy, Vol. 119, pp. 198-207.

67. *Tumor angiogenesis: thereapeutic implications.* **Folkman, Judah.** 1971, New England Journal of Medicine, pp. 1182-1186.

68. *Growth and metastasis of tumors in organ culture.* **Folkman, J., et al.** 1963, Cancer, p. 16.

69. *Tumor angiogenesis: Transfilter diffusion studies in the hamster by the transparent chamber technique.* **Greenblatt, M. and Shubik, P.** 1968, Journal National Cancer Insititute, Vol. 41, pp. 111-124.

70. *The hallmarks of cancer.* **Hanahan, D, Weinberg, R. A.** 2000, Cell, pp. 57-70.

71. *Modes of resistance to anti-angoigenic therapy.* **Bergers, Gabriele and Hanahan, Douglas.** 2008, Nat Rev Cancer, pp. 592-603.

72. *Evaluation of metastatic and angiogenic potentials of human colon carcinoma cells in chicken embryo model systems.* **Subauste, M. C., et al.** 2009, Clinical and Experimental Metastasis, Vol. 26, pp. 1033-1047.

73. *Soluble vascular endothelial growth factor levels in patients with primary colorectal carcinoma.* **Werther, K., et al.** 7, 2000, European Journal of Surgical Oncology, Vol. 26, pp. 657-662.

74. *Elevated perioperative serum vascular endothelial growth factor levels in patients with colon carcinoma.* **De Vita, F., et al.** 2004, Cancer, Vol. 100, pp. 270-278.

75. *Sunitinib malate for the treatment of metastatic renal cell carcinoma and gastrointestinal stromal tumors.* **Adams, V. R. and Leggas, M.** 2007, Clinical Therapeutics, Vol. 29, pp. 1338-1354.

76. **The Jackson Cancer Modeling Group.** Quantitative Cancer Research. [Online] 2011. [Cited: 06 13, 2011.] http://www.math.lsa.umich.edu/~tjacks/research.html.

77. *Abnormalities in pericytes on blood vessels and endothelial sprouts in tumors.* **Morikawa, L. E and al., et.** 2002, American Journal of Patholgy, Vol. 160, pp. 985-1000.

78. *Targeting vessels to treat hepatocellular carcinoma.* **Romanque, P., et al.** 2008, Clinical Science, Vol. 114, pp. 467-477.

79. *Targeting non-malignant disorders with tyrosine kinase inhibitors.* **Grimminger, F., et al.** 2010, Nature, Vol. 9, pp. 956-970.

80. *Understanding the causes of multidrug resistance in cancer: a comparison of doxorubicin and sunitinib.* **Broxterman, H. J, et al.** 2009, Drug Resistance Updates, Vol. 12, pp. 114-126.

81. *Uptake and retention of duanomycin by leukemic cellls as factors in drug response.* **Kessel, D., et al.** 1968, Cancer Research, Vol. 28, pp. 938-941.

82. *Anti-angiogenic therapeutic drugs for treatment of human cancer.* **Wu, H.-C., et al.** 2008, Journal of Cancer Molecules, Vol. 4, pp. 37-45.

83. *Antiangiogenic therapy elicits malignant progression of tumors to increased local invasion and distant metastasis.* **Paez-Ribes, M., et al.** 2009, Cancer Cell, pp. 220-231.

84. *Accelerated metastasis after short-term treatment with a potent inhibitor of tumor angiogenesis.* **Ebos, J. M., et al.** 2009, Cancer Cell, Vol. 15, pp. 232-239.

85. *Multiple circulating proangiogenic factors induced by sunitinib malate are tumor-independent and correlate with antitumor efficacy.* **Ebos, J. M., et al.** 2007, Proceedings of the National Academy of Sciences, Vol. 104, pp. 17069–17074.

86. *VEGF-targeted therapy: mechansims of anti-tumor activity.* **Ellis, L.M. and Hicklin, D.J.** 2008, Nature Reviews Cancer, Vol. 8, pp. 579-591.

87. *Seminars in Medicine of the Beth Israel Hostpital, Boston. Clinical applications of research on angiogenesis.* **Folkman, Judah.** 1995, New England Journal fo Medicine, Vol. 333, pp. 273-286.

88. *Bevacizumab, CCO Formulary.* **Roche.** s.l. : Roche, 2010.

89. *Avastin versus Lucentis: Why it matters.* **Kaufman, S. R, et al.** Medical Research Modernization Committee. [Online] 12 11, 2006. [Cited: 05 11, 2011.] http://www.mrmcmed.org/AvastinversusLucentis.pdf.

90. *Normalization of tumor vasculartur: an emerging concept in antiangiogenic therapy.* **Jain, R. K.** 2005, Science, Vol. 307, pp. 58-62.

91. *Health Canada endorsed important safety information on Avastin (bevacizumab)*. **HealthCanada.** December 16, 2008.

92. *Genetic heterogeneity of the vasculogenic phenotype parrallels angiogenesis; implications for cellular surrogate marker analusis of antiangiogenesis.* **Shaked, Y., et al.** 2005, Cancer Cell, Vol. 7, pp. 101-111.

93. *Antiangiogenic therapy in lung cancer: focus on vascular endothelial growth factor pathway.* **Korpanty, G., et al.** 2010, Experimental Biology and Medicine, Vol. 235, pp. 3-9.

94. *A randomized trial of Bevacizumab, an anti-vascular endothelial growth factor antibody for metastatic renal cancer.* **Yang, J. C., et al.** 2003, New England Journal of Medicine, Vol. 349, pp. 427-34.

95. *Activity of SU11248, a multitargeted inhibitor of vasular endothelial growth factor receptor and platelet-derived growth factor receptor, in patients with renal cell carcinoma.* **Motzer, R. J., et al.** 2006, Journal of Clinical Oncology, Vol. 24, pp. 16-24.

96. *Vessel fractions in tumor xenografts depicted by flow- or contrast-sensitive three- dimensional high frequency doppler ultrasound respond differently to antiangiogenic treatment.* **Palmowski, M., et al.** 2008, Cancer Research, Vol. 67, pp. 7042-7049.

97. *Safety, pharmacokinetic and antitumor activity of SU11248, a novel oral multitarget tyrosine kinase inhibitor, in patients with cancer.* **Faivre, S., et al.** 2006, Journal of Clinical Oncology, Vol. 24, pp. 24-35.

98. *In vivo antitumor activity of SU11248, a novel tyrosine kinase inhibitor targeting vascular endothelial growth factor and platelet derived growth factor receptors: determination of a pharmacokinetic/ pharmodynamic relationship.* **Mendel, D. B., et al.** 2003, Clinical Cancer Research, Vol. 13, pp. 327-37.

99. *Development and validation of an HPLC-UV-visible method for sunitinib quantification in human plasma.* **Blanchet, Benoit, et al.** 2009, Clinical Chimica Acta, Vol. 404, pp. 134-39.

100. *Approval summary: sunitinib for the treatment of imatinib refractory or intolerant gastrointestinal stromal tumors and advanced renal cell carcinoma.* **Goodman, V. L., et al.** 2007, Clinical Cancer Research, Vol. 13, pp. 1367-1373.

101. *Food and Drug Administration drug approval summary: sunitinib malate for the treatment of gastrointestinal stromal tumor and advanced renal cell carcinoma.* **Rock, E. P., et al.** 2007, Oncologist, Vol. 12, pp. 107-113.

102. *Pfizer Scores New Approval for Sutent in Europe.* **Genetic Engineering and Biotechnology News, GEN.** Genetic Engineering and Biotechnology News, GEN. [Online] December 2, 2010. [Cited: March 24, 2011.] http://www.genengnews.com/gen-news-highlights/pfizer-scores-new-approval-for-sutent-in-europe/81244326/.

103. *Overall survival and updated results from sunitinib compared with interferon alpha in metastatic renal-cell carcinoma.* **Motzer, R. J., et al.** 2009, Journal of Clinical Oncology, Vol. 27, pp. 3584-3590.

104. *Quantification of sunitinib in human plasma by high performance liquid chromatography-tandem mass spectrometry.* **Minkin, P., et al.** 2008, Journal Chromatography Biology, Vol. 15, pp. 84-88.

105. *Ligand-dependent platelet-derived growth factor receptor (PDGFR)-alpha activation sensitizes rare lung cancer and sarcoma cells to PDGFR kinase inhibitors.* **McDermott, U., et al.** 2009, Cancer Research, Vol. 69, pp. 3937-3946.

106. *Drug Discovery and Development*. **The Van Andel Research Institute.** VARI Scientists Turn Off Resistance to Sunitinib. [Online] 04 02, 2010. [Cited: 05 06, 2011.] http://www.dddmag.com/news-VARI-Scientists-Turn-Off-Resistance-to-Sunitinib-3210.aspx.

107. *The history of photodetection and photodynamic therapy.* **Ackroyd, Roger, et al.** 2001, Photochemistry and Photobiology, Vol. 74, pp. 656-669.

108. *Photodynamic thearpy in the treatment of head and nech neoplasia.* **Biel, M. A.** 1998, Laryngoscope, Vol. 108, pp. 1259-1268.

109. *A phase II/III study of tin ethyl etiopurpurin (Purlytin)-induced photodynamic therapy for the treatment of recurrent cutaneous metastatic breast cancer.* **Mang, T. S., et al.** 1998, Cancer Journal for Scienctific America, Vol. 4, pp. 378-384.

110. *Photodynamic therapy of brain tumors.* **Propovic, E. A., et al.** 1996, Journal of Clinical Laser Medical Surgery, Vol. 14, pp. 251-261.

111. *Photomedical approaches for the diagnosis and treatment of gynocoologic cancers.* **Hornung, R.** 2001, Current Drug Targets Immune Endocrine Metabolism Disorders, Vol. 2001, pp. 165-177.

112. *Results of combined photodynamic therapy (PDT) and high dose rate brachytherapy (HDR) in treatment of obstructive endobronchial non-small cell lung cancer (NSCLC).* **Weinberg, B. D., et al.** 2010, Photodyagnosis and Photodynamic therapy, Vol. 7, pp. 50-58.

113. *Differential cytotoxic responses to low- and high-dose photodynamic therapy in human gastric and bladder cancer cells.* **Yoo, J. O.** 2011, Journal of Cell Biochemistry.

114. *Guidelines on the use of phtotdynamic therapy for non-melanoma skin cancer: an international consensus.* **Braathen, L. R., et al.** s.l. : Journal of American Academic Dermatology, 2005. International Society for Photodynamic therapy in Dermatology. Vol. 56, pp. 125-43.

115. *Photodynamic Therapy for Cancer*. **National Cancer Institute.** National Cancer Institute at the National Institutes of Health. [Online] 12 05, 2004. [Cited: 05 23 , 2011.] http://www.cancer.gov/cancertopics/factsheet/Therapy/photodynamic.

116. *Phtotdynamic therapy: a review of the literature and documentation.* **Issa, M. C. A.** 2010, Anais Brasileiros de Dermatologia, Vol. 85, pp. 501-511.

117. *Photodynamic therapy for cancer.* **Dolmans, D., et al.** 2003, Nature.

118. *Visudyne therapy – a selective approach.* EPG online. [Online] 2011. [Cited: 05 06, 2011.] http://www.epgonline.org/warning.cfm?path=www.epgonline.org~page.cfm~pageid~789.

119. *Definition of Jablonski diagram.* Chemicool. [Online] May 2011. [Cited: 05 12, 2011.] http://www.chemicool.com/definition/jablonski_diagram.html.

120. *Scientific Discussion for Approval of Visudyne*. **EMEA.** EMEA. [Online] 12 01, 2003. [Cited: 05 10, 2011.] http://www.ema.europa.eu/docs/en_GB/document_library/EPAR_-_Scientific_Discussion/human/000305/WC500052403.pdf.

121. *Photodynamic therapy-mediated oxidative streess can induce expression of heat shock proteins.* **Gomer, C. J., et al.** 1996, Cancer Research, Vol. 56, pp. 2355-2360.

122. *The role of apoptosis in response to photodynamic therapy: what, where, why and how.* **Oleinick, N. L., et al.** 2002, Photochemical Photobiology, Vol. 1, pp. 1-21.

123. *Apoptosis-based therapies.* **Reed, J. C.** 2002, Naturee Review Drug Discovery, Vol. 1, pp. 111-121.

124. *TRAIL-induced apoptosis requires Bax-dependent mitochondrial release of Smac/DIABLO.* **Deng, Y. and al, et.** 2002, Genes Development, Vol. 16, pp. 33-45.

125. *Spectroscopic properties and photodynamic effects of new lipophilic porphyrin derivatives: efficacy, localisation and cell death pathways.* **Kramer-Marek, G.** 2006, Journal of Photochemisty and Photobiology, Vol. 84, pp. 1-14.

126. *Ranibizumab versus verteporfin photodynamic therapy for neovascular age-related acular degeneration: Two-year results of the ANCHOR study.* **Brown, D. M., et al.** 2009, Opthalmology, Vol. 116, pp. 57-65.

127. *Verteporfin photodynamic therapy combined with intravitreal bevacizumab for neovascular age-related macular degeneration.* **Kaiser, P. K. and Committee, Registry of Visudyne AMD Therapy Writing.** 2009, Opthalmology, Vol. 116, pp. 747-755.

128. *Inhibition of human vascular endothelial cells proliferationg by terbinafine.* **Ho, P. Y., et al.** 2004, International Journal of Cancer, Vol. 111, pp. 51-59.

129. *A hemangioendothelioma-derived cell line: its use as a model for the study of endothelial cell biology.* **Obeso, J., et al.** 1990, Laboratory Investigation, Vol. 63, pp. 259-269.

130. *The role of basement membrane in angiogenesis and tumor growth.* **Grant, D. S., et al.** 1994, Pathology Research and Practive, Vol. 190, pp. 854-863.

131. *Alchornea glandulosa ethyl acetate fraction exhibits antiangiogenic activity: preliminary findings from in vitro assays using human umbilical vein endothelial cells.* **Lopes, F. C., et al.** 2011, Journal of Medicinal Food.

132. *Growth of microvessels in serum-free matrix culture of rat aorta. A quantitative assay of angiognesis in vitro.* **Nicosia, R. F. and Ottinetti, A.** 1990, Laboratory Investigation, Vol. 63, pp. 115-122.

133. *The chick embryo aortic arch assay: a new, rapid, quantifiable in vitro method for testing the efficacy of angiogenic and anti-angiogenic factors in a three dimensional, serum-free organ culture system.* **Muthukkarruppan, V. R., et al.** 2000, Proceedings of the American Association for Cancer Research, Vol. 41, p. 65.

134. *A single local application of recombinant human basic fibroblast growth factor accelerates initial angiogenesis during wound healing in rabbit ear chamber.* **Komori, M., et al.** 2005, Anesthesia and Analgesia, Vol. 100, pp. 830-834.

135. *Effects of thalidomide on DMBA-induced oral carcinogenesis in hamster with respect to angiogenesis.* **Yang, Y. et al.** 2009, Journal of Oral Pathology and Medicine, Vol. 38, pp. 455-462.

136. *The dorsal skinfold chamber: studying angiogenesis by intravital microscopy.* **Sckell, A. and Leunig, M.** 2009, Methods of Molecular Biology, Vol. 467, pp. 305-317.

137. *Angiogenesis in the mous cornea.* **Muthukkaruppan, V. R., et al.** 1979, Science, Vol. 205, pp. 1416-1418.

138. *A simple, quantitative method for assessing angiogenesis and antiangiogenic agents using reconstituted basement membrane, heparin and fibroblast growth factor.* **Passaniti, A., et al.** 1982, Laboratory Investigation, Vol. 1982, pp. 519-528.

139. *The sponge/Matrigel angiogenesis assay.* **Akhtar, N., et al.** 2002, Angiogenesis, Vol. 5, pp. 75-80.

140. *Processing of fluorescence angiograms for the quantification of vascular effects induced by anti-angiogenic agents in the CAM model.* **Nowak-Sliwinska, P., et al.** 2010, Microvascular Research, Vol. 79, pp. 21-28.

141. *A new drug-screening procedure for photodynamic sensitizing agenst used in photodynamic therapy for CNV.* **Lange, N. and al., et.** 2001, Investigative Ophthalmology Visual Science, Vol. 42, pp. 38-46.

142. *Vascular regrowth following photodynamic therapy in the chicken embryo chorioallantoic membrane.* **Nowak-Sliwinska, P., et al.** 2010, Angiogenesis, Vol. 13, pp. 281-292.

143. *Angiostatic kinase inhibitors to sustain photodynamic angio-occlusion.* **Nowak-Sliwinska, P., et al.** 2011, Under Review.

144. *Verteporfin, photofrin II, and merocyanine 540 as PDT photosensitizers against melanoma cells.* **Nowak-Sliwinska, P., et al.** 2006, Biochemical and Biophysical Research Communications, Vol. 349, pp. 549-55.

145. *Efficacy and safety of sunitinib malate (SU11248) in bevacizumab-refractory metastatic renal cell carcinoma (mRCC).* **Rini, B. I., et al.** Atlanta, GA : s.n., 2006. ASCO Anual Meeting. p. Abstract 9540.

146. *Inhibition of vascular endothelial growth factor-induced angiogenesis suppresses tumor growth in vivo.* **Kim, K. J., et al.** 1993, Nature, Vol. 362, pp. 841-844.

147. *Phase II study of SU11248, a multitargeted receptor tyrosine kinase inhibitor (TKI), in patietns (pts) with previously treated metastatic breast cancer (MBC).* **Miller, K. D., et al.** Orlando Fla. : s.n., 2005. ASCO Annual Meeting. p. Abstract 563.

148. *Sunitinib for patients (pts) with advanced imatinib (IM)-refractory GIST: Early results from a "treatment-use" trial.* **Morgan, J. A., et al.** Atlanta, GA : s.n., 2006. ASCO Annual Meeting. p. Abstract 9540.

149. *Efficacy and safety of sunitinib in previously treated, advanced non-small lung cancer (NSCLC): Preliminary results of a multicenter phase II trial.* **Socinski, M. A., et al.** Atlanta, GA : s.n., 2006. ASCO Annual Meeting. p. Abstract 7001.

150. *Phase II study of sunitinib administered.* **George, S., et al.** Atlanta, GA : s.n., 2006. p. Abstract 9532.